ELECTROMAGNETIC BIAS IN RADAR ALTIMETRY AT MICROWAVE FREQUENCIES

by

David V. Arnold

B.S. Brigham Young University
(1983)
M.S. Brigham Young University
(1987)

Submitted to the Department of
Electrical Engineering and Computer Science
in Partial Fulfillment of the Requirements
for the Degree of

DOCTOR OF PHILOSOPHY

at the

MASSACHUSETTS INSTITUTE OF TECHNOLOGY

August 1992

Author_____
Department of Electrical Engineering and Computer Science

Certified by_____
Professor Jin Au Kong
Thesis Supervisor

Certified by_____
Professor W. Kendall Melville
Thesis Supervisor

Accepted by_____
Campbell Searle, Chairman
Departmental Committee on Graduate Students

ABSTRACT

The electromagnetic (EM) bias ϵ is an error present in radar altimetry of the ocean surface due to non-uniform reflection from wave troughs and crests. The electromagnetic bias is defined as the difference between the mean reflecting surface and the mean sea surface. A knowledge of the electromagnetic bias is necessary to permit error reduction in mean sea level measurements by satellite radar altimeters. Direct measurements of the EM bias were made from a Shell Offshore oil production platform in the Gulf of Mexico for a six month period during 1989 and 1990. Measurements of the EM bias were made at 5 GHz and 14 GHz. During the experiment the significant wave height $H_{1/3}$ varied from 0.6 to 3.2 m, and the wind speed at 25 m above the surface varied from 0.1 m/s to 14.3 m/s. For wind speeds greater than 3-4 m/s but less than 10 m/s, the bias was found to increase linearly with wind speed. For wind speeds greater than 11-12 m/s, the C band bias reaches a saturation, and similarly, the Ku band bias reaches a saturation and then begins to decrease for wind speeds greater than 9-10 m/s. The C band bias was found to be smaller than the Ku band bias for low wind speeds and larger for high wind speeds. The EM bias is explained using physical optics scattering and an empirical model for the short wave modulation. Measurements of the short wave modulation using a wire wave gauge demonstrated a linear dependence of the normalized bias on the short wave modulation strength M. The theory accurately predicts this dependence by the relation $\epsilon = -\alpha M H_{1/3}$. The wind speed dependence of the normalized bias is explained by the dependence of the short wave modulation strength on the wind speed. While other effects such as long wave tilt and curvature will have an effect on the bias, the primary cause of the bias is shown to be due to the short wave modulation.

Supervisor: Jin Kong
Supervisor: W. Kendall Melville

ACKNOWLEDGEMENTS

I wish to express my appreciation to Professors Jin Kong and Ken Melville for the productive years I spent under their direction. I appreciate their many suggestions and the opportunity they provided to perform this work. I would like to thank Eric Lamarre for the extensive support he provided during the Gulf of Mexico experiment. I would like to thank Bill Keller of the Naval Research Laboratory for the use of the C band scatterometer, the construction of the Ku band scatterometer, and for his assistance in calibrating and maintaining the scatterometers. I also wish to thank Bob Shin for being a reader on my thesis committee, Bob Stewart for many helpful suggestions, and Francis Felizardo for the two week-long trips he made to the platform in the Gulf of Mexico.

I would like to thank my wife Linda and my children Amy, Benjamin and Matthew, all born since beginning this work, for their continuing love and support. I would also like to thank Linda for her help in the typing and preparation of this thesis.

Finally, I would like to thank my parents Verl and Shirley. It was 14 years ago that I began college as a 13 year old boy. I thank them for their wisdom and the large part they have played in the accomplishment of my goals. I have become a well balanced and happy adult thanks to their careful but purposeful child rearing.

Table of Contents

List of Tables

LIST OF FIGURES

Chapter 1

Introduction

The electromagnetic bias ϵ is an error present in radar altimetry of the ocean surface due to non-uniform reflection from wave troughs and crests. The electromagnetic bias is defined as the difference between the mean reflecting surface and the mean sea surface. A study of the electromagnetic bias became necessary to permit error reduction in mean sea level measurements by satellite radar altimeters. If not corrected, the electromagnetic bias could introduce errors in mean sea level measurements, possibly as large as 50 cm [*Slinn,* 1990].

1.1 Experimental Observations of the Electromagnetic Bias

The electromagnetic bias was first measured by *Yaplee et al.* [1970] from an ocean platform using a one-nanosecond-pulse X-band radar. Examples of the normalized radar cross section versus wave displacement for a calm and wind driven sea were reported and are shown in figure 1.1. It was demonstrated that the reflectivity in these two cases was not uniform but increased toward the trough. This caused the mean reflecting surface to be lower than the mean sea surface. The equivalent

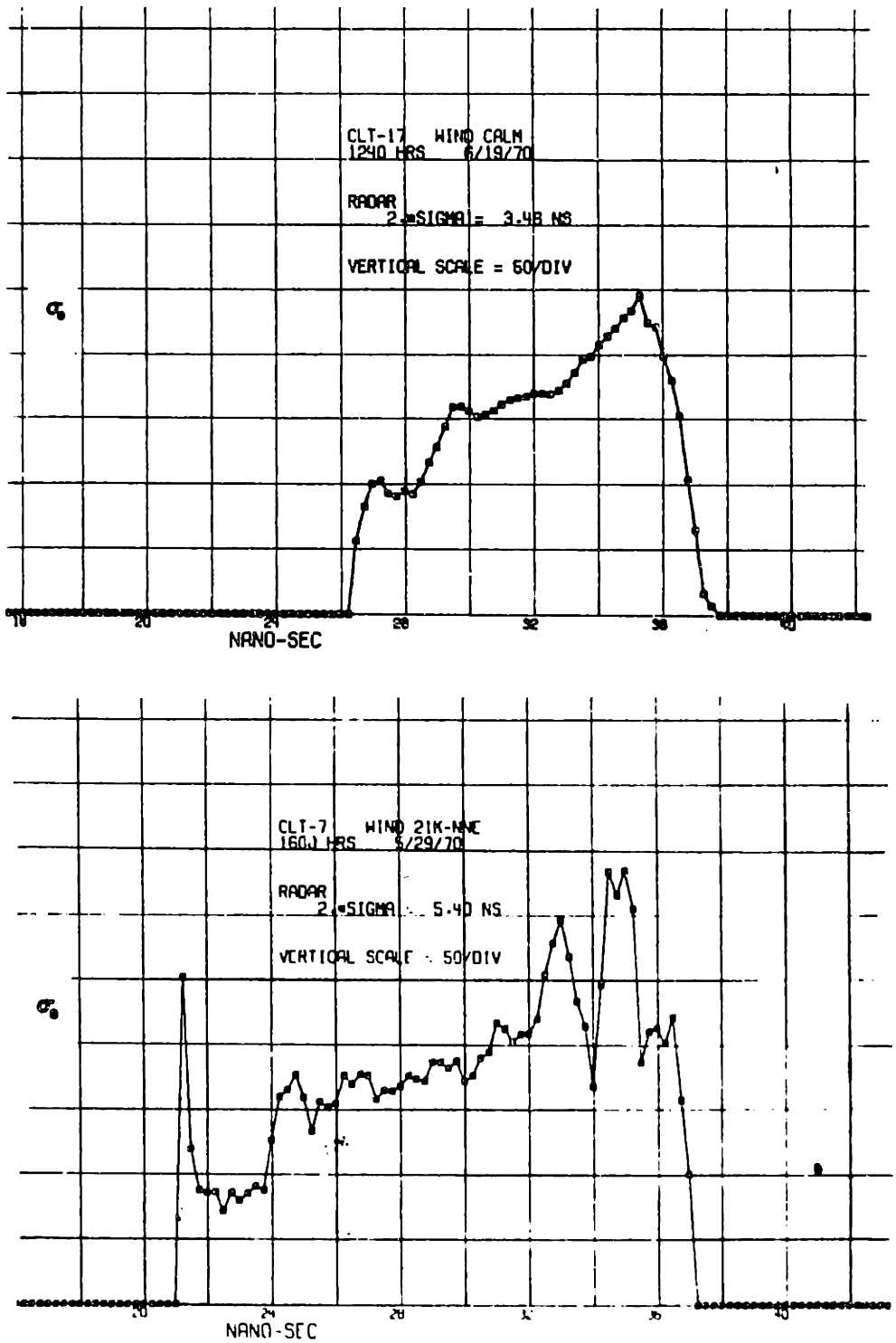

Figure 1.1: Normalized radar cross section versus wave depth, top: calm sea, bottom: wind driven sea. (Figures 9 and 10 from *Yaplee et al.* [1970].)

impulse responses for the reflecting surface and sea surface are shown in figure 1.2 for the calm and wind driven sea cases. As seen in figure 1.2, the mean reflecting surface was lower than the mean sea surface. The mean reflecting surface was 5% of the significant wave height (SWH) lower than the mean sea surface in both examples.

During 1980 three airborne electromagnetic bias experiments were performed. *Walsh et al.* [1984] measured the electromagnetic bias at 36 GHz as 1.1% of the SWH. *Choy et al.* [1984] measured the electromagnetic bias at 10 GHz as 3-5% of the SWH. At optical frequencies the electromagnetic bias was measured by *Hoge et al.* [1984] as biased toward the crests by 2% of the SWH for a low wind speed case and biased toward the troughs by 0.75% of the SWH for a high wind speed case. *Walsh et al.* [1989] report additional measurements of the electromagnetic bias at optical frequencies for high wind speed conditions. They found the electromagnetic bias at optical frequencies to be unbiased or biased toward the crests by as much as 0.5% of the SWH.

The work of *Walsh et al.* [1984] and *Choy et al.* [1984] showed a clear dependence of the electromagnetic bias on significant wave height. It is useful to define a dimensionless bias as

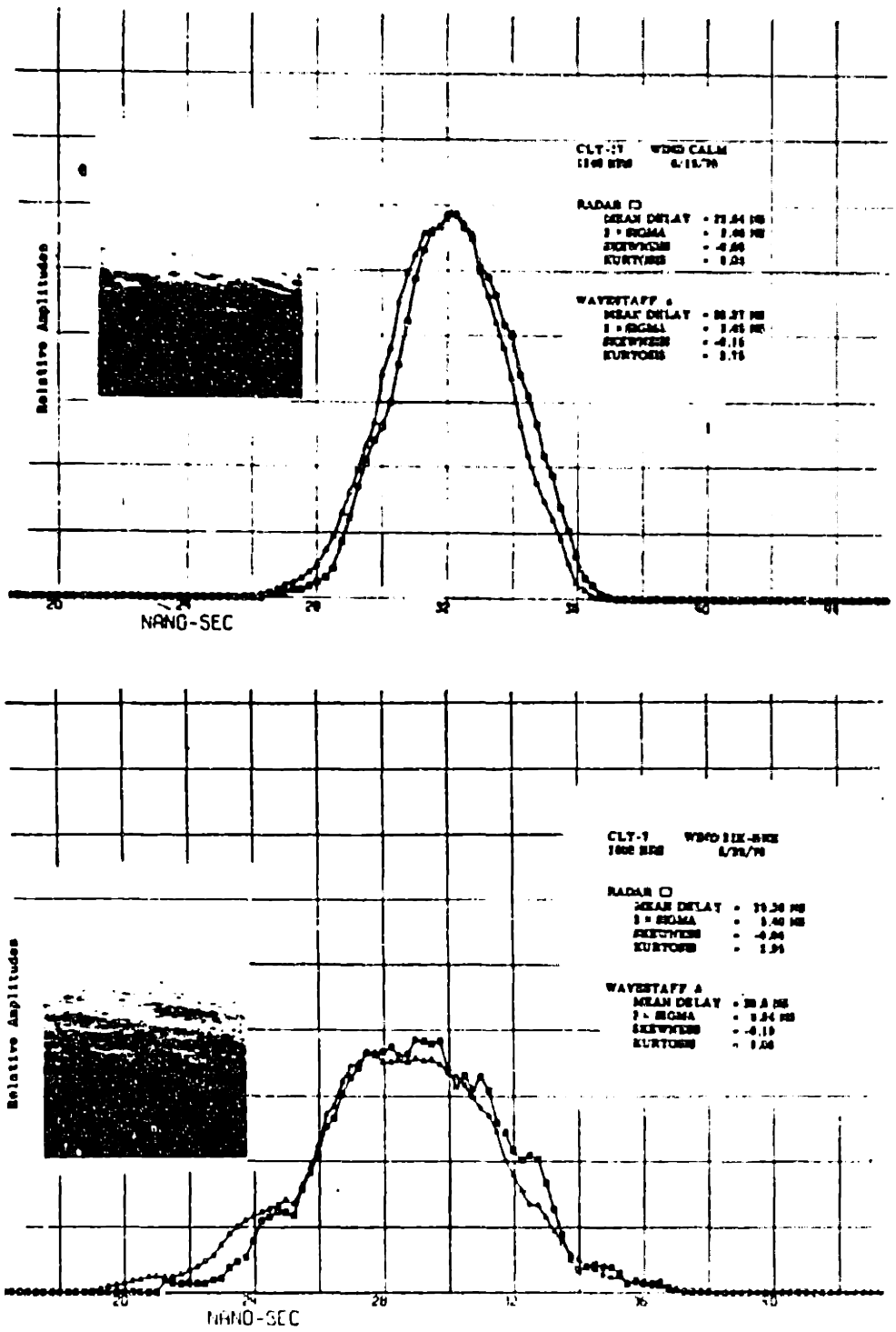

Figure 1.2: Equivalent impulse response, top: calm sea, bottom: wind driven sea. (Figures 11 and 12 from *Yaplee et al.* [1970].)

$$\beta = \frac{\epsilon}{H_{1/3}} \qquad (1.1)$$

where $H_{1/3}$ is the significant wave height defined as four times the standard deviation of the wave displacement. The measurements of *Choy et al.* [1984] showed a dependence of the dimensionless bias β on the wind speed. Figure 1.3 shows a plot of β versus the wind speed from Table 2[1] of *Choy et al.* [1984]. Figure 1.3 shows the electromagnetic bias increases with increasing wind speed. A linear regression fit to the *Choy et al.* [1984] data gives

$$\beta(\%SWH) = -0.146 - 0.288U \qquad r^2 = 0.672. \qquad (1.2)$$

During 1988, as part of the SAXON-CLT experiment, *Melville et al.* [1991] measured the electromagnetic bias from an ocean platform at 14 GHz as 3.3% of the SWH (see Appendix A). A dependence of β on wind speed similar to the result of *Choy et al.* [1984] was found. However, the SAXON-CLT electromagnetic bias experiment contained many more sample points (347 hourly averages over a 3-week time span) and more accurate wind speed measurements than *Choy et al.* [1984]. The observed dependence of β on the wind speed for the SAXON-CLT experiment is shown

[1]In working with the *Choy et al.* [1984] data points, *Walsh et al.* [1991] discovered an error in their Table 2. For the November 26, 1980 flight, the wind speed should be 6 m/s, not the 10 m/s shown in Table 2.

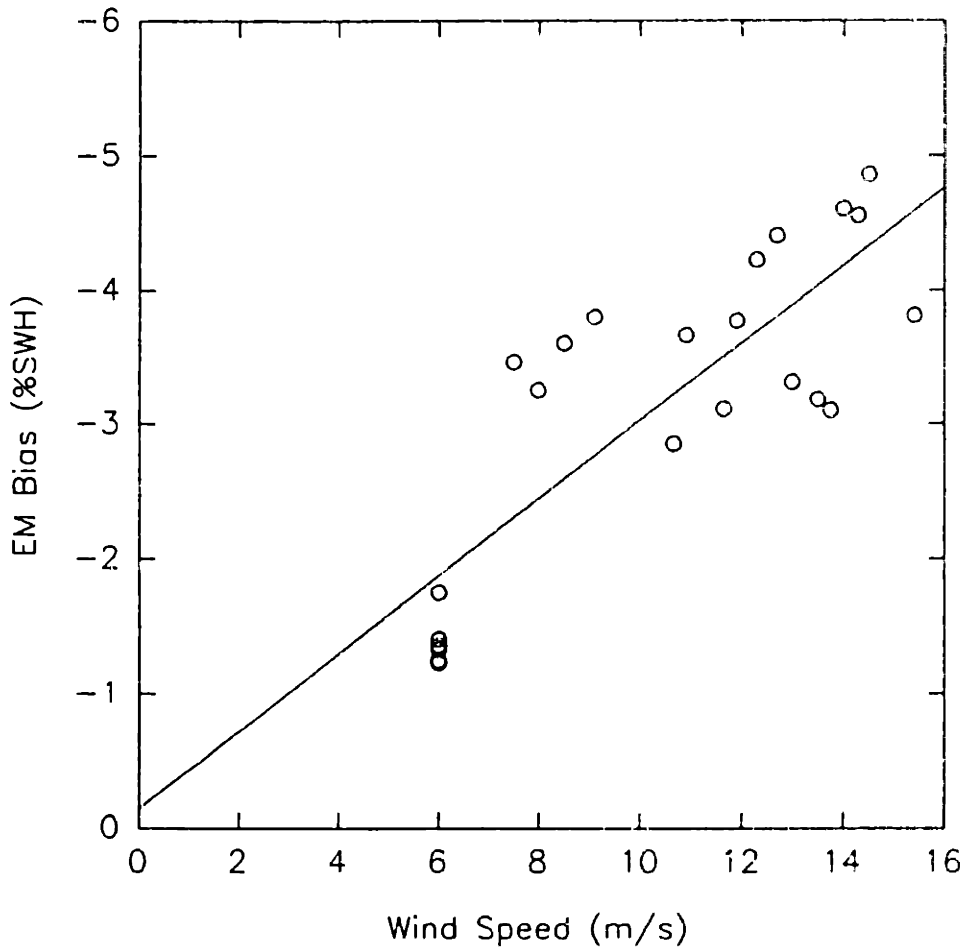

Figure 1.3: *Choy et al.* [1984] normalized X band electromagnetic bias as a function of wind speed. The line through the data is the linear regression fit $\beta(\%SWH) = -0.146 - 0.288U$ ($r^2 = 0.672$).

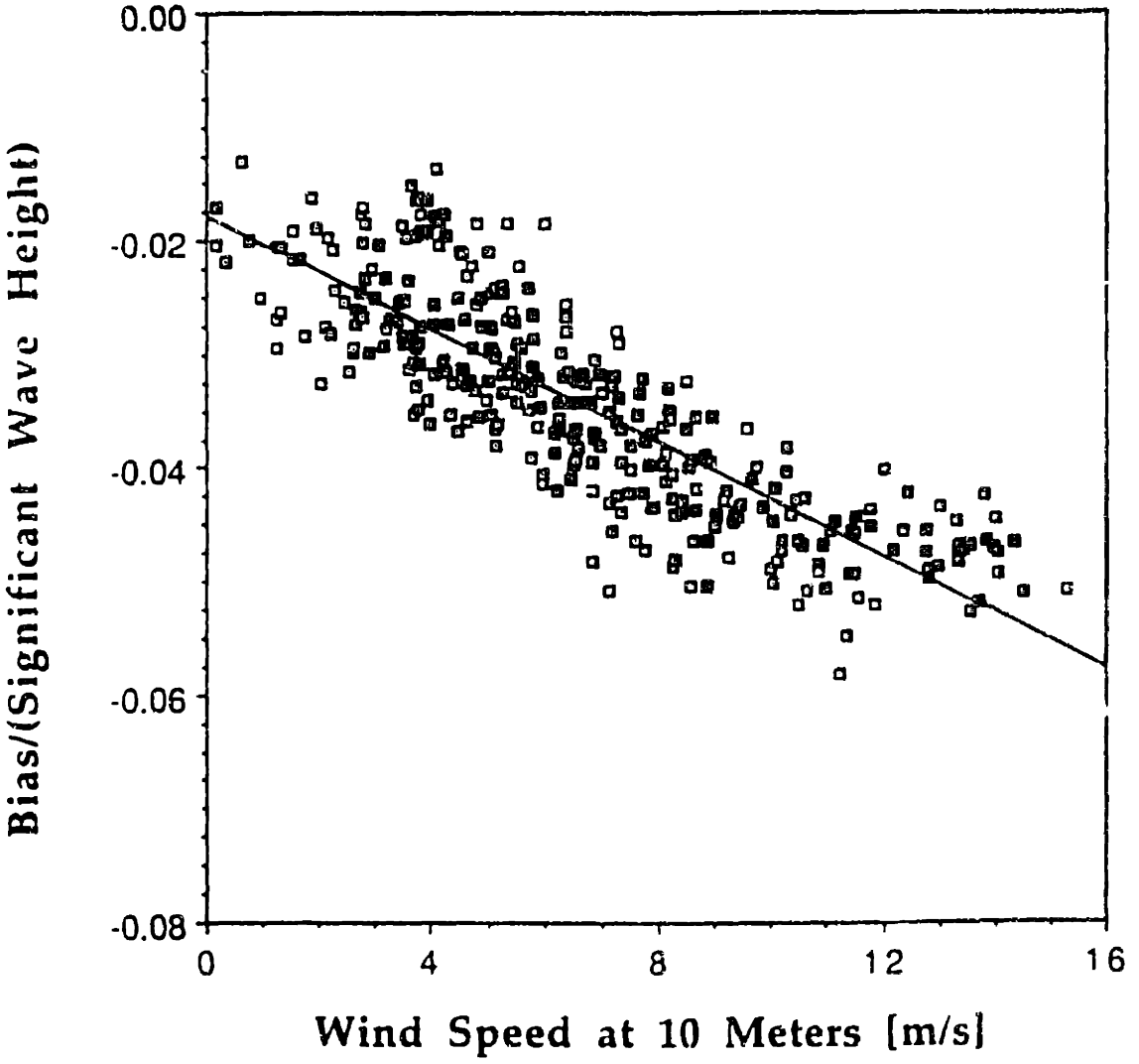

Figure 1.4: Normalized electromagnetic bias β, which is bias B divided by significant wave height $H_{1/3}$, as a function of wind speed 10 m above the sea surface, U_{10}. The line through the data is the least squares regression line $\beta = -0.0179 - 0.00250U_{10}$ ($r^2 = 0.707$) for wind speed in meters per second. (Figure 6 from *Melville et al.* [1991].)

in figure 1.4. A linear regression fit to the SAXON-CLT electromagnetic bias data gave

$$\beta(\%SWH) = -1.79 - 0.25U_{10} \qquad r^2 = 0.707. \qquad (1.3)$$

This measurement is similar to the *Choy et al.* [1984] result of equation (1.1) with differences at low wind speeds.

During 1989 *Walsh et al.* [1991] measured the electromagnetic bias at 5.3 GHz, 13.6 GHz, and 36 GHz. Similar to the previous experiments β was found to depend on the wind speed and the electromagnetic frequency. The measurements of *Walsh et al.* and some previous experimental data for comparison are shown in figure 1.5. A linear regression of the electromagnetic bias on wind speed for the *Walsh et al.* data at each frequency yielded

$$\beta_{5.3}(\%SWH) = -0.74 - 0.25U \qquad r^2 = 0.609 \qquad (1.4)$$

$$\beta_{13.6}(\%SWH) = -1.10 - 0.140U \qquad r^2 = 0.238 \qquad (1.5)$$

$$\beta_{36}(\%SWH) = 0.19 - 0.12U \qquad r^2 = 0.537. \qquad (1.6)$$

The airborne electromagnetic bias measurements of *Walsh et al.* [1991] (see figure 1.5) suggest about the same wind speed dependence as the tower measurements of

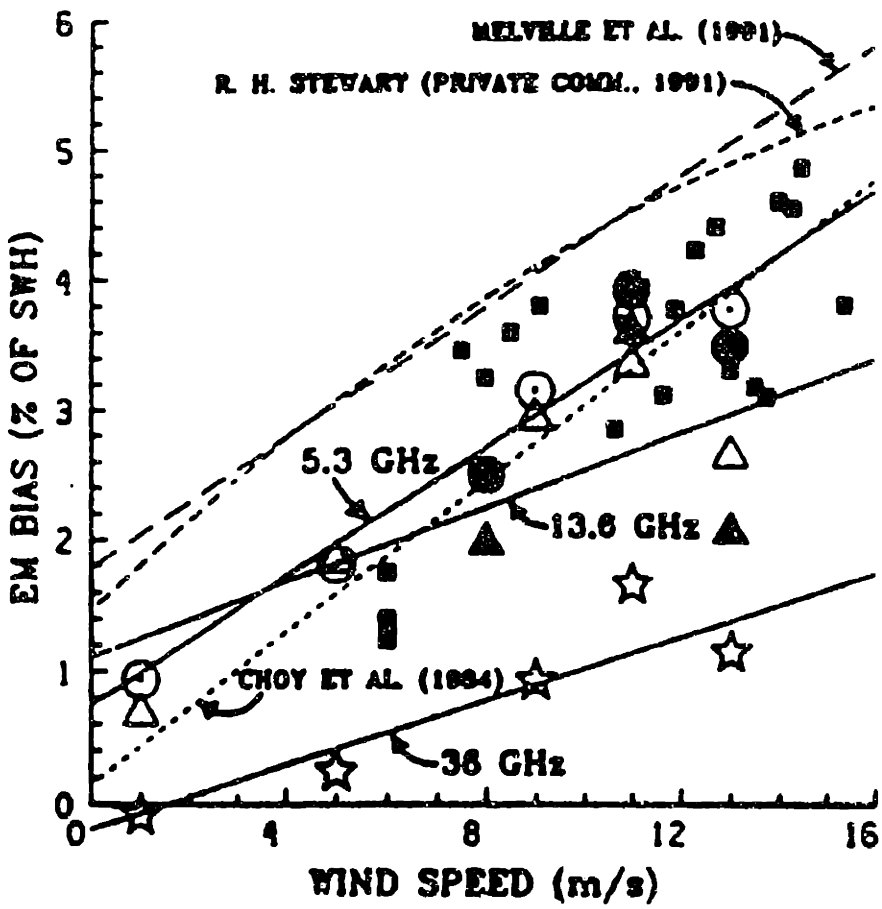

Figure 1.5: Mean values of EM bias for each day of the present experiment versus wind speed for 5.3 GHz (circles), 13.6 GHz (triangles), and 36 GHz (stars), with the solid symbols indicating use of AOL elevations and the open symbols indicating use of SCR elevations. The squares are airborne observations of *Choy et al.* [1984]. The solid lines are linear regressions to the data of the present experiment, and the dashed curves are regressions to data from earlier experiments. (Figure 18 from *Walsh et al.* [1991].)

Melville et al. [1991], but the magnitude of the airborne measurements is about 1% of SWH lower than the tower measurements. *Walsh et al.* [1991] suggested that since the tower and airborne heights differed by more than a factor of 7 (22 m versus 180 m) it might be useful to consider focusing/defocusing effects of the sea surface wave structure in trying to explain disparities.

During 1989 and 1990, measurements of the electromagnetic bias at 5 and 14 GHz were made from a platform in the Gulf of Mexico by the author and his colleagues. Results similar to the SAXON-CLT measurements of *Melville et al.* [1991] were found with some differences. The structure of the dependence of β on wind speed was different than found previously. A saturation and roll off of β at wind speeds greater than 10 m/s was observed. Also the C band bias was found to be smaller than the Ku band bias at low wind speeds but larger at high wind speeds. These results will be discussed in detail and extensively compared with previous measurements in Chapter 2.

Satellite radar altimeter measurements have been used to find upper and lower bounds for the electromagnetic bias (see Appendix A.1.2). Studies of the GEOS-3, SEASAT and GEOSAT altimeter data [*Lipa and Barrick,* 1981; *Born et al.,* 1982;

Hayne and Hancock, 1982; *Douglas and Agreen,* 1983; *Nerem and Shum,* 1990] lead to an electromagnetic bias that is in the range of 2-4% of the SWH.

1.2 Theoretical Investigations of the Electromagnetic Bias

Jackson [1979] was the first to study the electromagnetic bias theoretically. He based his work upon specular point theory [*Barrick,* 1968] where the relative back scatter coefficient is given in terms of the joint height-slope probability density function of the sea surface. Jackson used a model for the joint height-slope probability density function based upon the work of *Longuet-Higgins* [1963], which used a Gram-Charlier series to describe the departure of the probability density function from the normal curve. After making several approximations, Jackson reached the result

$$\epsilon = -\lambda_{30}\mu_{20}^{1/2} \tag{1.7}$$

with

$$\lambda_{30} = \frac{\mu_{30}}{\mu_{20}^{3/2}} \tag{1.8}$$

$$\mu_{mn} = \langle \eta^m \eta_x^n \rangle \tag{1.9}$$

where η is the surface displacement and η_x is the surface slope. This result accurately showed the bias to depend upon wave height, but a strong correlation with the skewness λ_{30},

as indicated in equation (1.1), has not been found in any of the electromagnetic bias experiments.

Barrick and Lipa [1985] and *Srokosz* [1986] continued the use of specular point theory while improving the model used for the joint height-slope probability density function. They found, using the notation of *Barrick and Lipa* [1985], that

$$\epsilon = -\frac{\lambda_2}{8} H_{1/3} \tag{1.10}$$

with

$$\lambda_2 = \frac{\mu_{002}\mu_{120} + \mu_{020}\mu_{102} - 2\mu_{011}\mu_{111}}{\mu_{200}^{1/2}(\mu_{020}\mu_{002} - \mu_{011}^2)} \tag{1.11}$$

$$\mu_{mnp} = \langle \eta^m \eta_x^n \eta_y^p \rangle \tag{1.12}$$

where η_x and η_y are the surface slopes in the x and y directions respectively. Using a JONSWAP (Joint North Sea Wave Project) spectrum [Hasselmann et al., 1973], *Barrick and Lipa* [1985] computed the necessary moments to compute λ_2. A regression, power-law fit to their numerical results gave

$$\lambda_2 \approx 0.25 H_{1/3}^{-0.28}. \tag{1.13}$$

This result shows the bias to depend upon $(H_{1/3})^{0.72}$, but this correlation has not been found in any of the electromagnetic bias experiments.

During the electromagnetic bias measurements of *Melville et al.* [1990, 1991] a wire wave gauge was used to obtain the modulation of the high frequency waves by the low frequency waves. It became apparent that the electromagnetic bias was primarily caused by the modulation of the short waves. This was reported by *Arnold et al.* [1989, 1990, 1991]. Physical optics scattering and an empirical model of the short wave modulation were used to estimate the C and Ku band electromagnetic bias from wire wave gauge measurements made independently of the scatterometer measurements. This theory accurately showed the bias to depend upon wave height as the earlier theories, but most importantly it explained the wind speed dependence through a short-wave modulation parameter. This theory will be discussed in detail in chapter 3.

Recently, *Rodriguez et al.* [1992] performed a numerical investigation of the dependence of the electromagnetic bias on small (short) wave modulation and long wave tilting. Their results are summarized in figures 1.6-1.8. As seen in figures 1.6a and 1.6b, the electromagnetic bias is seen to depend on the wave height in agreement with earlier work.

Figures 1.6c and 1.6d show the wind speed dependence of the electromagnetic bias for a nonlinear surface and a Gaussian surface respectively. The nonlinear surface accounts for long

wave tilting. The results of figures 1.6d and 1.7 will be discussed in Chapter 3.

The large-scale surface slope variance as a function of height is shown in figure 1.8. This shows the tilt modulation increases with wind speed up to 10 m/s and then decreases. This causes the bias to increase with wind speed up to 10 m/s and then decrease, as shown in figure 1.6c. This is in qualitative agreement with the measurements of chapter 2, but with a much stronger roll off than measured.

An in-depth discussion of the 1989-1990 Gulf of Mexico electromagnetic bias experiment follows in chapter 2, and a detailed description of a theory explaining the electromagnetic bias in terms of the short wave modulation will be presented in chapter 3.

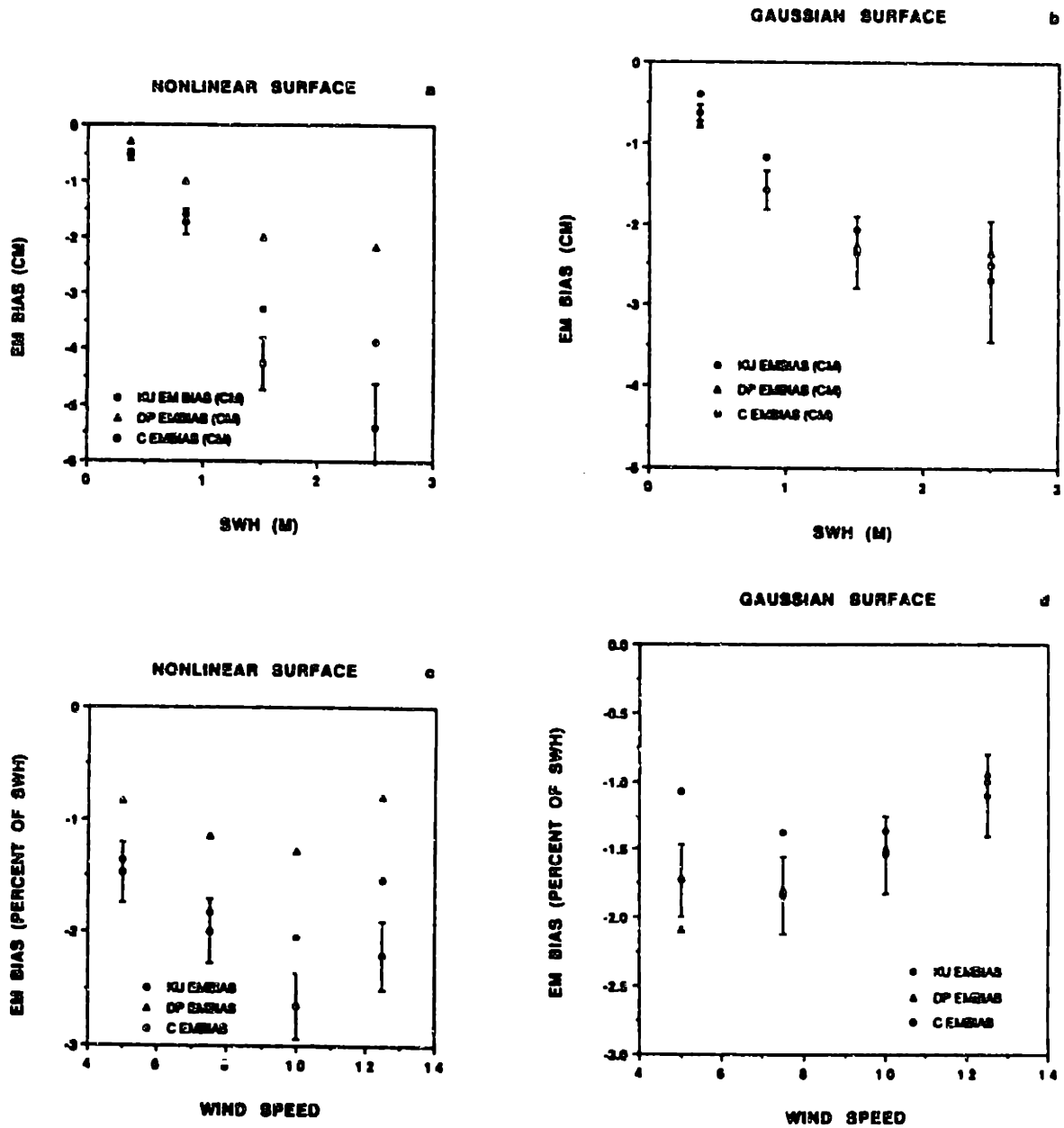

Figure 1.6: EM bias as a function of SWH for (a) modulated surfaces and (b) Gaussian surfaces (note the nearly linear dependence), and EM bias divided by SWH as a function of wind speed for (c) modulated and (d) Gaussian surfaces. Notice that this residual bias also increases with both increasing wind speed and electromagnetic wavelength. (Figure 9 from *Rodriguez et al.* [1992].)

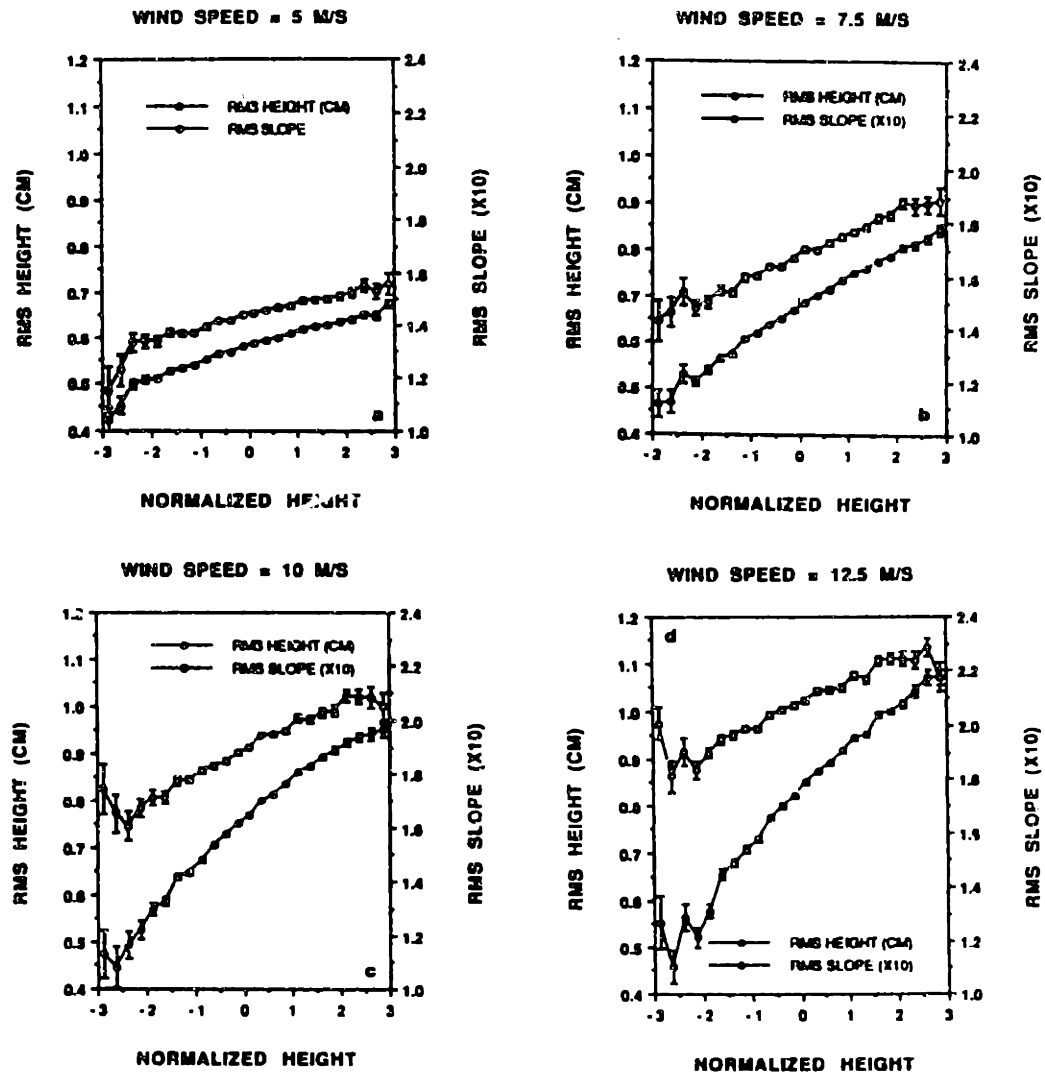

Figure 1.7: Modulation of small scale surface height and slope for wind speeds of (a) 5 m/s, (b) 7.5 m/s, (c) 10 m/s, and (d) 12.5 m/s from the Monte Carlo simulation. The error bars show the standard deviation of the simulation results about the reported means. Notice the almost linear dependence with normalized surface height, defined as height above mean sea level divided by the surface height standard deviation. (Figure 4 from *Rodriguez et al.* [1992].)

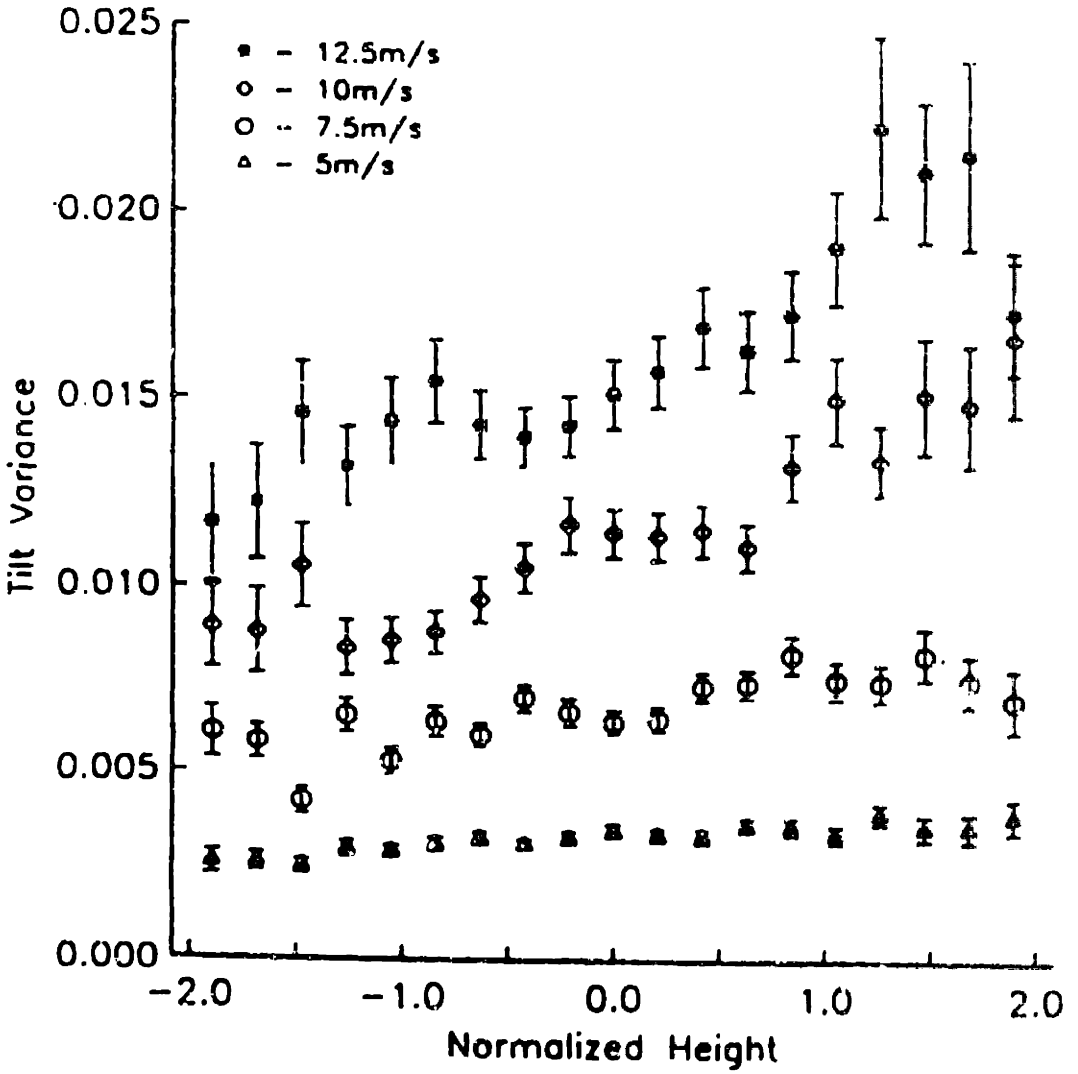

Figure 1.8: Large-scale surface tilt variance modulation as a function of wind speed obtained from the Monte Carlo simulation. The error bars show the standard deviation of the simulation results about the reported means. Notice increased modulation with increased wind speed. (Figure 3 from *Rodriguez et al.* [1992].)

Chapter 2

Gulf of Mexico Experiment

Direct measurements of the electromagnetic bias were made from the Shell Offshore oil production platform complex Brazos 19 in the Gulf of Mexico for a six month period from December 1, 1989 to May 31, 1990. The platform complex is located south of Houston, Texas at 28° 10' N and 95° 35' W. The closest land is 58 km to the north of the platform complex, and the platform is in water 40 m deep. The platform complex consists of three platforms connected by two bridges forming an L shape (see figures 2.1, 2.2 and 2.3). Each platform was rectangular in shape with dimensions of 20 m by 50 m. The bridge connecting platforms B and C was 60 m in length and the bridge connecting platforms B and D was 50 m in length.

2.1 DESCRIPTION OF EXPERIMENT AND DATA PROCESSING

2.1.1 INSTRUMENTATION

Nadir looking, 5 GHz and 14 GHz continous wave scatterometers (see figure 2.4), designed and built at the U.S. Naval Research Laboratory, were mounted 18 m above mean sea level at the center of the 60 m bridge connecting platforms B and C.

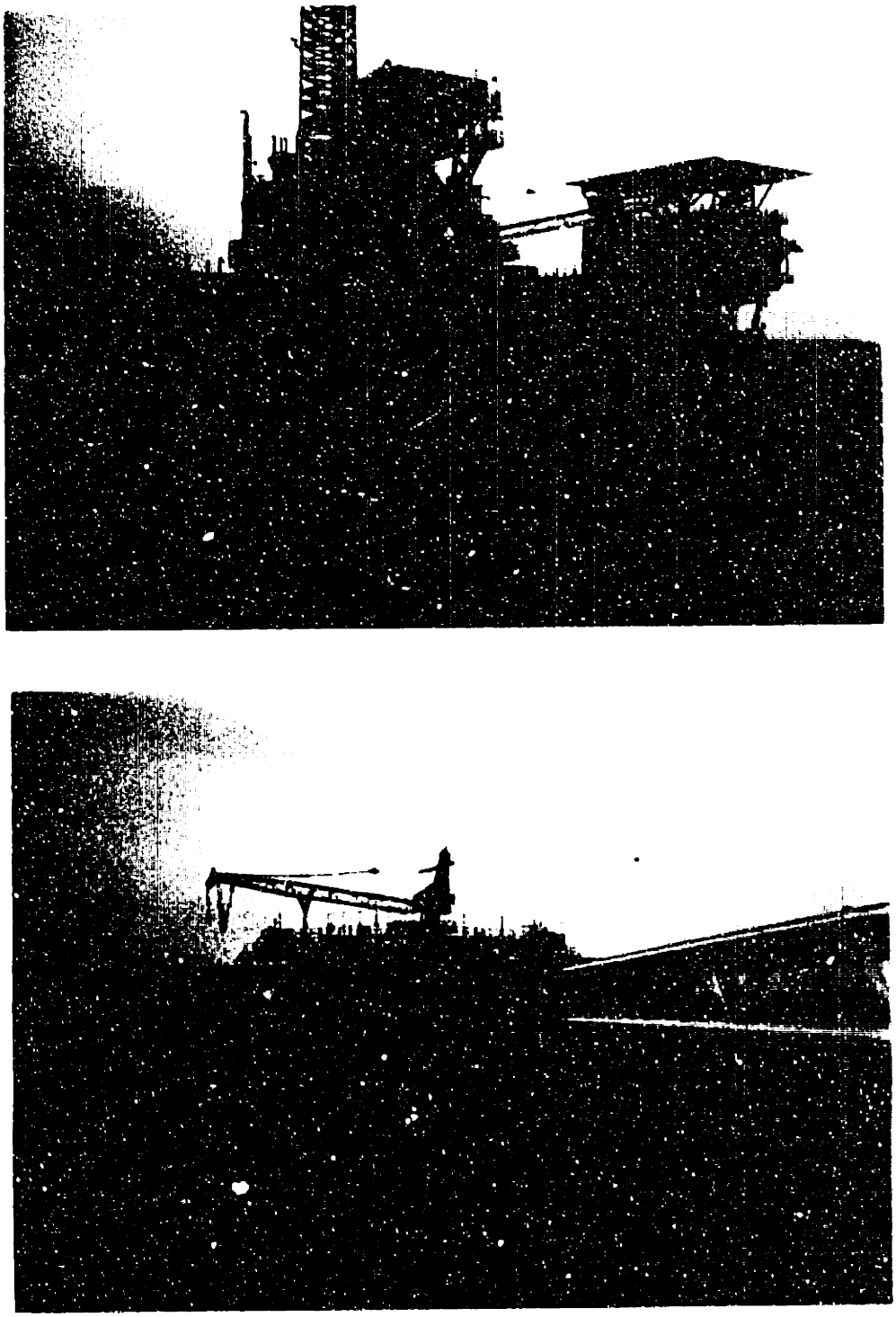

Figure 2.1: Shell Offshore oil production platform complex Brazos 19, top: platform C, bottom: platform B.

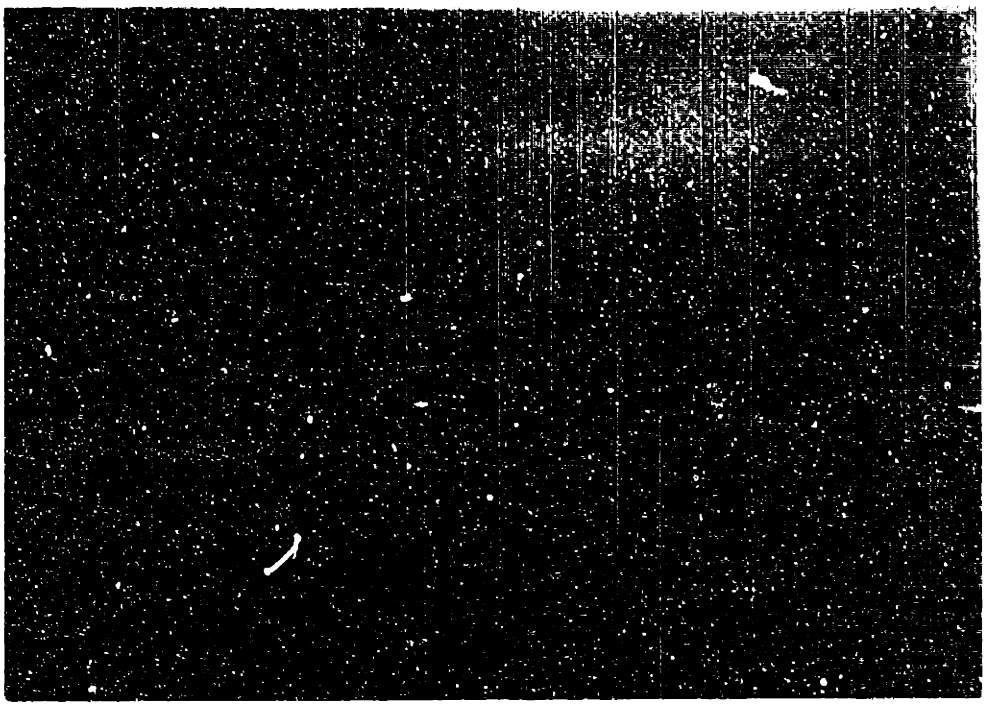

Figure 2.2: Shell Offshore oil production platform complex Brazos 19, platform D.

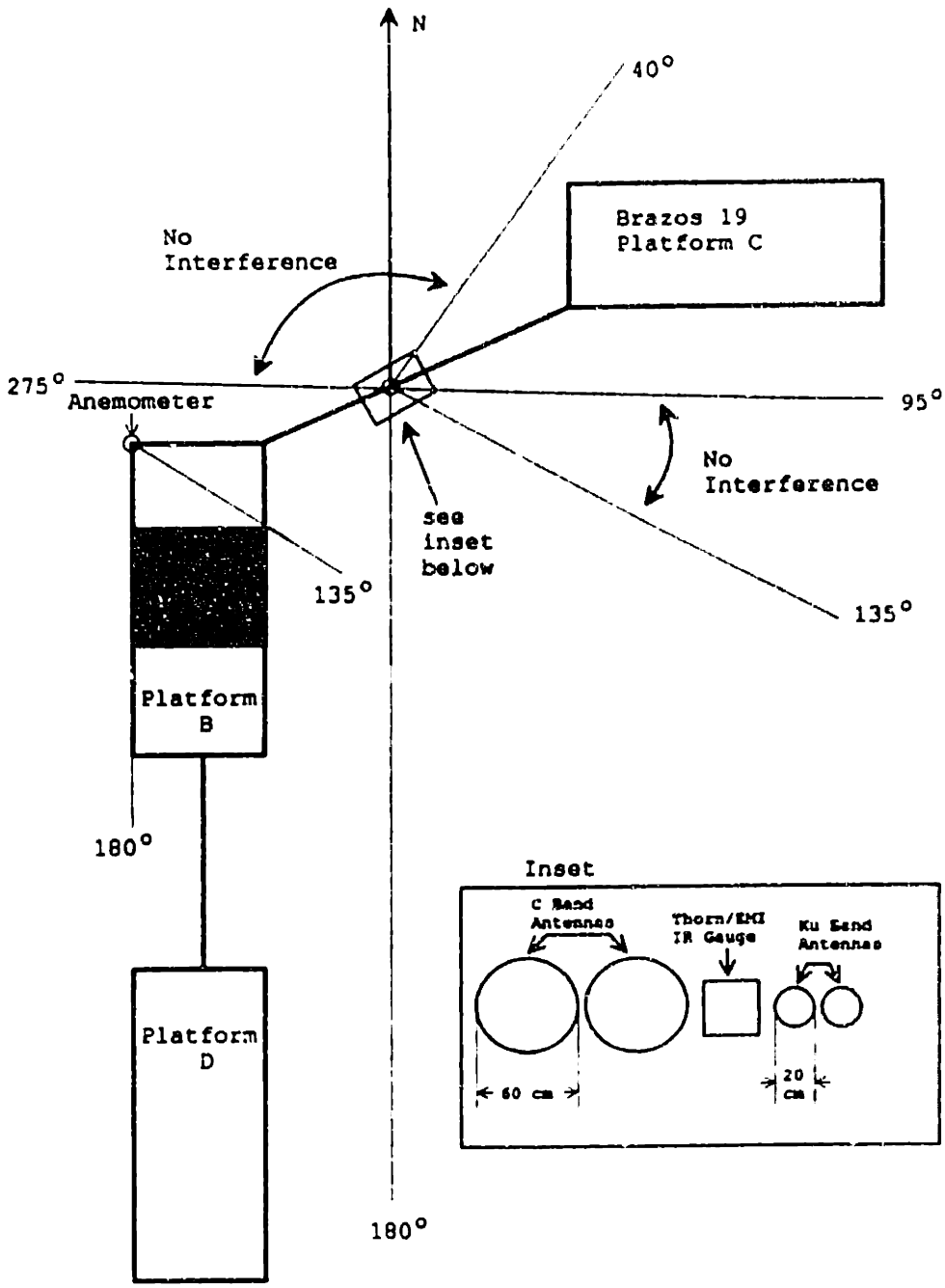

Figure 2.3: Layout of Brazos 19 platform complex. The platforms are 20 m by 50 m. The bridge between platforms B and C is 60 m in length, and the bridge between platforms B and D is 50 m in length. The scatterometers were placed in the middle of the bridge between platforms B and C. The layout of the scatterometers is shown in the inset. The platform caused interference with the wave field for directions between 40° and 95° and between 180° and 275°. Structures on platform B caused interference with the wind measurement for directions between 135° and 180°.

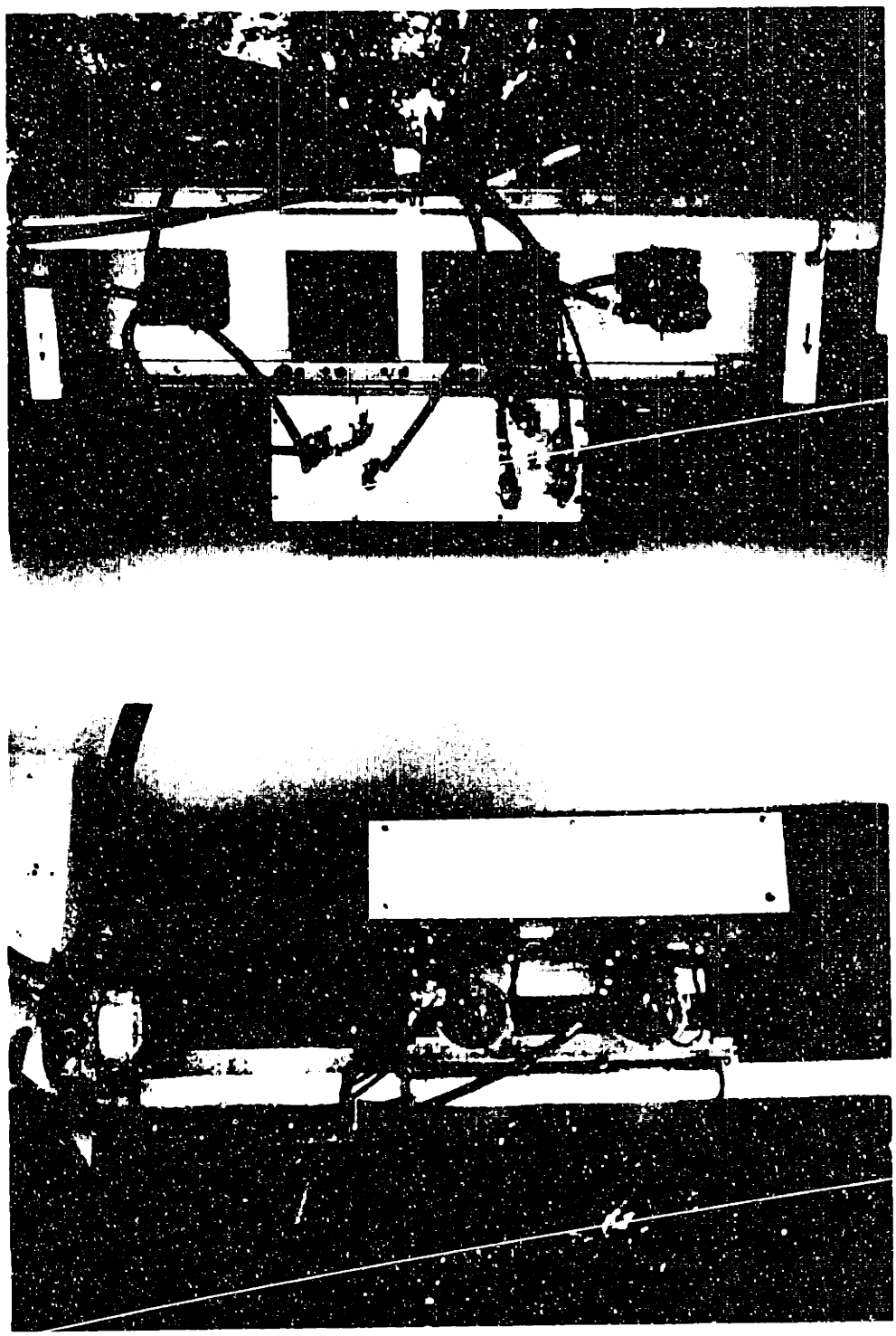

Figure 2.4: Top: C band scatterometer, bottom: Ku band scatterometer and the Thorn/EMI infrared wave gauge.

The scatterometers transmit and measure the power reflected from the ocean surface. While the scatterometers do not measure the range to the surface directly, they can infer the wave displacement from the Doppler of the return signal, as will be demonstrated later. The 5 GHz scatterometer antennas had a two-way 3 dB beam width of 4.5°, corresponding to a 1.4 m diameter foot print. The 14 GHz scatterometer antennas had a two-way 3 dB beam width of 5.0°, corresponding to a 1.6 m diameter foot print. A Thorn/EMI infrared wave gauge with a beam width of 1°, corresponding to a 0.3 m diameter foot print, was placed between the two scatterometers where its foot print would lie within the foot prints of the scatterometers. An 8 m capacitance wire wave gauge was suspended from the bridge during one week intensive experiment periods. The wire gauge was positioned so as to be outside the scatterometer beams. The wire wave gauge was calibrated in situ.

Wind speed and direction, air temperature, water temperature, rain fall and relative humidity were measured using an R. M. Young meteorological package. The wind speed and direction and rain fall were measured at the northwest corner of platform B at a height of 25 m above mean sea level. The air temperature and relative humidity were measured at the southwest corner of platform B at a height of 19 m above mean

sea level. The water temperature was measured at the south end of platform B at a water depth of 1 m. Unfortunately, the relative humidity and water temperature measurements were valid for only a small portion of the experiment.

Without the relative humidity and water temperature measurements, it was not possible to accurately translate the wind speed at 25 m to the reference 10 m height. Therefore, wind speed at 25 m will be used in the analysis of the data. Assuming the mean wind velocity profile is logarithmic and the drag coefficient based on the velocity at 10m is on the order of 10^{-3}, then winds at 25 m are about 10% larger than winds at 10 m for a neutral atmosphere.

2.1.2 DATA PROCESSING

A digital data acquisition system was used to sample the scatterometer IF (intermediate frequency) signals at 2 KHz, the wind speed, wind direction and wave gauges at 8 Hz and the other environmental measurements once every ten minutes. The received power and mean Doppler frequency were computed with an integration time of 0.125 s. The mean Doppler frequency was estimated using a time domain covariance processing technique commonly used in weather radar [*Doviak and Zrnic,* 1984]. This technique was also used by *Jessup et al.* [1991] for measuring the Doppler frequency mean and bandwidth for

their breaking wave studies (see also *Jessup* [1990]). The data were stored in 10 minute records on optical disks. The mean power and mean doppler frequency for each scatterometer and the wave gauge signals were stored at an 8 Hz rate. Averages of the wind speed and wind direction for the 10 minute interval and the other environmental measurements were stored once every 10 minutes.

The back scattered power changes with range as r^{-4}, but since the illuminated foot print changes as r^2, the net change in the back scattered power with range is r^{-2}. The back scatter coefficient is given by

$$\sigma^o = \frac{K(z_o - \eta)^2}{z_o^2} \sigma_m^o \qquad (2.1)$$

where z_o = 18 m is the height above mean sea level, η is the surface displacement, K is a calibration constant for each scatterometer and σ_m° is the measured back scattered power[1].

The electromagnetic bias was calculated from the measured back scatter coefficient and the measured sea surface displacement

---

[1]It should be noted that there was a typographical error in the first equation on page 4918 of *Melville et al.* [1991]. The equation should read

$$\sigma_o = [K(z_o - \zeta)^2/z_o^2]\,\sigma_m.$$

as

$$\epsilon = \frac{\Sigma \sigma^o \eta}{\Sigma \sigma^o}. \qquad (2.2)$$

Unfortunately, the Thorn/EMI infrared wave gauge was operational during the month of February only. This necessitated an alternate method for measuring the sea surface displacement during the remaining five months of the experiment. Beginning with the assumption that the mean Doppler frequency of the scatterometer is proportional to the vertical velocity of the long ocean waves, the mean Doppler frequency was integrated in time, providing an estimate of the sea surface displacement. A calibration of the estimated displacement was obtained by comparing it to the wave displacement measured with the Thorn/EMI infrared wave gauge during the month of February.

Hourly averages of the electromagnetic bias, significant wave height, wind speed, wind direction and the other environmental measurements were computed from the 10 minute data records.

2.1.3 DATA EDITING

The six months of data were first edited by hand to remove data for known periods of instrument malfunction and obvious spurious data points caused by glitches and other unknown

factors, which invariably occur in an experiment of this length. Next, data contaminated by interference from the platform on the wind and waves were removed.

Interference occurred when the waves travelled through the platform structure. The directions corresponding to the platform interference were between 40° and 95° for platform C and between 180° and 275° for platforms B and D (see figure 2.3). Also, there was interference with the wind speed measurement for directions between 135° and 180° due to blockage from structures on platform B (see figure 2.3). This left two angular regions 95° to 135° and 275° to 40° where the waves and wind were unaffected by the platform structure. Since no measurement of the wave direction was made, the wave direction was assumed to be given by the wind direction for the purpose of removing the platform interference.

2.2 RESULTS

2.2.1 DATA FROM MONTH OF FEBRUARY

The experimental data from the month of February 1990 will be analyzed first because the Thorn/EMI infrared wave gauge was operating during this month. In February 1990 the significant wave height varied from 0.7 m to 2.3 m, the wind speed varied from 0.5 m/s to 14.2 m/s, the Ku bias varied from -1.2 cm to -10.7 cm or from -1.6% to -5.0% of the significant wave

height, and the C bias varied from -1.0 cm to -12.0 cm or from -1.4% to -5.7% of the significant wave height (see Table 1). A total of 186 hours of usable data were collected.

Variable	Minimum	Maximum	Mean	Stdv
$H_{1/3}$ (m)	0.65	2.28	1.41	0.39
U_{25} (m/s)	0.5	14.2	6.8	2.8
ϵ_C (cm)	-0.9	-12.0	-5.2	2.5
β_C (%$H_{1/3}$)	-1.44	-5.67	-3.52	0.98
ϵ_{Ku} (cm)	-1.2	-10.7	-5.2	2.1
β_{Ku} (%$H_{1/3}$)	-1.59	-5.03	-3.58	0.71

Table 1 - Summary for month of February

The February data were used to find the empirical relationships between the electromagnetic bias ϵ, the significant wave height $H_{1/3}$, and the wind speed U_{25}. The relationships between the bias and the significant wave height for Ku and C bands are shown in figures 2.5 and 2.6 respectively. The linear correlation of the biases and the significant wave height were found to be

$$\epsilon_{Ku}(cm) = 1.86 - 5.02\ H_{1/3}(m) \qquad r^2 = 0.859 \qquad (2.3)$$

$$\epsilon_{c}(cm) = 2.82 - 5.70\ H_{1/3}(m) \qquad r^2 = 0.797. \qquad (2.4)$$

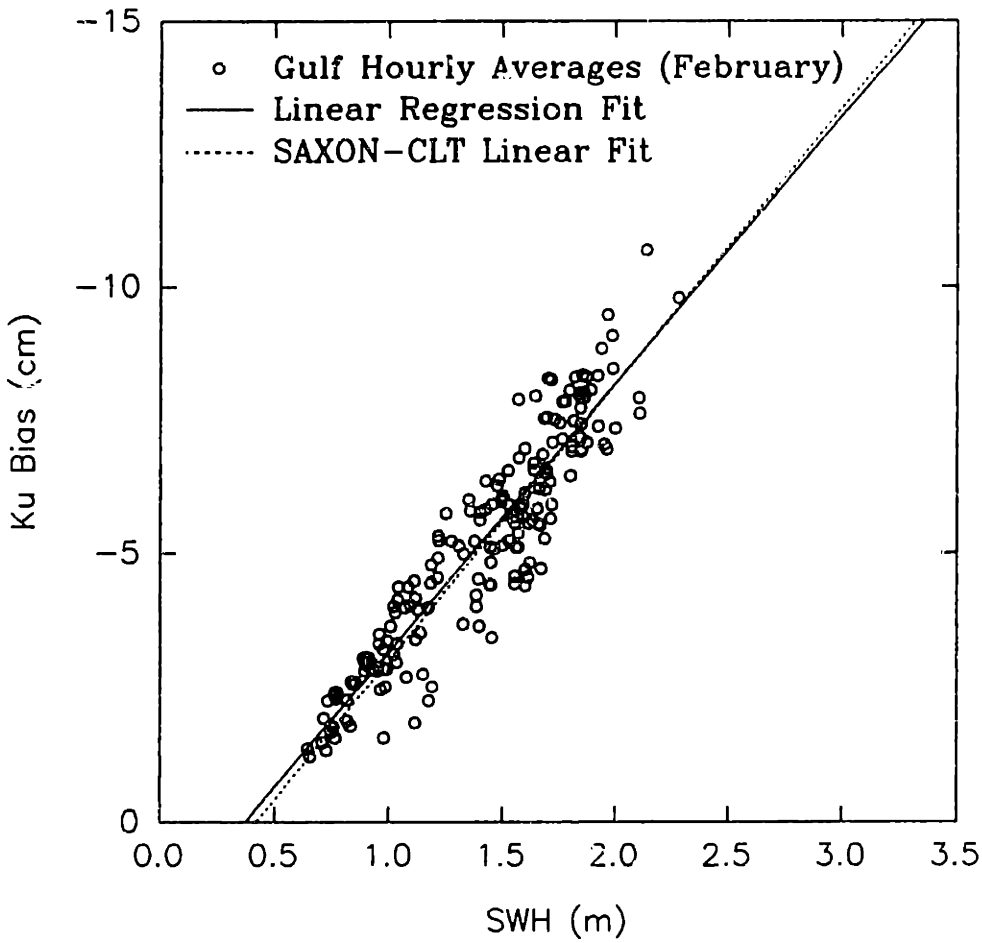

Figure 2.5: Ku band electromagnetic bias as a function of significant wave height for the month of February. The solid line is the linear regression fit ϵ_{Ku}(cm) = 1.86 - 5.02$H_{1/3}$(m) (r^2 = 0.859). The dashed line is the linear regression fit to the data of *Melville et al.* [1991] given by ϵ_{Ku}(cm) = 2.16 - 5.17$H_{1/3}$(m) (r^2 =0.873).

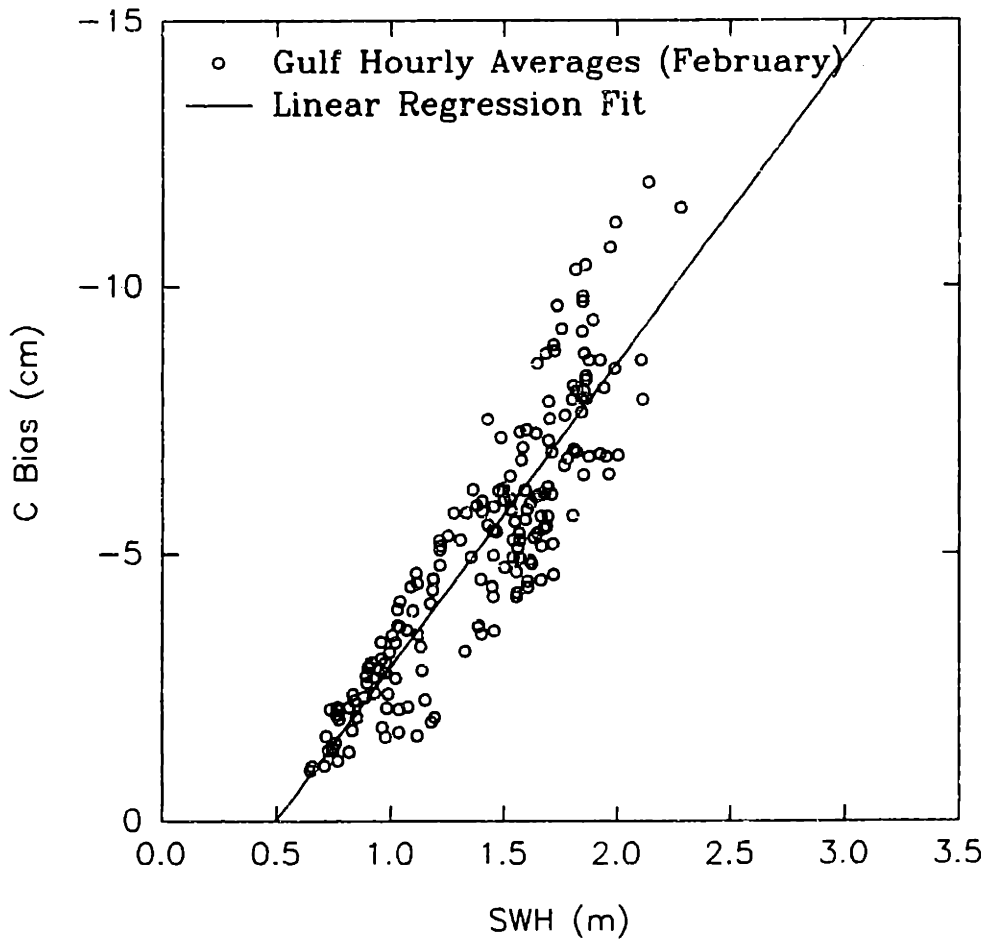

Figure 2.6: C band electromagnetic bias as a function of significant wave height for the month of February. The solid line is the linear regression fit given by $\epsilon_c(\text{cm}) = 2.82 - 5.70 H_{1/3}(\text{m})$ ($r^2 = 0.797$).

The correlation of Ku bias and significant wave height, found as part of the SAXON-CLT experiment by *Melville et al.* [1991][2], was

$$\epsilon_{Ku}(cm) = 2.16 - 5.17\, H_{1/3}(m) \qquad r^2 = 0.873. \quad (2.5)$$

The linear regressions of equations (2.3) and (2.5) are shown as solid and dashed lines respectively in figure 2.5. Both experiments exhibit the same correlation between the Ku bias and the significant wave height.

Because of the strong correlation between the bias and the significant wave height, the dimensionless bias, $\beta = \epsilon / H_{1/3}$, is used in the following analysis. The mean value of β_{Ku} was -3.6% with a standard deviation of 0.7%. The mean value of β_c was -3.5% with a standard deviation of 1.0%. For SAXON-CLT [*Melville et al.*, 1991] the mean value of β_{Ku} was -3.5% with a standard deviation of 1%.

The relationships between β and the wind speed for Ku and C bands are shown in figures 2.7 and 2.8 respectively. The linear correlations between β and the wind speed were found to

---

[2]It should be noted that there was a typographical error in the caption of figure 5 of *Melville et al.* [1991]. The linear and quadratic fits should be

$$B = 0.0216 - 0.0517 H_{1/3}$$
$$B = 0.001 - 0.0210 H_{1/3} - 0.0104 (H_{1/3})^2.$$

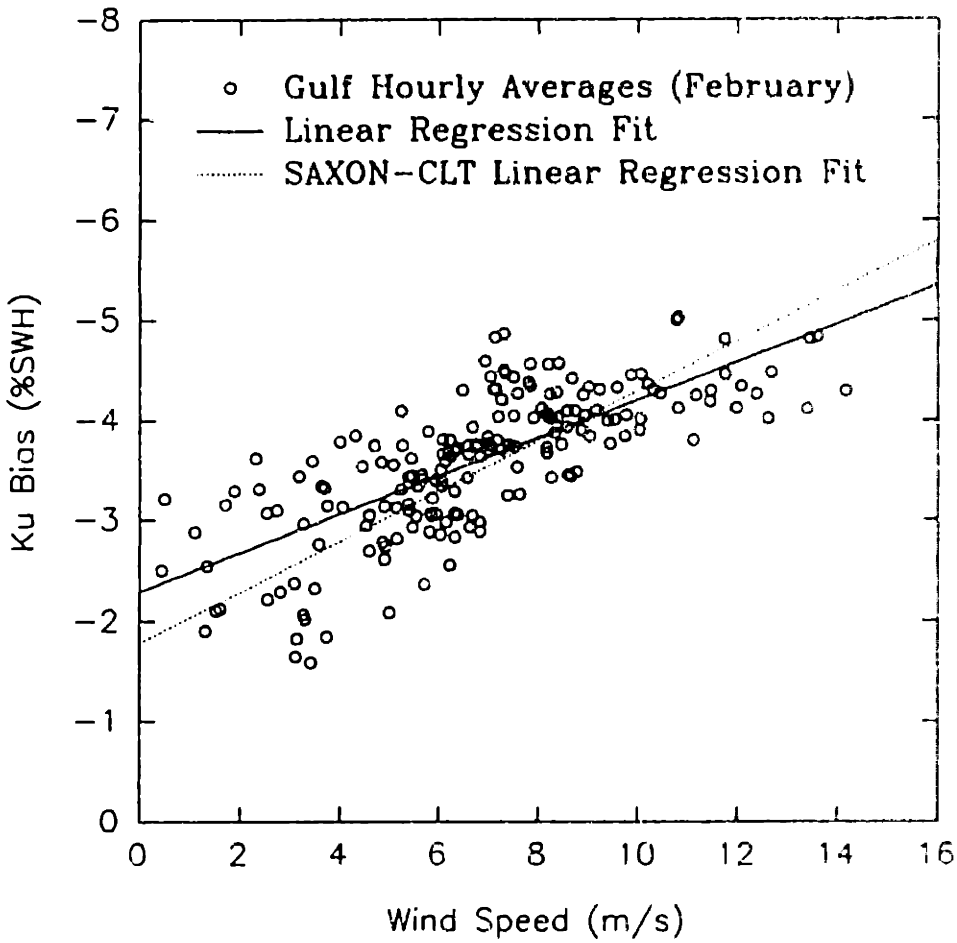

Figure 2.7: Normalized Ku band electromagnetic bias as a function of wind speed at 25 m above the sea surface for the month of February. The solid line is the linear regression fit $\beta_{Ku}(\%SWH) = -2.30 - 0.190U_{25}(m/s)$ ($r^2 = 0.545$). The dashed line is the linear regression fit to the data of *Melville et al.* [1991] given by $\beta_{Ku}(\%SWH) = -1.79 - 0.25U_{10}(m/s)$ ($r^2 = 0.707$).

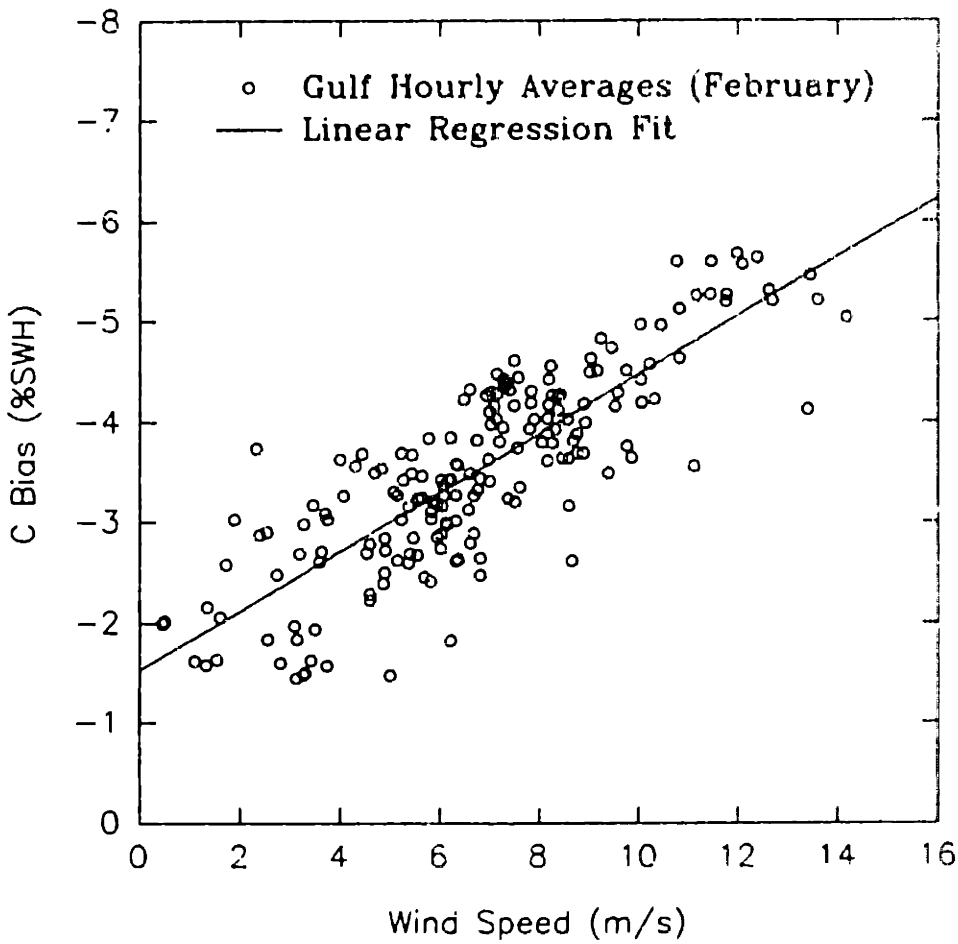

Figure 2.8: Normalized C band electromagnetic bias as a function of wind speed at 25 m above the sea surface for the month of February. The solid line is the linear regression fit $\beta_c(\%SWH) = -1.53 - 0.294U_{25}(m/s)$ ($r^2 = 0.689$).

be

$$\beta_{Ku}(\%H_{1/3}) = -2.30 - 0.190\ U_{25}(m/s) \qquad r^2 = 0.545 \quad (2.6)$$

$$\beta_{c}(\%H_{1/3}) = -1.53 - 0.294\ U_{25}(m/s) \qquad r^2 = 0.689. \quad (2.7)$$

The correlation of β_{Ku} and the wind speed for SAXON-CLT [*Melville et al.*, 1991] was

$$\beta_{Ku}(\%H_{1/3}) = -1.79 - 0.25\ U_{10}(m/s) \qquad r^2 = 0.707. \quad (2.8)$$

The linear regressions of equations (2.6) and (2.8) are shown as solid and dashed lines respectively in figure 2.7. The difference between these two linear regressions can be attributed to the lower bias at wind speeds greater than 10 m/s for the present experiment as compared to the SAXON-CLT experiment.

The residual bias, after removing the correlation of β with the wind speed, had a standard deviation of 0.48% and 0.55% of significant wave height respectively for Ku and C bands. The residual bias for SAXON-CLT, after removing the correlation of β with the wind speed, had a standard deviation of 0.51%. Both the present experiment and SAXON-CLT experiment had the

same residual bias. The difference between the correlation coefficients of equations (2.6) and (2.8) is a result of the variability of β_{Ku} of the present experiment (0.7%) being less than the variability of β_{Ku} for SAXON-CLT (1.0%), since the variability of the residuals in both experiments is the same. The lower variability of β_{Ku} for the present experiment is a result of the lower bias at wind speeds greater than 10 m/s.

The Ku and C band biases are compared in figure 2.9. For low values of bias, the Ku bias is about 0.8% of significant wave height larger than the C bias. For high values of bias the C bias is about 1% of significant wave height larger than the Ku bias. Since the bias is a function of wind speed, this result can also be stated in terms of wind speed. For wind speeds less than 10 m/s the C bias is less than the Ku bias, but for wind speeds greater than 10 m/s, the C bias is larger than the Ku bias.

To provide some indication that the data were properly edited in regards to wind direction, figure 2.10 shows the difference between the measured β_c and equation (2.7) as a function of wind direction. The hatched angular regions were removed from the data set. Based on *Melville et al.* [1991] and equations (2.6) and (2.7), a residual β standard deviation of 0.5% of SWH, corresponding to a ±1% variability, is expected. An

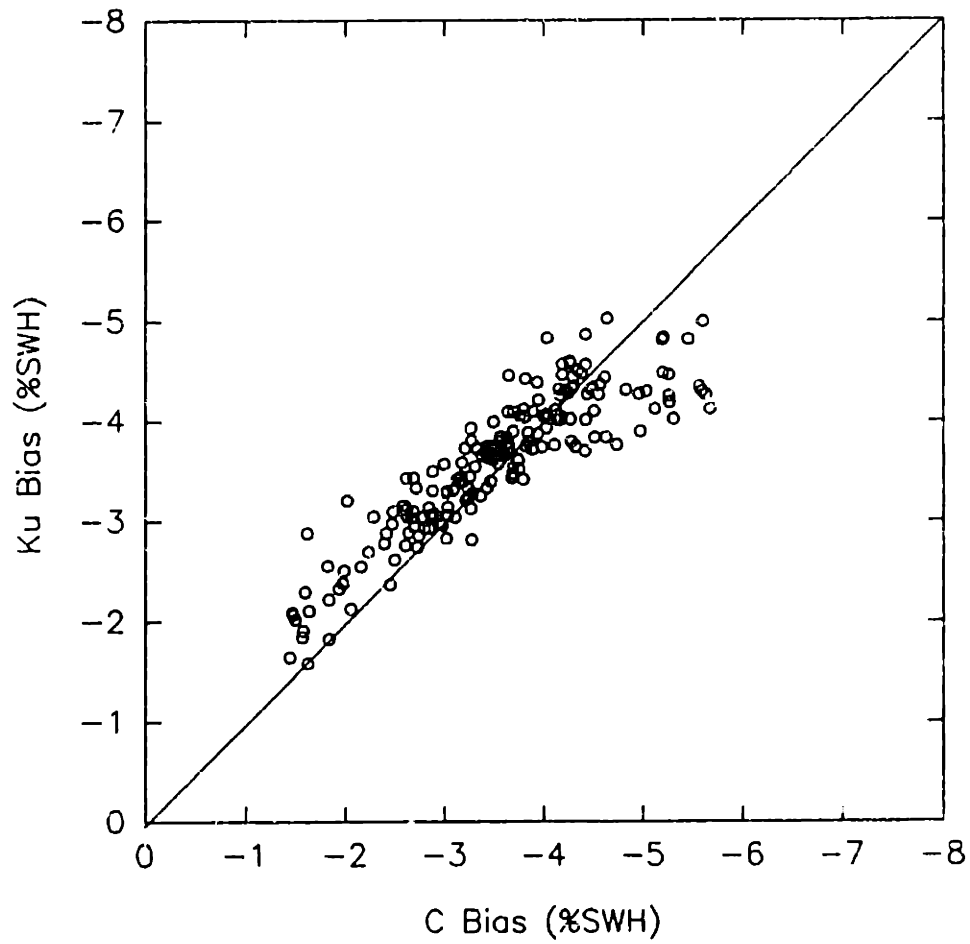

Figure 2.9: Normalized Ku band electromagnetic bias compared to the normalized C band electromagnetic bias for the month of February.

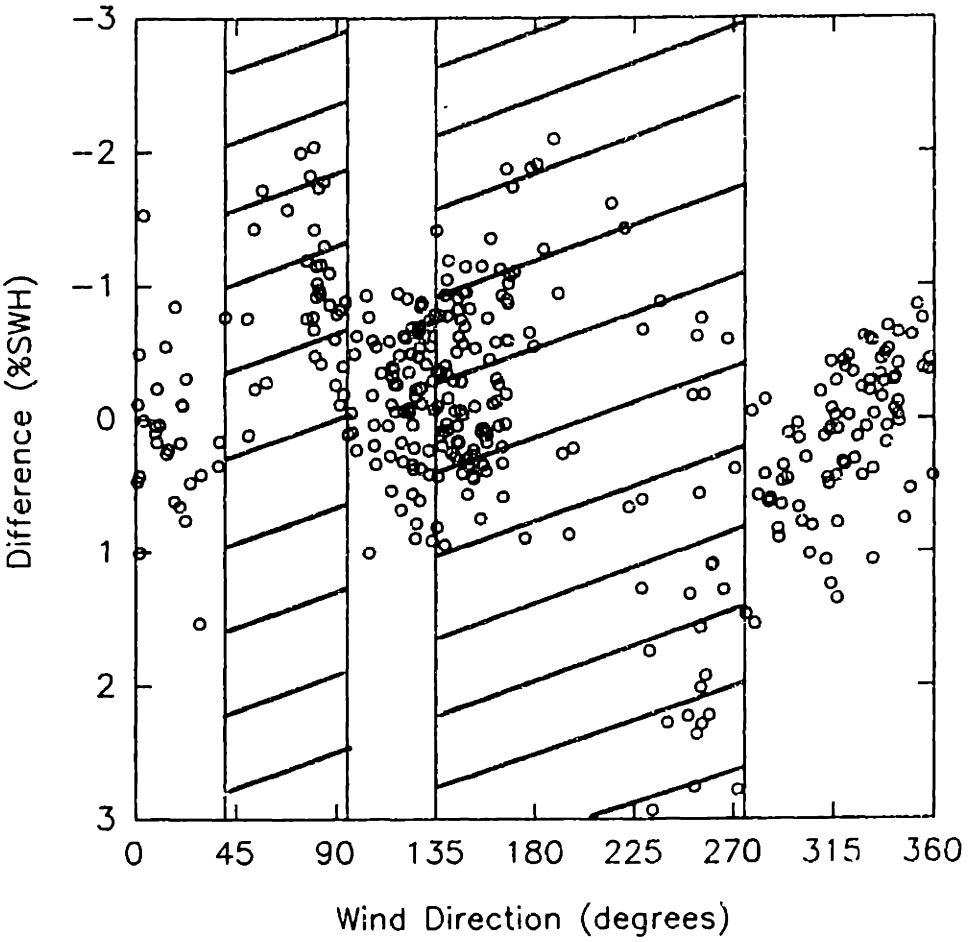

Figure 2.10: Difference between the measured normalized C band electromagnetic bias and equation (2.7) as a function of wind direction. The hatched angular regions were removed from the data set due to interference from the platform.

examination of figure 2.10 shows the variability in the usable regions to be ±1% and the variability in the removed regions to be ±2%. This indicates that the regions of interference were correctly identified.

2.2.2 ESTIMATED WAVE DISPLACEMENT FROM DOPPLER

Since the Thorn/EMI infrared wave gauge was operational during only one month of the experiment, it would be desirable to use the integrated radar Doppler as a measure of the surface wave displacement. Beginning with the assumption that the mean Doppler frequency of the scatterometer is proportional to the vertical velocity of the long ocean waves, the mean Doppler frequency was integrated in time, providing an estimate of the sea surface displacement. Figure 2.11 shows a time series comparison of the surface displacement measured with the Thorn/EMI infrared wave gauge and the C and Ku band integrated Doppler. Figure 2.12 shows a comparison of the significant wave height measured with the Thorn/EMI infrared wave gauge during the month of February as compared to the significant wave height estimated from the scatterometer Doppler. It should be noted that wave heights less than 0.5 m were not used because the wave height estimated from the scatterometer Doppler was grossly in error for small wave heights. Also, since using the Ku Doppler to estimate the wave displacement was slightly better than using the C Doppler, the Ku Doppler

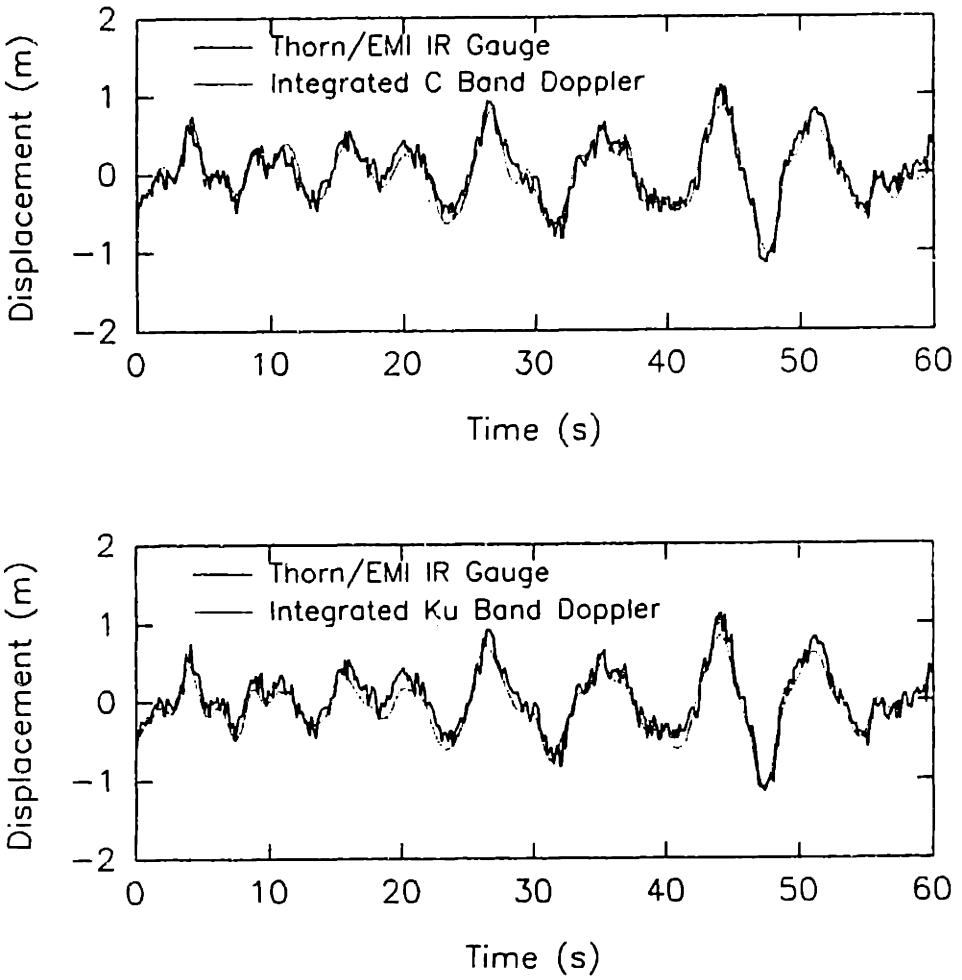

Figure 2.11: Wave displacement measured using the Thorn/EMI infrared wave gauge compared to the wave displacement measured using the integrated scatterometer Doppler.

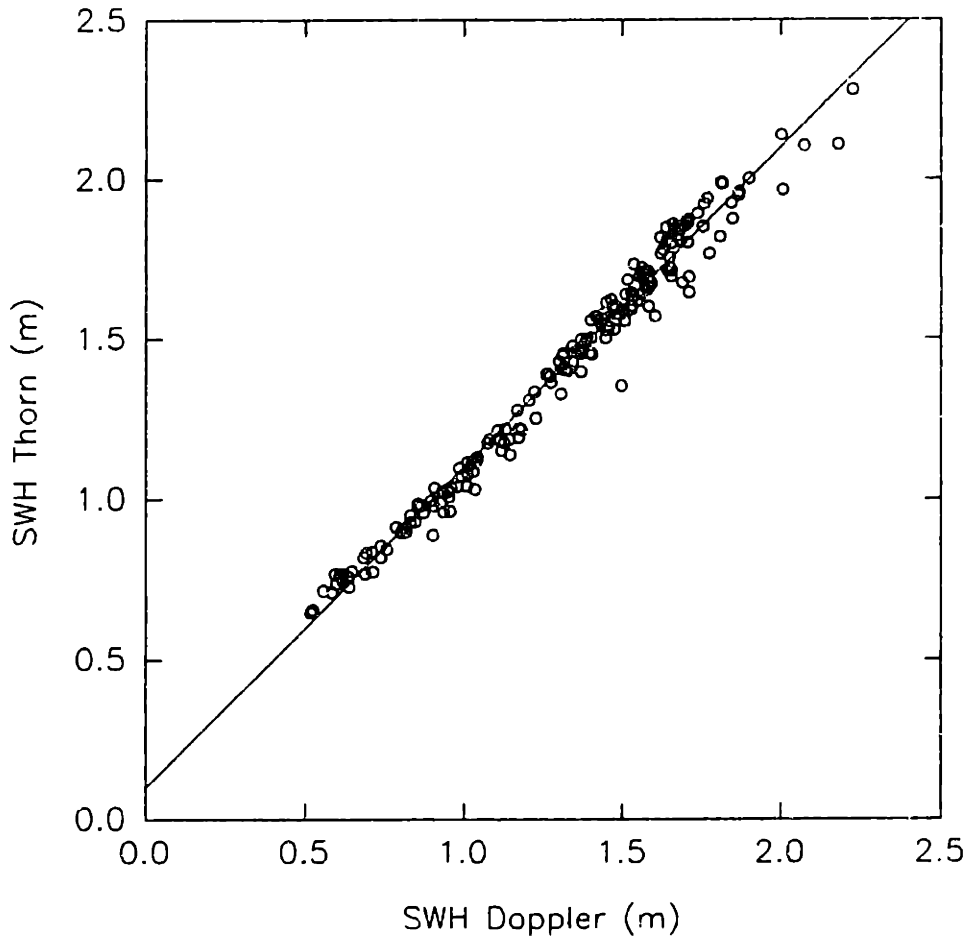

Figure 2.12: Significant wave height measured using the Thorn/EMI infrared wave gauge compared to the significant wave height measured using the integrated scatterometer Doppler. The solid line is $(H_{1/3})_{\text{Thorn}} = 0.1\text{m} + (H_{1/3})_{\text{Doppler}}$.

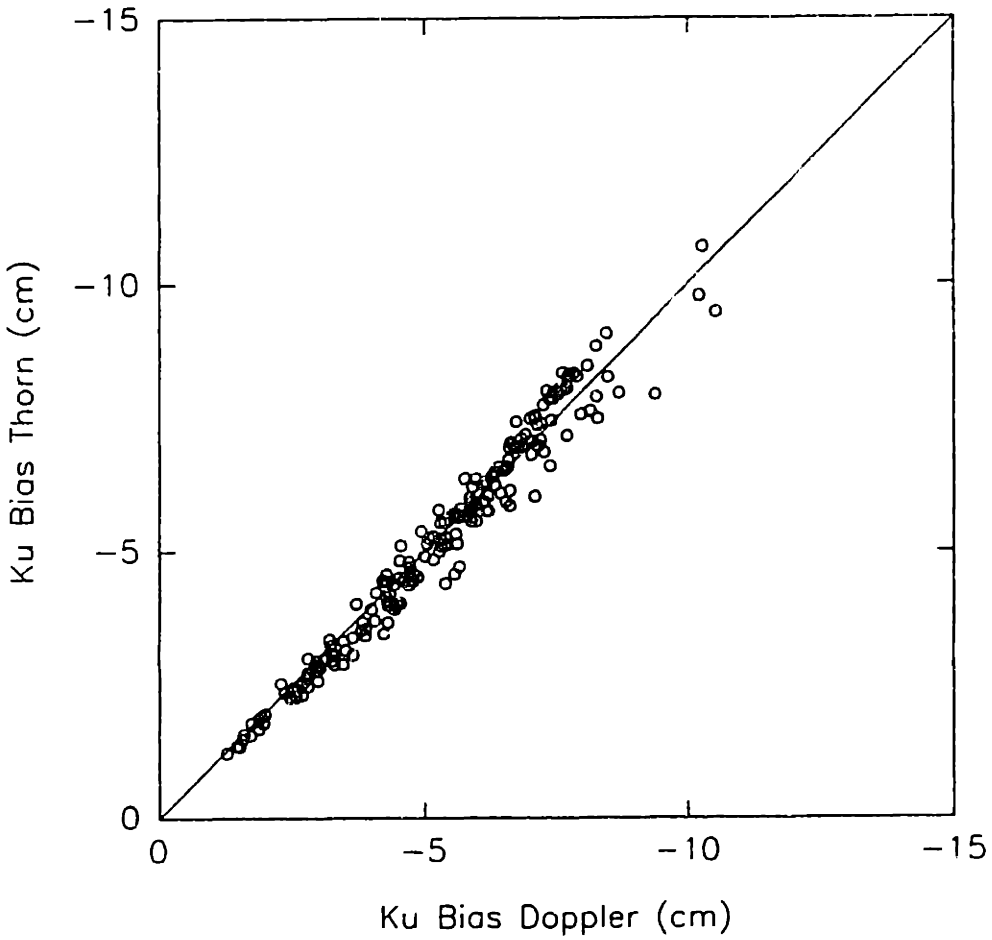

Figure 2.13: Ku band electromagnetic bias measured using the Thorn/EMI infrared wave gauge compared to the Ku band electromagnetic bias measured using the integrated scatterometer Doppler. The solid line is $(\epsilon_{Ku})_{Thorn} = (\epsilon_{Ku})_{Doppler}$.

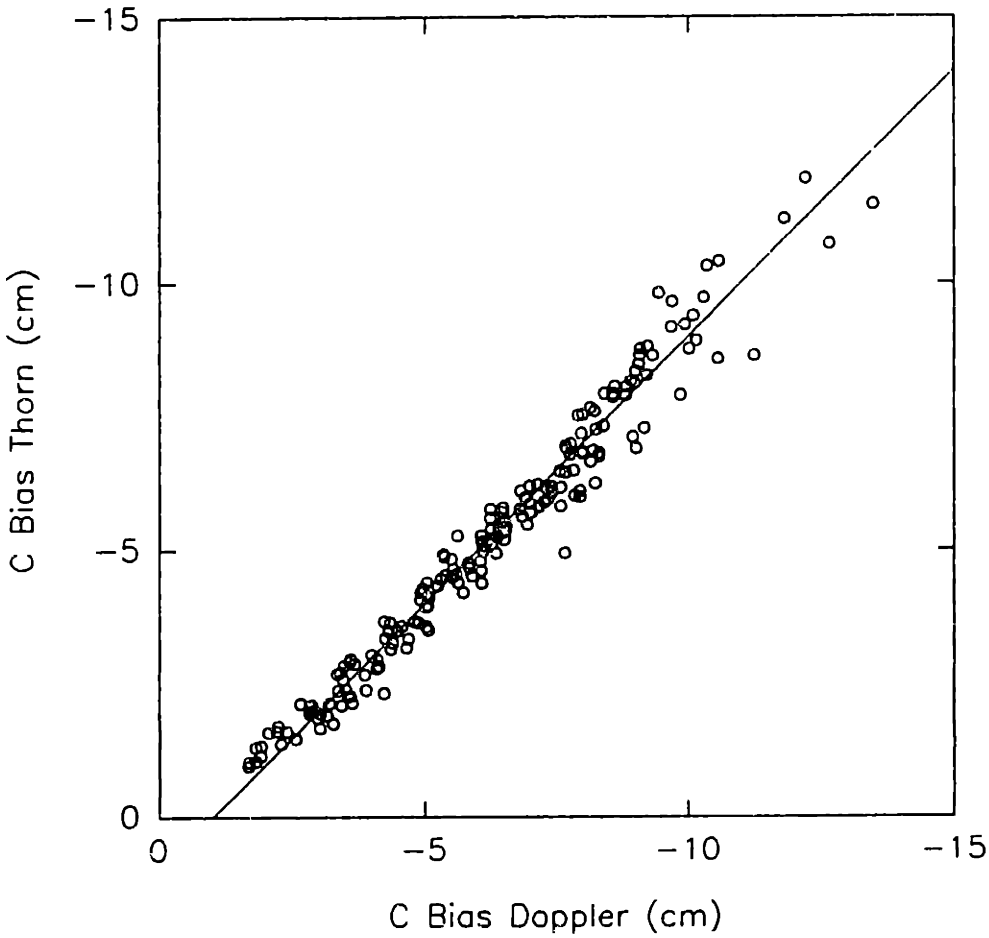

Figure 2.14: C band electromagnetic bias measured using the Thorn/EMI infrared wave gauge compared to the C band electromagnetic bias measured using the integrated scatterometer Doppler. The solid line is $(\epsilon_c)_{Thorn} = 1cm + (\epsilon_c)_{Doppler}$.

was used.

As seen in figure 2.12, there is a linear relationship between the SWH measured with the Thorn/EMI infrared wave gauge and the SWH estimated from the scatterometer Doppler, given by

$$(H_{1/3})_{Thorn} = 0.1m + (H_{1/3})_{Doppler}. \qquad (2.9)$$

The SWH estimated from the scatterometer Doppler is a constant 10 cm less than the SWH measured with the Thorn/EMI wave gauge. This difference is due to the integrated scatterometer Doppler underestimating the wave displacement at the wave troughs and crests, where the vertical velocity of the long waves and the corresponding Doppler is near zero.

The biases computed using the estimated surface displacement from the scatterometer Doppler are compared to the bias computed using the Thorn/EMI wave gauge measured surface displacement in figures 2.13 and 2.14. As seen in figures 2.13 and 2.14, there is no difference between the biases computed using the Thorn/EMI wave gauge and the scatterometer Doppler for Ku band, but the C band bias computed using the scatterometer Doppler is a constant 1 cm larger than the bias computed with the Thorn/EMI wave gauge. The reason for this difference is not known. The correspondence between the biases computed using the Thorn/EMI wave gauge and the

scatterometer Doppler are given as

$$(\epsilon_{Ku})_{Thorn} = (\epsilon_{Ku})_{Doppler} \tag{2.10}$$

$$(\epsilon_{c})_{Thorn} = 1cm + (\epsilon_{c})_{Doppler}. \tag{2.11}$$

Using the Thorn/EMI wave gauge displacement as the standard, the biases and SWH computed using the scatterometer Doppler were adjusted according to equations (2.9), (2.10) and (2.11). Figure 2.15 shows the dimensionless bias β, measured using the Thorn/EMI wave gauge, compared to the adjusted dimensionless bias, measured using the scatterometer Doppler. The standard deviation of the error between the adjusted bias and the bias computed using the Thorn/EMI wave gauge was 0.233% of SWH for C band and 0.201% of SWH for Ku band. Figure 2.15 indicates that the adjusted C band bias underestimates the bias for small values of bias.

2.2.3 DATA FROM ENTIRE SIX MONTHS OF EXPERIMENT

The experimental data from the entire six months of the experiment will now be analyzed using the adjusted bias, computed using the integrated scatterometer Doppler for the wave displacement. During the six months of the experiment, the significant wave height varied from 0.6 m to 3.2 m, the wind speed varied from 0.1 m/s to 14.3 m/s, the Ku bias varied from -1.0 cm to -13.8 cm or from -1.6% to -5.3% of the

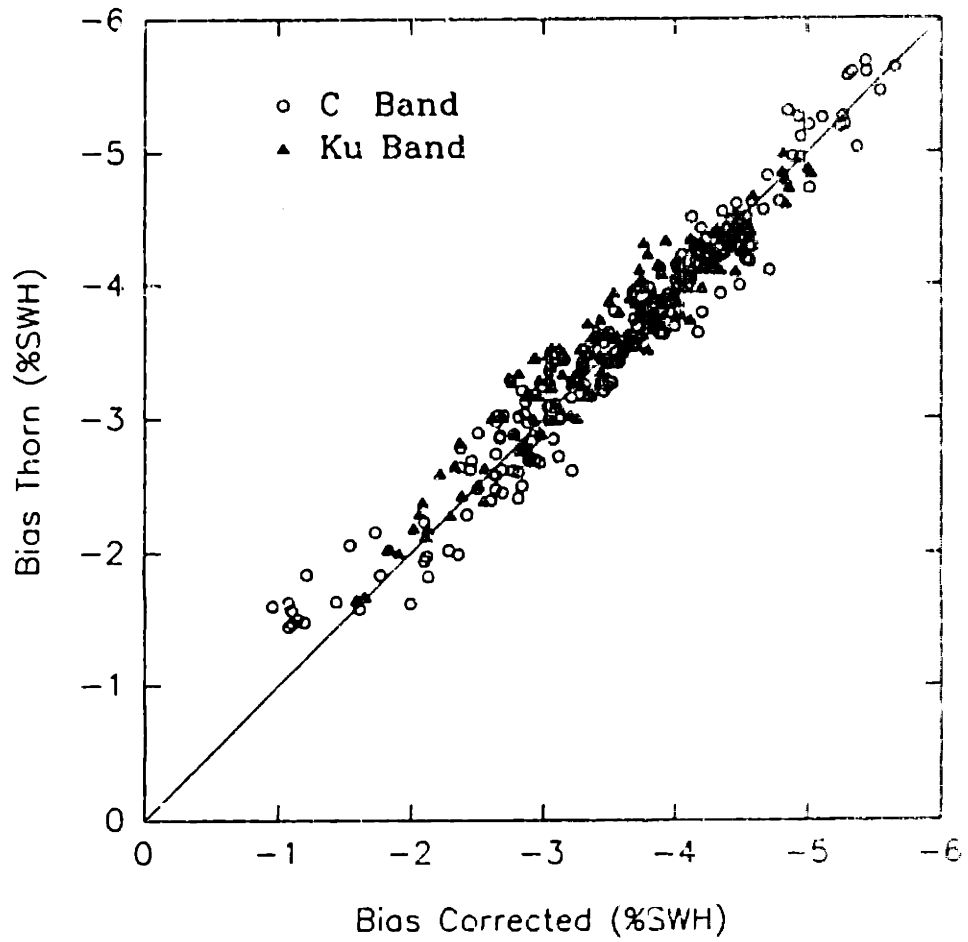

Figure 2.15: Normalized electromagnetic bias measured using the Thorn/EMI infrared wave gauge compared to the normalized electromagnetic bias measured using the integrated scatterometer Doppler adjusted according to equations (2.9), (2.10) and (2.11). The standard deviation of the error was 0.233% of SWH for C band and 0.201% of SWH for Ku band.

significant wave height, and the C bias varied from -0.4 cm to -19.9 cm or from -0.6% to -6.3% of the significant wave height (see Table 2). There were a total of 1280 hours of usable data.

Variable	Minimum	Maximum	Mean	Stdv
$H_{1/3}$ (m)	0.61	3.19	1.44	0.47
U_{25} (m/s)	0.1	14.3	6.9	2.9
ϵ_C (cm)	-0.6	-18.7	-6.6	3.3
β_C (%$H_{1/3}$)	-1.31	-6.54	-3.59	1.04
ϵ_{Ku} (cm)	-1.1	-13.4	-5.5	2.3
β_{Ku} (%$H_{1/3}$)	-1.44	-5.30	-3.65	0.70

Table 2 - Summary for December 1989 - May 1990

The relationships between β and the wind speed for Ku and C bands are shown in figures 2.16 and 2.17 respectively. The linear correlations between β and the wind speed were found to be

$$\beta_{Ku}(\%\ H_{1/3}) = -2.76 - 0.139\ U_{25} \qquad r^2 = 0.417 \qquad (2.12)$$

$$\beta_{C}(\%\ H_{1/3}) = -1.44 - 0.309\ U_{25} \qquad r^2 = 0.661. \qquad (2.13)$$

The residual bias, after removing the correlation of β with the wind speed, had a standard deviation of 0.48% and 0.65% of

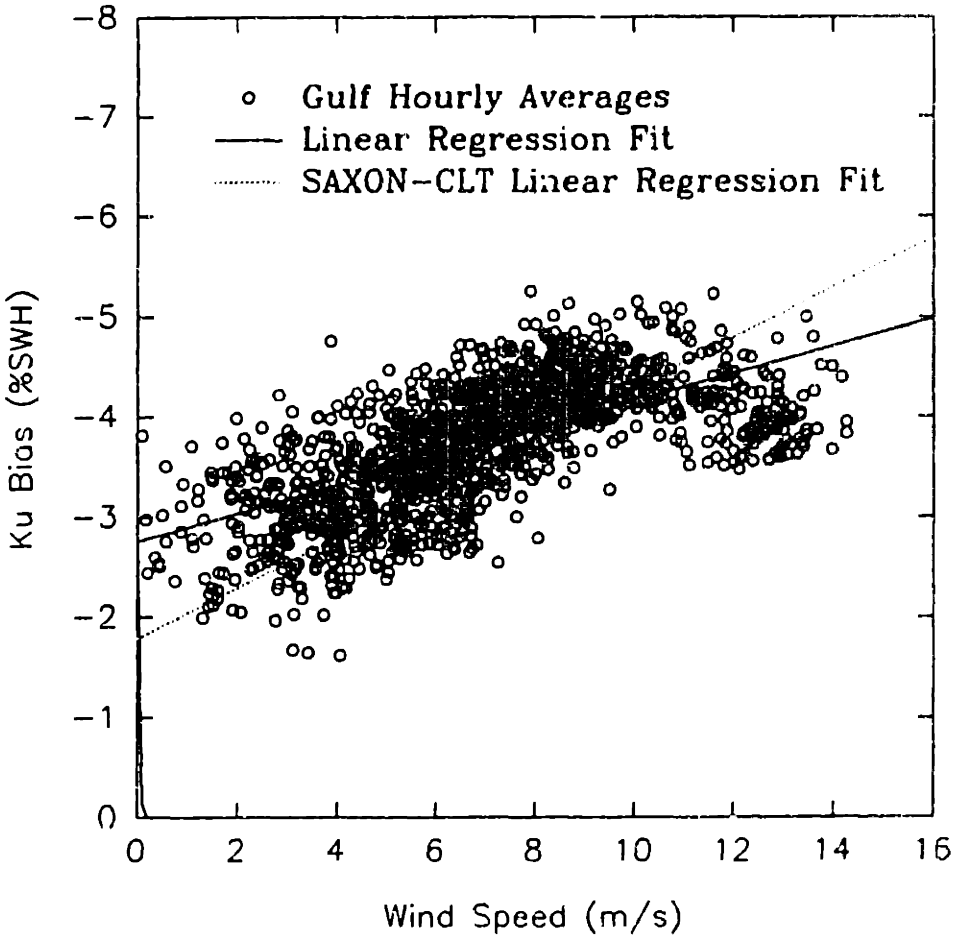

Figure 2.16: Normalized Ku band electromagnetic bias as a function of wind speed at 25 m above the sea surface for the six months of the experiment. The solid line is the linear regression fit $\beta_{Ku}(\%SWH) = -2.76 - 0.139U_{25}$ ($r^2 = 0.417$). The dashed line is the linear regression fit to the data of *Melville et al.* [1991] given by $\beta_{Ku}(\%SWH) = -1.79 - 0.25U_{10}(m/s)$ ($r^2 = 0.707$).

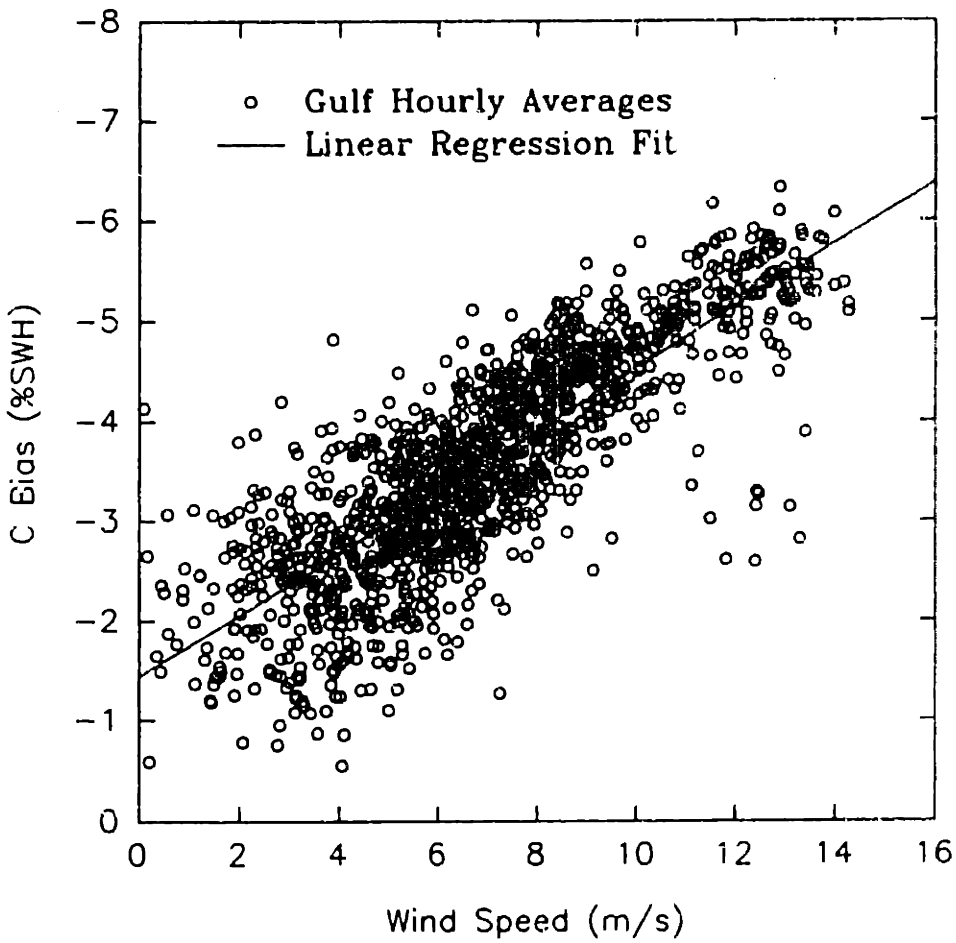

Figure 2.17: Normalized C band electromagnetic bias as a function of wind speed at 25 m above the sea surface for the six months of the experiment. The solid line is the linear regression fit $\beta_c(\%SWH) = -1.44 - 0.309U_{25}(m/s)$ ($r^2 = 0.661$).

significant wave height respectively for Ku and C bands. As seen in figure 2.17, there is a lot of scatter for small values of C band bias. This is due to the underestimation of the C band bias for small values of bias as was indicated in figure 2.15.

Figure 2.16 clearly shows a nonlinear dependence of the Ku band dimensionless bias β on the wind speed. To better represent the nonlinear behavior, the bias was binned with wind speed. For each 1 m/s interval in wind speed the bias was averaged. Figure 2.18 shows the number of hours of data occurring at each 1 m/s interval of wind speed, and figure 2.19 shows the average bias at each 1 m/s interval. For wind speeds less than 3-4 m/s the C and Ku band biases are almost constant. Above wind speeds of 3-4 m/s, the biases increase linearly until they reach a saturation level. The Ku band bias reaches a saturation at wind speeds of 9-10 m/s above which it decreases. The C band bias reaches a saturation at wind speeds of 11-12 m/s, above which it levels out.

Figure 2.20 shows a comparison of the C and Ku band biases. Similar to the data from the month of February shown in figure 2.9, the C band bias is smaller than the Ku band bias for low wind speeds and larger for high wind speeds.

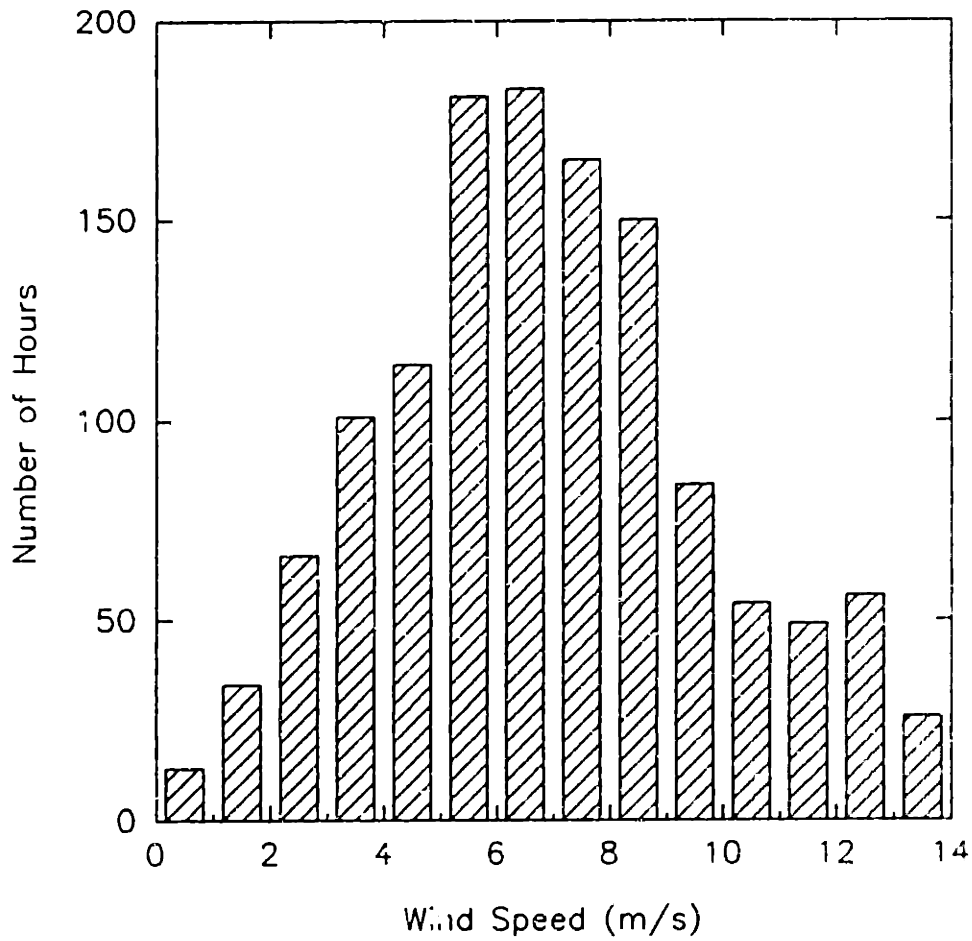

Figure 2.18: Histogram showing the number of hours of data occuring at each 1 m/s interval of wind speed.

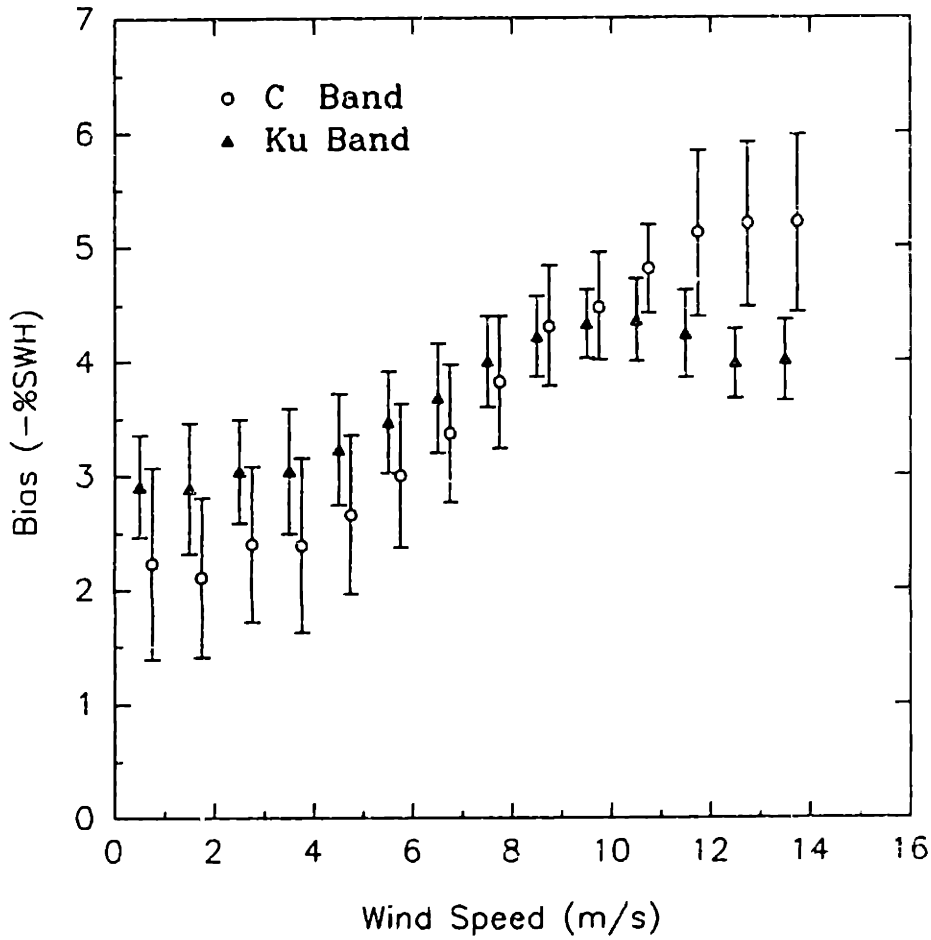

Figure 2.19: Average normalized electromagnetic bias at each 1 m/s interval of wind speed as a function of wind speed at a height of 25 m. The vertical error bars show the standard deviation about the mean.

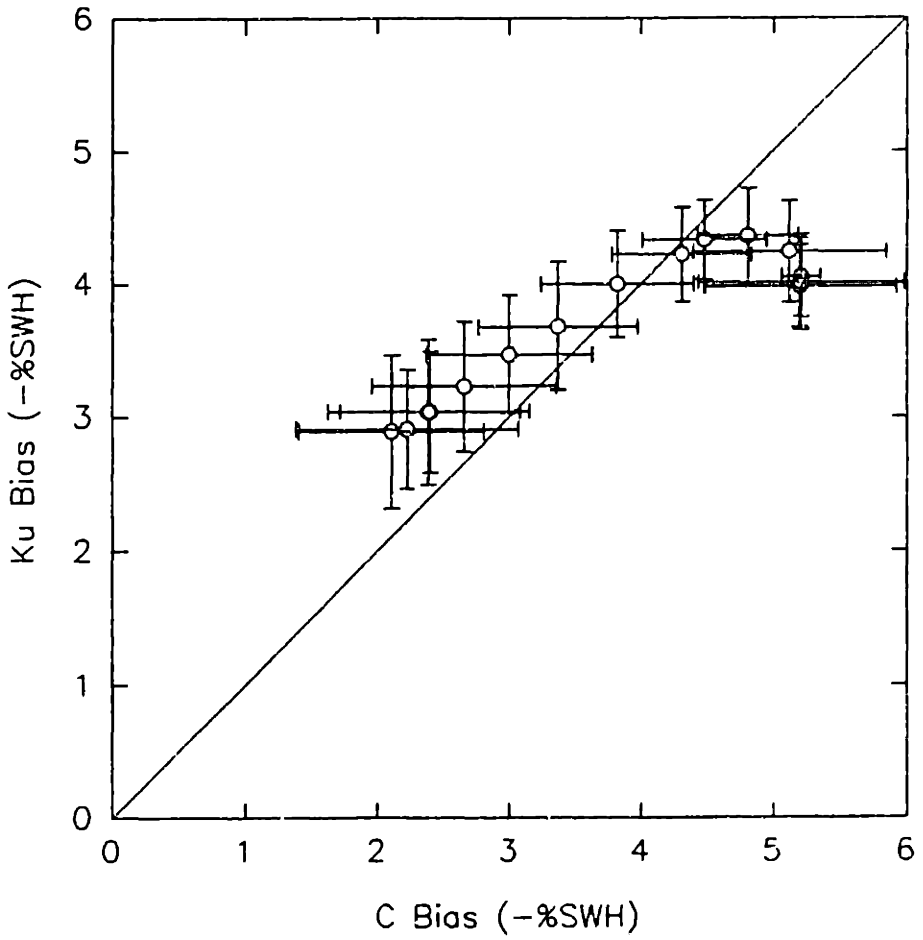

Figure 2.20: Average normalized Ku band electromagnetic bias compared to the average normalized C band electromagnetic bias. The vertical error bars show the standard deviation of the Ku band bias about its mean. The horizontal error bars show the standard deviation of the C band bias about its mean.

2.3 DISCUSSION

As in previous experiments the dimensionless bias β has been found to depend on the wind speed and the electromagnetic frequency. Figure 2.21 summarizes the measurements of the present experiment, the SAXON-CLT EM bias measurements of *Melville et al.* [1991] and the aircraft EM bias measurements of *Walsh et al.* [1991].

The results for the month of February shown in figures 2.7 and 2.8 compare well with the results for the entire experiment shown in figure 2.19. The only observable difference between the two is the different behavior of the Ku band bias at wind speeds above 10 m/s. The Ku band bias, as measured in the month of February (see figure 2.7), showed a saturation at wind speeds above 10 m/s, whereas the Ku band bias measured during the entire experiment (see figure 2.19) shows a decrease in bias above 10 m/s. Measurements from SAXON-CLT [*Melville et al.*, 1991] showed a similar saturation at high wind speeds as the measurements for the month of February.

Measurements from the months of December and January of the present experiment (see figure 2.22) show a decreasing bias at wind speeds greater than 10 m/s. The primary difference between the months of December and January and the month of

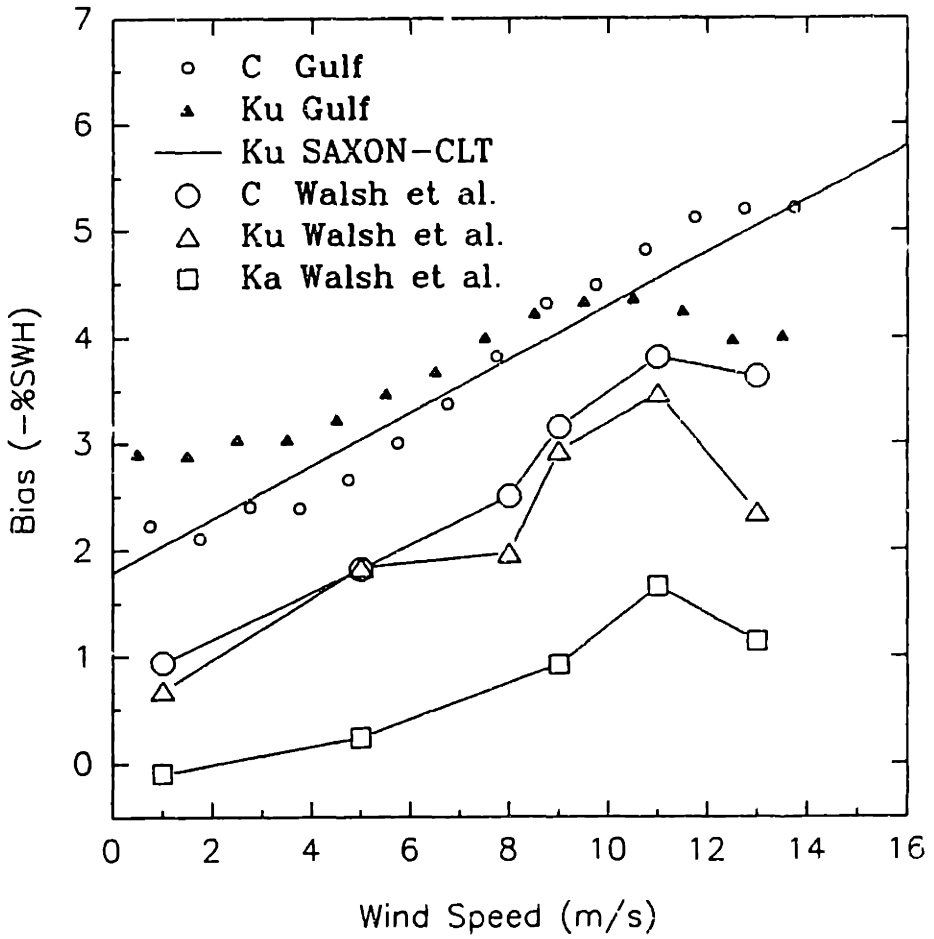

Figure 2.21: Summary plot showing the normalized electromagnetic bias as a function of wind speed for the present Gulf of Mexico measurements, the SAXON-CLT measurements of *Melville et al.* [1991], and the aircraft measurements of *Walsh et al.* [1991].

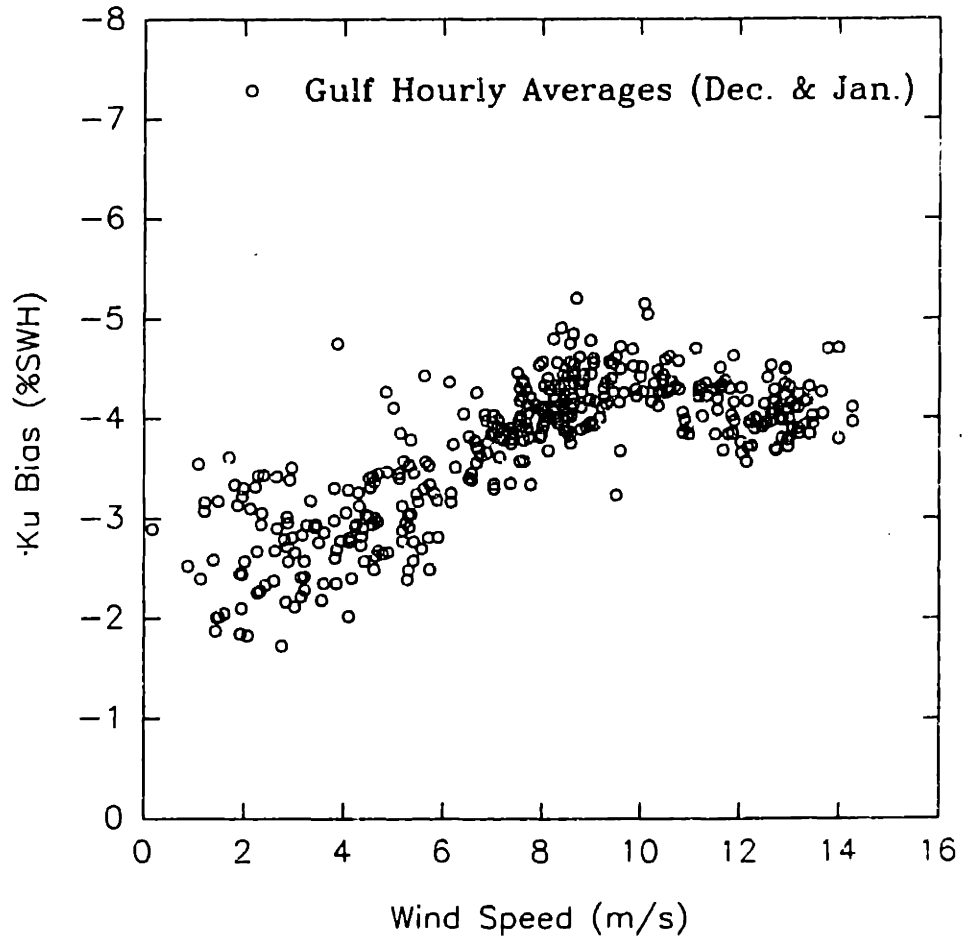

Figure 2.22: Normalized Ku band electromagnetic bias as a function of wind speed at 25 m above the sea surface for the months of December and January.

February was the range of wave heights. During December and January the wave height ranged from 0.6 m to 3.2 m, whereas during the month of February the wave height ranged from 0.7 m to 2.3 m. The range of wind speed was the same for the three months with wind speed ranging up to 14 m/s. This indicates a possible dependence of the dimensionless bias upon the wave height or the wave development at wind speeds above 10 m/s.

A comparison of the aircraft measurements of *Walsh et al.* [1991] with the present experiment show similar saturations of the bias at high wind speeds. The C band bias as measured by *Walsh et al.* [1991] reached a saturation at wind speeds above 10-11 m/s and the Ku band bias decreased at wind speeds above 10-11 m/s in agreement with the present experiment. The constant bias at wind speeds below 3-4 m/s, as observed in the present experiment, were also observed during SAXON-CLT [*Melville et al.*, 1991]. An examination of figure A.6 in Appendix A shows a constant bias for wind speeds less than 4 m/s with an exception of the 5 hours of data in the 0-1 m/s wind speed range.

For wind speeds less than 10 m/s, the Ku bias as measured in the present experiment was nearly a constant 0.3% of significant wave height larger than the Ku bias measured in

SAXON-CLT, and the bias as measured in SAXON-CLT was nearly a constant 1% of significant wave height larger than the Ku bias measured by *Walsh et al.* [1991]. This difference may be due to the different heights from the surface at which the measurements were taken. The present experimental measurements, the SAXON-CLT bias measurements and the aircraft bias measurements were taken at 18 m, 22 m and 160 m above mean sea level respectively. This could indicate that the closer the measurements are made to the sea surface, the larger the measured bias.

Walsh et al. [1991] suggested the height difference may be due to focusing/defocusing effects of the sea surface wave structure. While a detailed analysis of this suggestion is beyond the scope of this thesis, some general remarks are appropriate. The curvature of the sea surface would be expected to have an asymmetric distribution about mean sea level with the wave crests having larger curvatures than the troughs. At the sea surface the electromagnetic phase front is spherical, causing an artificial curvature to be added to the sea surface. This has the effect of shifting the effective curvature distribution even more toward the crests which results in a larger electromagnetic bias. Since the curvature of the spherical electromagnetic phase front is larger at heights close to the surface, the bias measured

close to the surface would be larger than when measured far from the surface.

Overall, the present experimental measurements compare well with the earlier SAXON-CLT bias measurements [*Melville et al*, 1991], with the noted exceptions at high wind speeds and the possible measurement height dependence. Also, the tower measurements and the aircraft measurements of *Walsh et al.* [1991] are in good agreement except for the noted constant difference of 1%-1.3% of significant wave height. It has been shown, based on the measurements presented in this chapter, that the bias is not well described by a linear relation between dimensionless bias and wind speed at low and high wind speeds. For wind speeds less than 3-4 m/s, the bias was found to be constant. For wind speeds greater than 3-4 m/s but less than 10 m/s, the bias was found to increase linearly with wind speed. For wind speeds greater than 11-12 m/s, the C band bias reaches a saturation, and similarly, the Ku band bias reaches a saturation and then begins to decrease for wind speeds greater than 9-10 m/s.

Chapter 3

Electromagnetic Bias Theory

During the EM bias experiments reported by *Melville et al.* [1990,1991] a wire wave gauge was used to obtain the modulation of the high frequency waves by the low frequency waves. It became apparent that the EM bias was primarily caused by the modulation of the short waves. This was reported by *Arnold et al.* [1989,1990,1991]. This chapter will present a theory using physical optics scattering and an empirical model of the short wave modulation to estimate the EM bias. The estimated EM bias will be compared to measurements at C and Ku bands.

3.1 EM Bias Dependence on Short Wave Modulation

The back scattered power from a small patch on the ocean surface depends on the displacement of the patch from mean sea level. It has been observed that more power is reflected from the troughs of waves than from the crests. A typical measurement of the relative back scatter coefficient as a function of wave displacement is shown in figure 3.1.

The EM bias ϵ can be defined mathematically as the ratio of

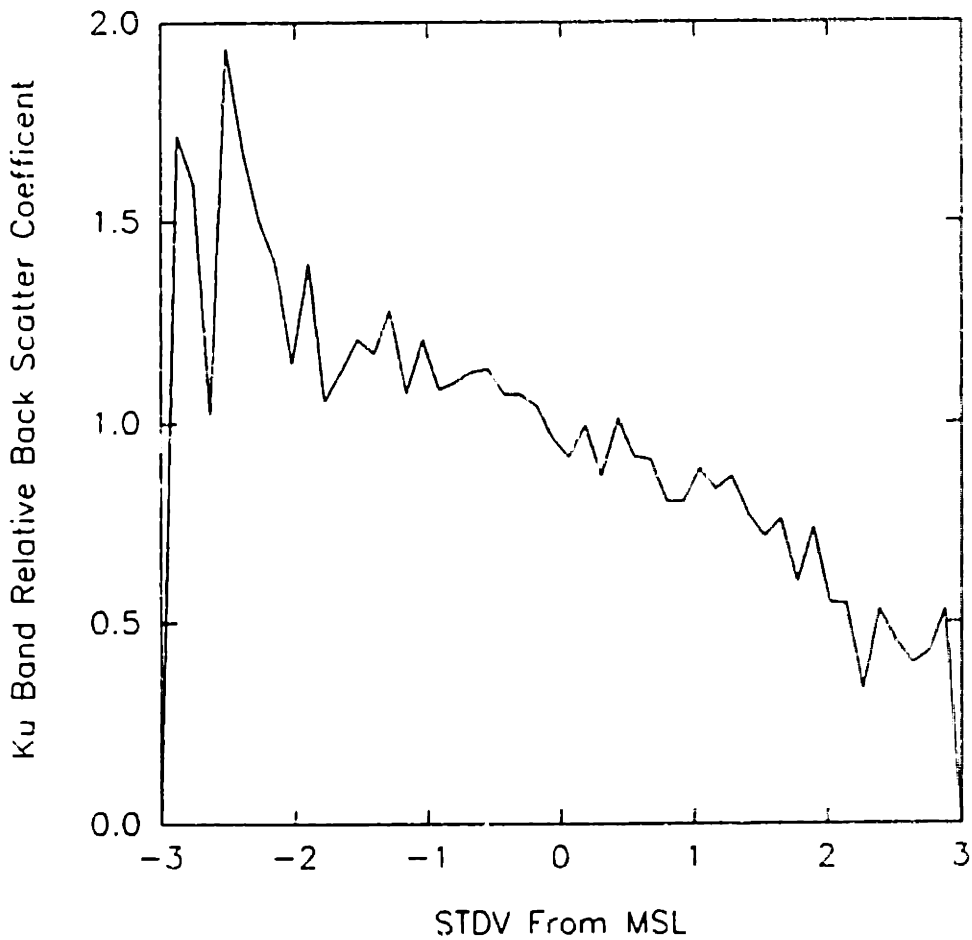

Figure 3.1: Ku band relative back scatter coefficient as a function of displacement from mean sea level in standard deviations.

the first two moments of the back scatter coefficient profile σ_η° given by

$$\epsilon = \frac{E[\eta \sigma_\eta^\circ(\eta)]}{E[\sigma_\eta^\circ(\eta)]} \tag{3.1}$$

where η is the surface displacement, and E[] denotes an ensemble average. The back scatter coefficient σ° is related to the back scatter coefficient profile by

$$\sigma^\circ = \int_{-\infty}^{\infty} d\eta \; \sigma_\eta^\circ(\eta) \; p_\eta(\eta) \tag{3.2}$$

where $p(\eta)$ is the surface displacement probability density function. The task is to develop a theory to predict the back scatter coefficient profile from which the EM bias can be calculated.

The primary cause of the EM bias at C and Ku bands will be assumed to be the modulation of the short wave amplitude by the long waves. The short wave amplitude modulation will be found empirically by measuring the energy in the short waves as a function of long wave displacement. Physical optics scattering will be used to predict the back scatter coefficient profile from the short wave modulation profile.

A model relating the EM bias to the important parameters describing the ocean surface will be developed. It will be

shown that the bias can be described by a relationship between wave height and a short wave modulation strength parameter.

3.1.1 Short Wave Modulation Model

The ocean wave field is separated into long and short waves at a separation wave length L with corresponding wave number k_s (see figure 3.2). The separation wave length is much larger than the electromagnetic wave length λ_{EM} of the microwave scatterometers and much smaller than the dominant wave length λ_o of the ocean waves. The short waves have a variance σ_s^2 and the long waves have a variance σ_l^2. The scatterometers used to make the measurements had illuminated spot sizes on the order of one meter; which was chosen as the separation wave length satisfying the relationship:

$$[\lambda_{EM} = O(10^{-2}m)] \ll [L = O(1m)] \ll [\lambda_o \approx O(10m)]. \qquad (3.3)$$

The long waves can be modeled by a surface tilt and curvature. The tilt and curvature of the surface will be considered to be of secondary importance to the short wave modulation and thus will be neglected. The possible effects of neglecting the tilt and curvature of the long wave surface will be discussed later.

The wavenumber modulation of the short waves will be neglected allowing the short wave spectrum to be described by a constant

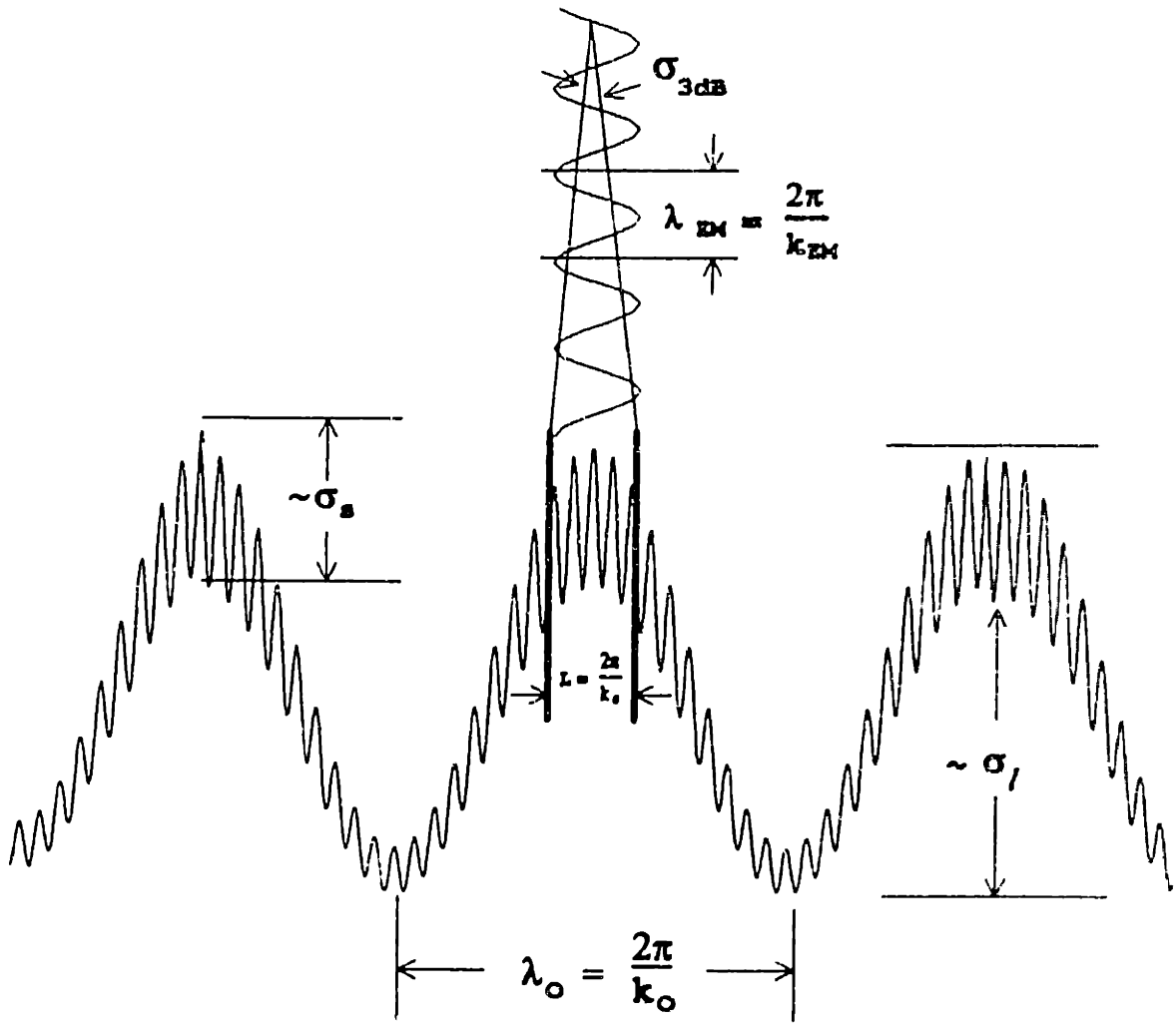

Figure 3.2: Short wave modulation model parameters. L is the separation wavelength corresponding to the illuminated spot size. λ_{EM} is the electromagnetic wavelength. λ_o is the dominant ocean wave length. σ_l is the long wave RMS height. σ_s is the local short wave RMS height. σ_{3dB} is the beamwidth of the scatterometers.

spectral shape. The wavefield at scales less than L will be modelled as unidirectional with a k^{-p} spectral shape. The short wave modulation can then be described by a short wave height variance which varies with long wave displacement. The short wave model spectrum for p greater than one is given by

$$S_p(k,\eta) = \begin{cases} (p-1)\,\sigma_s^2(\eta)\,k_s^{p-1}k^{-p} & k \geq k_s = \frac{2\pi}{L} \\ 0 & k < k_s \end{cases} \qquad (3.4)$$

so that the variance of the short waves is given by

$$\sigma_s^2(\eta) = \int_{k_s}^{\infty} S_p(k,\eta)\,. \qquad (3.5)$$

The corresponding autocorrelation function and correlation coefficient are

$$R_p(x,\eta) = \sigma_s^2(\eta)\,C_p(x) \qquad (3.6)$$

$$C_p(x) = \int_{k_s}^{\infty} dk\,(p-1)\,k_s^{p-1}k^{-p}\cos kx. \qquad (3.7)$$

The correlation coefficient can be rewritten as

$$C_p(k_s x) = (p-1)\,(k_s x)^{p-1} \int_{k_s x}^{\infty} du\; u^{-p} \cos u. \qquad (3.8)$$

This transform can be performed resulting in a power series representation for small argument and an asymptotic series representation for large argument (see Appendix B for details). The correlation coefficient is shown in figure 3.3 for three different values of p.

Values of p = 2.5 and 3.0 will be used later in comparing with measured results. A value of p = 3.0 for a unidirectional surface corresponds to a k^{-4} two-dimensional spectrum and a value of p = 2.5 corresponds to a $k^{-3.5}$ two-dimensional spectrum. These values of p were chosen to agree with the measurements of *Banner et al.* [1989], *Shemdin et al.* [1988] and *Jahne and Riemer* [1990].

3.1.2 Physical Optics Scattering Theory

Physical optics, or the Kirchhoff approximation, is a well known scattering theory, having been used for rough surface scattering by *Beckman and Spizzichino* [1963], *Hagfors* [1966], *Fung and Moore* [1966], *Holliday et al.* [1986] and many others.

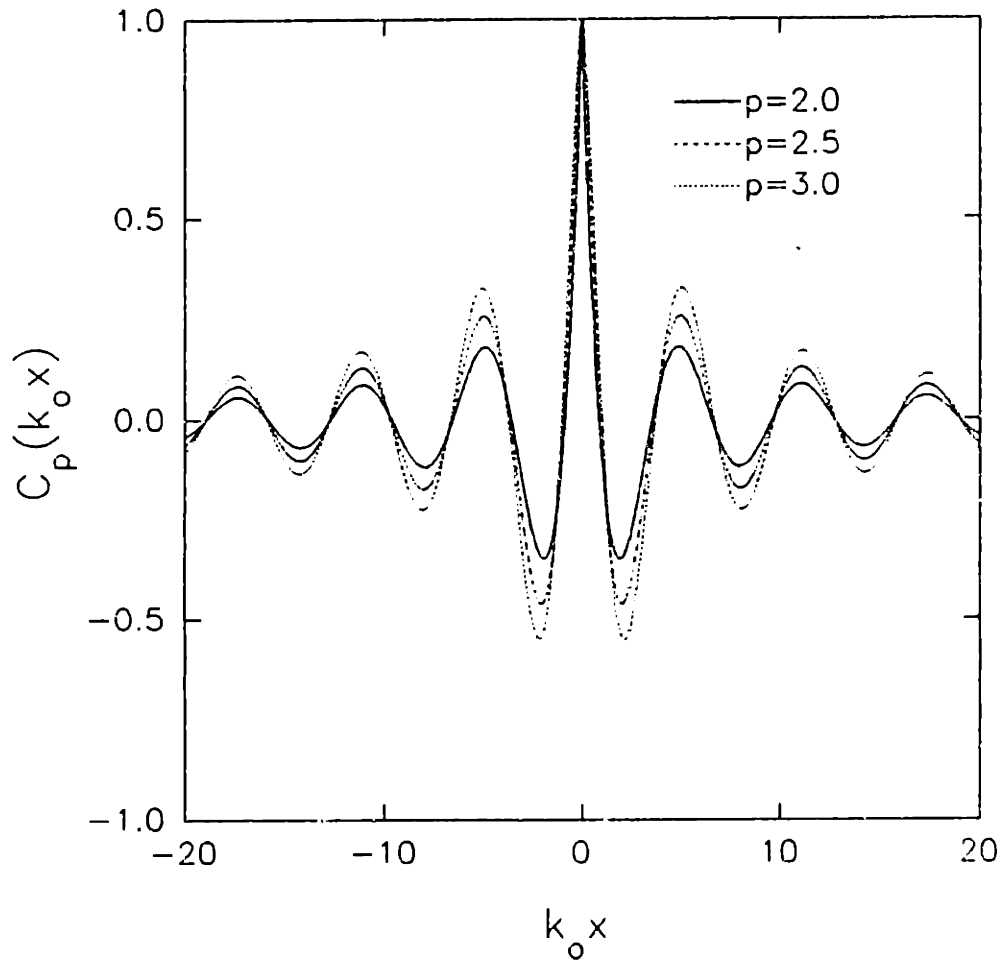

Figure 3.3: Correlation coefficient for p = 2.0, 2.5 and 3.0.

The physical optics integral at normal incidence for a unidirectional surface is given by (for derivation, see Appendix C)

$$\sigma^o = \left(\frac{k_{EM}^2 A_o}{\pi}\right) \int_{-1}^{1} du(1-|u|)\, e^{-4\sigma_s^2 k_{EM}^2 [1-C_p(k_s L u)]} \qquad (3.9)$$

where σ^o is the backscatter coefficient, k_{EM} is the electromagnetic wave number, A_o is the illuminated area, σ_s is the RMS wave height of the short waves, k_s is the separation wave number of the surface spectrum, L is the illuminated spot diameter and C_p is the surface correlation coefficient given by equation (3.7). Two assumptions were made in the development of equation (3.9); namely, a tangent plane approximation for the electric surface current and a Gaussian probability density distribution for the surface displacement.

Barrick [1970] argued that the only valid use of physical optics was in the limit as electromagnetic frequency becomes infinite, resulting in geometric optics or specular point theory. Specular point theory has been discussed by *Kodis* [1966], *Barrick* [1968], and *Barrick and Bahar* [1981], where it was shown that specular point theory depends only on the slope statistics of the surface, not the shape of the correlation coefficient. *Fung and Chan* [1971], *Fung and Eom* [1981] and *Chan and Fung* [1988] showed, using method of moment

calculations, that the high frequency restriction of *Barrick* [1970] is too restrictive. The validity of the Kirchhoff approximation requires only that the average radius of curvature of the surface be large compared to the electromagnetic wavelength. This insures that the surface will be smooth enough for the tangent plane surface current approximation to be applicable. Stated explicitly, the validity of equation (3.9) requires

$$\frac{\lambda_{EM}}{\rho_c} < 1 \qquad (3.10)$$

where ρ_c is the average radius of curvature of the surface.

The high frequency portion of the ocean wave spectrum causes the average radius of curvature to be small. This apparently renders invalid the use of either specular point or physical optics scattering theory when observations of the ocean surface are made at microwave frequencies. However, *Tyler* [1976] showed that the high frequency features of a surface should be smoothed prior to application of specular point theory. The common practice is to include only the portion of the ocean surface with wave lengths longer than the electromagnetic wave length [*Valenzuela,* 1978].

The physical optics integral of equation (3.9) does not

require a filter function as proposed by *Tyler* [1976] to be explicitly applied to the ocean surface. A filter function is inherent in the physical optics integral, for a surface with spectrum given by equation (3.4), because the high frequency waves are weighted less because of their small heights. These statements will be verified by comparing the results of the physical optics integral to results obtained using exact method of moment calculations for the employed short wave model.

The physical optics integral was evaluated numerically for a surface with a spectrum given by equation (3.4) with $p = 3$. The results are shown by the solid line in figure 3.4. The physical optics scattering coefficients computed using a Monte Carlo simulation are shown by the squares. A method of moments technique *described by Axline and Fung* [1978] was used to obtain the exact scattering coefficients for k_{EM} = 104.7 rad/m, and the results are shown by the triangles. It can be seen that the physical optics theory provides excellent agreement with the exact method of moment results. This establishes the validity of using physical optics scattering for the employed short wave spectrum model.

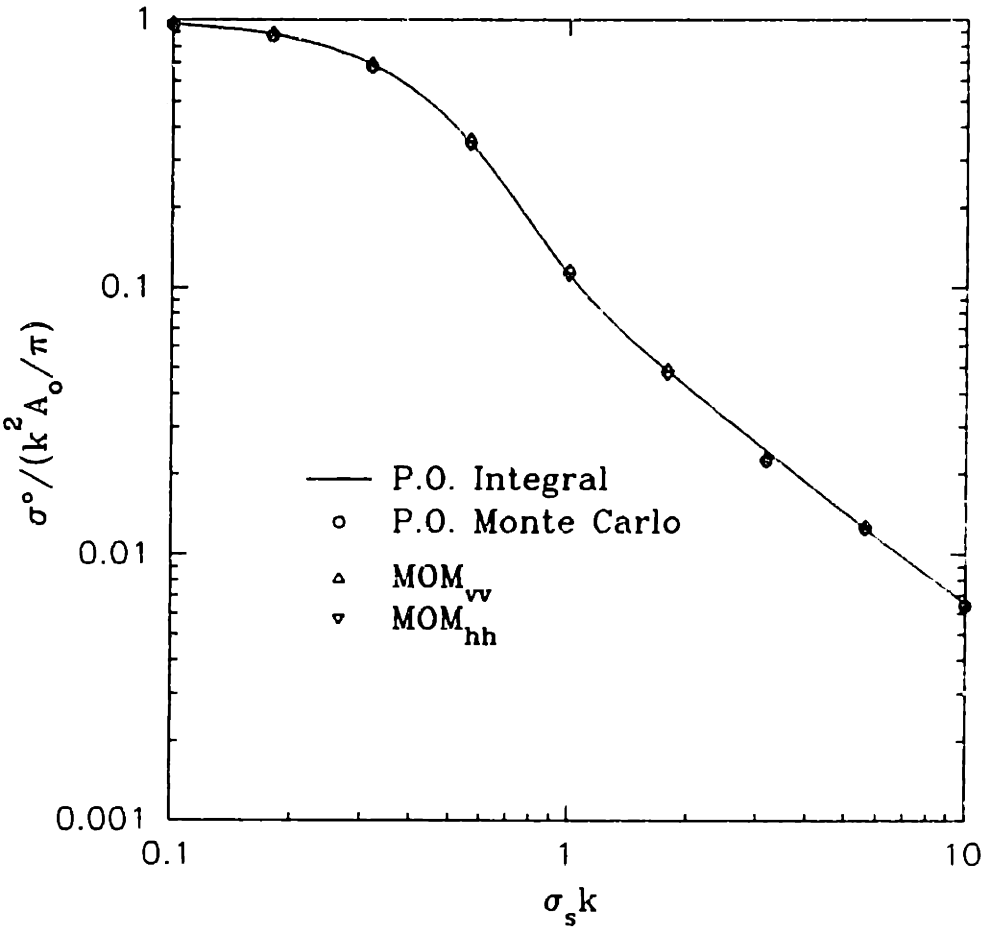

Figure 3.4: Back scatter coefficient as a function of $\sigma_s k$. The solid line is the numerical evaluation of the physical optics integral. The circles are physical optics scattering coefficients computed using a Monte Carlo simulation. The triangles are the exact scattering coefficients, computed using a method of moments technique.

In order to study the implicit filter function in the physical optics integral, the following spectrum with a variable high wave number cut off will be used:

$$S_p(k) = \begin{cases} 0 & k > k_h \\ S_o k^{-p} & k_g \le k \le k_h \\ 0 & k < k_g = \frac{2\pi}{L} \end{cases} \quad (3.11)$$

A corresponding correlation coefficient can easily be found similar to equation (3.7).

For a separation length L = 2 m, a typical short wave height σ_s = 2 cm, k_{EH} = 105 rad/m and 293 rad/m corresponding to C and Ku bands, and with p = 3, figure 3.5 shows the back scatter coefficient as a function of k_h normalized by the scatter coefficient for an effective infinite k_h. Physical optics integral results are shown by the solid line. Physical optics scattering coefficients computed using a Monte Carlo simulation are shown by the squares, and the exact method of moments results are shown by the triangles. It is easily recognized that the back scatter coefficient is less influenced by shorter waves. The same dependence of exact method of moment and physical optics results on high wave number cutoff, demonstrates that physical optics applies the

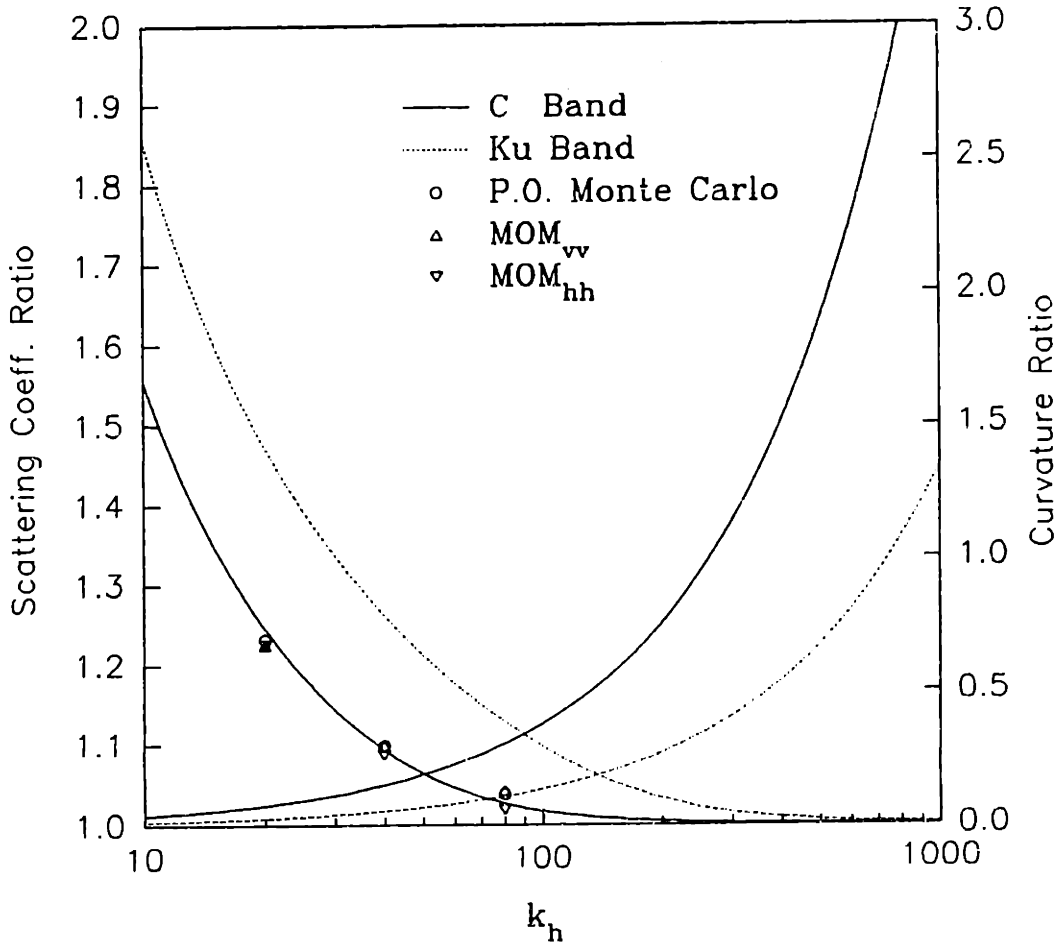

Figure 3.5: The left axis and the decreasing curves show the backscatter coefficient normalized by the back scatter coefficient for an effective infinite k_h as a function of k_h, where k_h is the high wave number cutoff. The right axis and the increasing curves are the ratio of the electromagnetic wavelength to the average radius of curvature.

correct filter function implicitly. The applicability of physical optics becomes obvious by considering figure 3.5, which also shows equation (3.10) computed as a function of k_h. It is seen that the ratio of electromagnetic wave length to the average radius of curvature is less than one for the portion of the spectrum that contributes to the scattering coefficient, thus satisfying the validity criteria of equation (3.10).

The physical optics integral of equation (3.9) is difficult to solve using standard asymptotic techniques. The exponential argument in equation (3.9) contains the correlation coefficient given by equation (3.7). The correlation coefficient is not well represented by the first few terms of a Taylor series as used in standard asymptotic techniques. An alternate method is to use a series with a fractional power term to represent the exponential argument of equation (3.9) as

$$4\sigma_s^2 k_{EM}^2 [1 - C_p(k_s Lu)] = \left(\frac{k_s Lu}{Z_o}\right)^{2/\alpha} + \ldots \qquad (3.12)$$

Assuming the parameter $\sigma_s k_{EM}$ is large, only the first term of equation (3.12) is needed. Substituting equation (3.12) into equation (3.9), and extending the limits to infinity gives

$$\sigma^o = 2\left(\frac{k_{EM}^2 A_o}{\pi}\right)\int_o^\infty du\; e^{-\left(\frac{k_s L u}{z_o}\right)^{\alpha/\alpha}}. \qquad (3.13)$$

Making a variable substitution and using the definition of the gamma function

$$\Gamma(p) = \int_0^\infty dx\; x^{p-1}e^{-x} \qquad (3.14)$$

gives equation (3.9) as

$$\sigma^o = \left(\frac{k_{EM}^2 A_o}{\pi}\right)\alpha\,\Gamma\left(\frac{\alpha}{2}\right)\frac{z_o}{k_s L}. \qquad (3.15)$$

The exponential argument of equation (3.9) is expanded in equation (3.12) about $k_s Lu = z_o$ where z_o is chosen according to the relation

$$4\sigma_s^2 k_{EM}^2[1 - C_p(Z_o)] = 1 \qquad (3.16)$$

so as to provide a good fit at the e^{-1} point of the exponential of equation (3.9). Keeping the first term of equation (3.12), differentiating both sides with respect to $k_s Lu$, and solving for α about z_o gives

$$\alpha = \frac{1}{2\sigma_s^2 k_{EM}^2 [-C_p'(z_o)]\, z_o}. \qquad (3.17)$$

Figure 3.6 compares the back scatter coefficient, calculated using the asymptotic result of equations (3.15), (3.16) and (3.17) with the numerical integration of equation (3.9) for $k_s L = 2\pi$. As seen in figure 3.6, the asymptotic back scatter coefficient is a good approximation when $\sigma_s k_{EM} > 1$.

3.1.3 EM Bias - Linear Short Wave Modulation Model

A model relating the EM bias directly to the short wave modulation will be described. It will be shown that the bias can be described by a simple relationship with the wave height and a short wave modulation strength parameter.

The short wave modulation profile is approximated linearly by

$$\sigma_s(\eta) = \sigma_m(1 + m\frac{\eta}{\sqrt{\eta^2}}) \qquad (3.18)$$

where σ_s is the local RMS short wave height, σ_m is the global RMS short wave height, and m is a measure of the modulation strength. The back scatter coefficient profile can be computed by substituting equation (3.18) into equation (3.9). For the modulation strength much less than one, the back scatter coefficient profile becomes

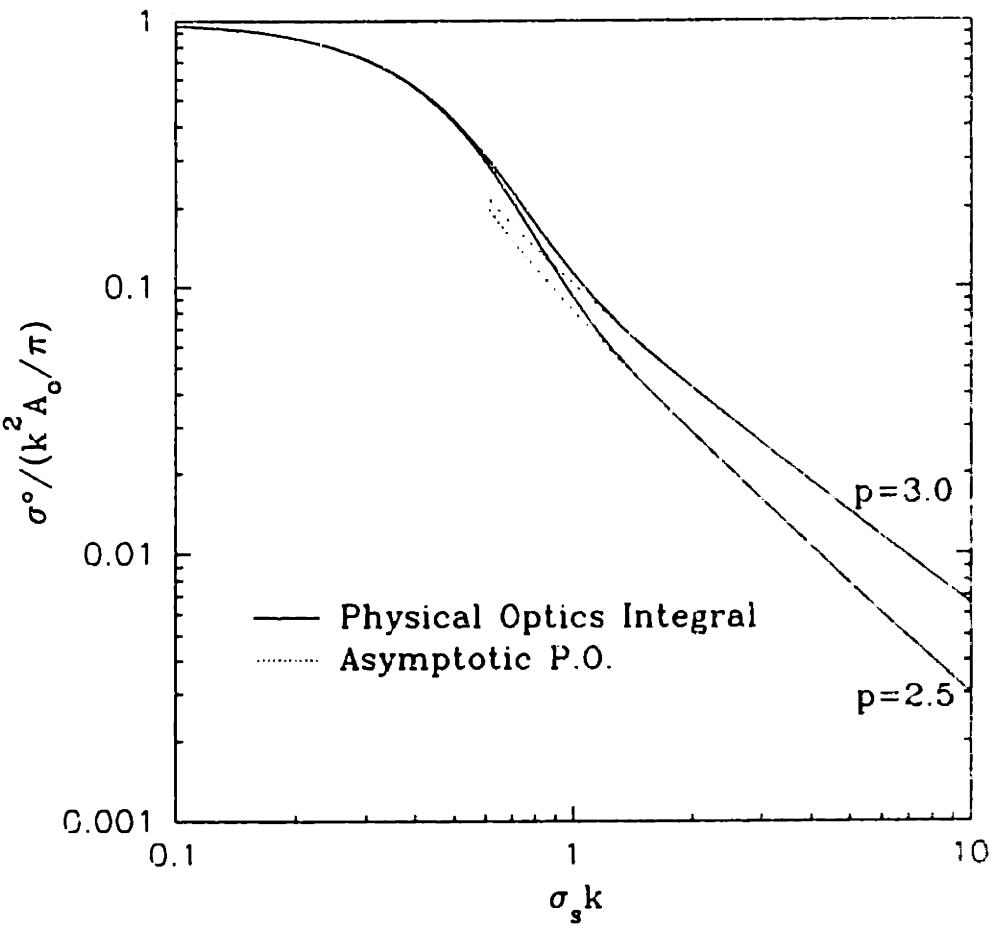

Figure 3.6: Back scatter coefficient as a function of $\sigma_s k$. The solid lines were computed numerically using the physical optics integral of equation (3.9). The dashed curves were computed using the asymptotic solution of equations (3.15)-(3.17).

$$\sigma^o(\eta) = \frac{k^2 A_o}{\pi}\int_{-1}^{1} du(1-|u|)\, e^{-4(\sigma_m k_{EM})^2(1+2m\eta/\sqrt{\eta^2})[1-C_p(k_g L u)]}. \quad (3.19)$$

Representing the back scatter coefficient profile by its Taylor series expansion about mean sea level gives

$$\sigma^o(\eta) = \sigma^o(0) + \eta\frac{\partial\sigma^o(0)}{\partial\eta} + \ldots \quad (3.20)$$

where the bias can be determined using equation (3.1) giving

$$\epsilon = \frac{\overline{\eta}^2\frac{\partial\sigma^o(0)}{\partial\eta} + \ldots}{\sigma^o(0)}. \quad (3.21)$$

Substituting equation (3.19) into (3.21), the bias can be written in terms of a short wave modulation strength parameter m and the wave height as

$$\epsilon = -\alpha m\sqrt{\overline{\eta^2}} \quad (3.22)$$

where

$$\alpha = \frac{\int_0^1 du(1-u)\,8(\sigma_m k_{EM})^2[1-C_p(k_g L u)]\, e^{-4(\sigma_m k_{EM})^2[1-C_p(k_g L u)]}}{\int_0^1 du(1-u)\, e^{-4(\sigma_m k_{EM})^2}[1-C_p(k_g L u)]}. \quad (3.23)$$

The linear dependence of the EM bias on wave height has been well known from experimental observations for some time [*Walsh et al.,* 1989]. A correspondence between the short wave modulation profile and the EM bias was established by *Arnold et al.* [1990], but equation (3.22) specifies the correspondence by showing the bias to be proportional to the short wave modulation strength.

Equation (3.23) can be solved asymptotically by using the methods of the last section given by equations (3.12-3.17). Equation (3.23) is found to be well approximated by equation (3.17) for $\sigma_m k > 1$. Figure 3.7 compares the numerical integration of equation (3.23) with the asymptotic result with $p = 2.5$ and 3 and $k_s L = 2\pi$. For $\sigma_m k > 1$, the asymptotic results are good approximations.

3.2 Experiment Description

An experiment to measure the EM bias at C and Ku bands (the frequencies of the TOPEX/Poseidon altimeters) was conducted from December 1989 through May 1990 [*Melville et al,* 1990] from a Shell Offshore production complex (Brazos-19) in 40 meters of water off the coast of Texas in the Gulf of Mexico. Nadir looking coherent scatterometers at 5 and 14 GHz and a Thorn/EMI IR wave gauge were mounted 18 meters above mean level in the middle of a 60 meter bridge joining two platforms. For

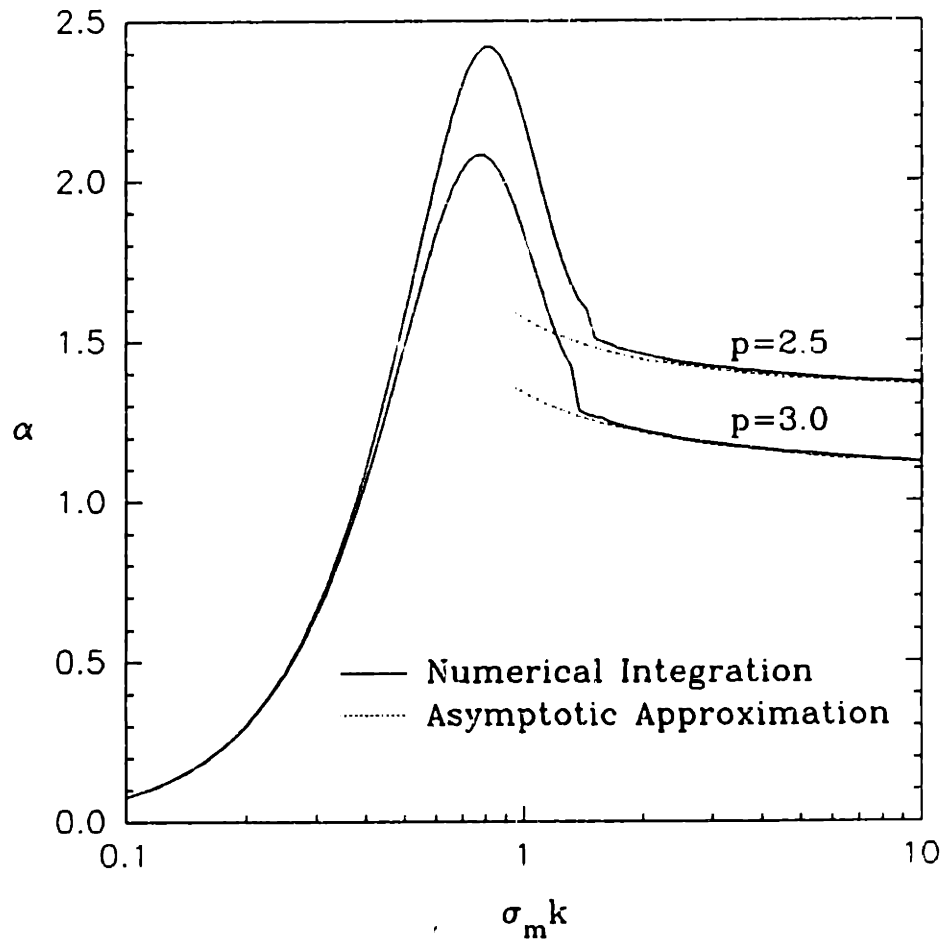

Figure 3.7: α of equation 3.23 as a function of $\sigma_m k$. The dashed curves are given by the asymptotic solution of equation (3.17).

short periods of the experiment, a capacitance wire wave gauge was mounted adjacent to the footprints of the scatterometers. The wind speed and direction, air and sea temperature, humidity and rain fall were measured by an R. M. Young instrument package. The 105 hours of data contained in this chapter comes from a week during May 1990.

The EM bias was measured using the back scatter and doppler of the C and Ku band scatterometers. The wave displacement was obtained by integrating the Doppler centroid, which is proportional to the vertical wave velocity, over time to give the displacement. The simultaneous measurements of back scatter and wave displacement were then used to calculate the EM bias.

The capacitance wire wave gauge was used to measure the short wave modulation. The short wave RMS height was measured by calculating the energy in the high pass filtered wave gauge output. The wave gauge output was high pass filtered at 0.88 Hz corresponding to a two meter illuminated spot size (estimated using the linear deep-water dispersion relation of $\omega^2 = gk$.)

3.3 Results

The investigation of the effect of short wave modulation on

the bias is begun by first examining the relationships between the measured RMS short wave height and the back scatter coefficients. Figure 3.8 shows hourly averages of the C and Ku band relative back scatter coefficients, RMS short wave height, and wind speed. A visual examination reveals the back scatter coefficients decrease as the RMS short wave height increases and vice versa. This is easily explained by noting that a rougher surface will scatter less energy in the back scatter direction. It also establishes a correlation between the back scatter coefficients at C and Ku bands and short waves with wavelengths of the order of one meter and less.

Figure 3.9 shows a direct comparison between the scatter coefficients and the RMS short wave height. The solid curve represents the back scatter coefficient as computed using the physical optics integral of equation (3.9). The circles and triangles are measured C and Ku band back scatter coefficients respectively. An absolute calibration of the scatterometers was not possible because of a slow drift (8dB drift in the Ku band scatterometer and 15dB drift in the C band scatterometer for the six month period) in the RF electronics. Therefore, the measured back scatter coefficients have been adjusted by constant gains so as to fit the physical optics integral curve. The C band scatter coefficients were adjusted by one gain and the Ku band scatter coefficients by another gain.

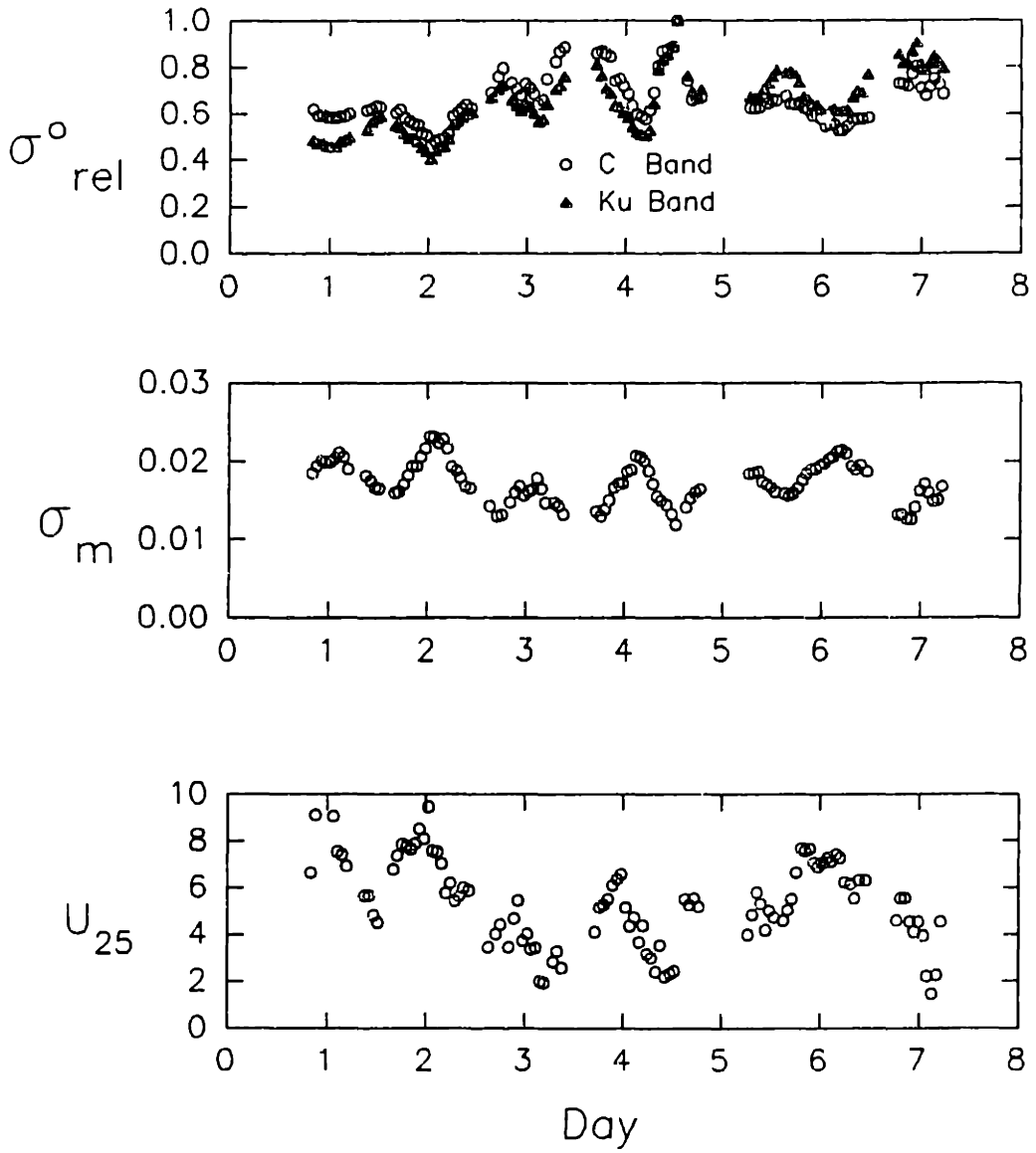

Figure 3.8: Time series of relative back scatter coefficient, short wave RMS height (m) and wind speed (m/s) recorded during the 7 days of the experiment.

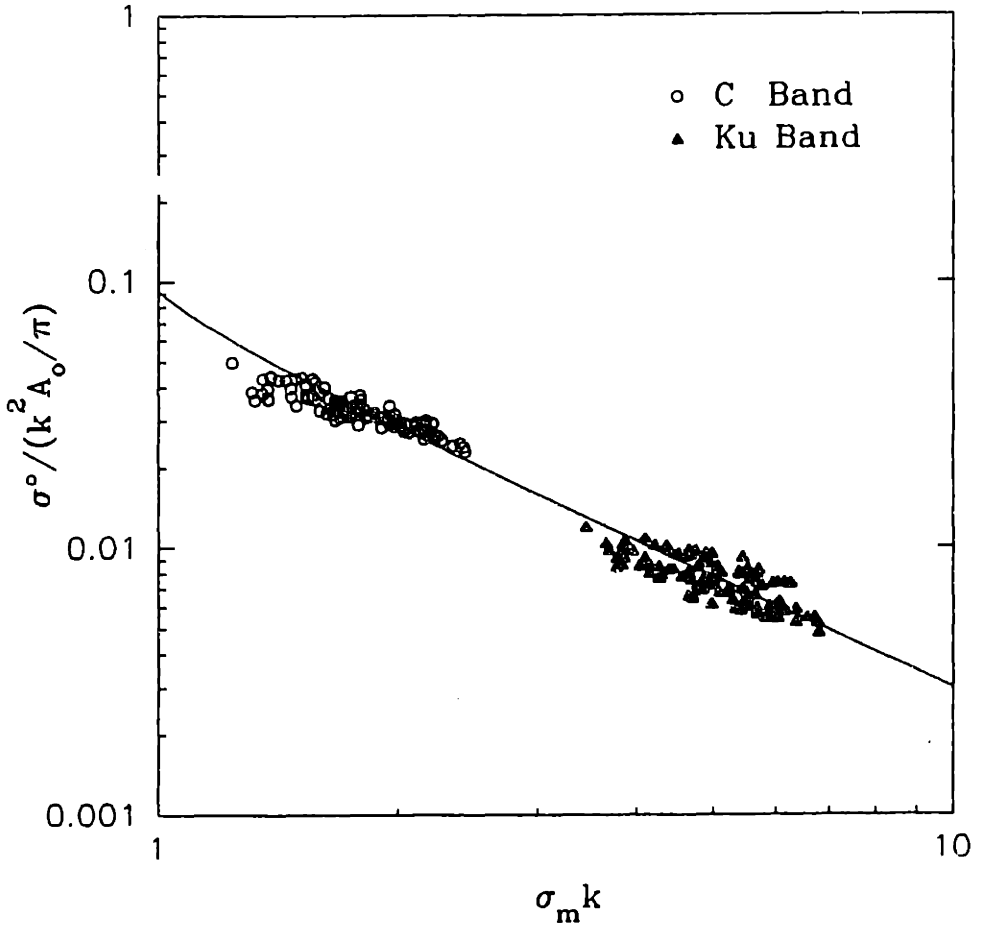

Figure 3.9: Back scatter coefficient as a function of $\sigma_m k$. The solid line was computed numerically using the physical optics integral of equation (3.9). The circles and triangles are measurements made using the scatterometers for σ° and the wire wave gauge for σ_m.

The measured scatter coefficients were approximately 10dB less then the predicted values. This is probably due to the assumption of a unidirectional surface. However, the bias does not depend on a constant gain difference in the back scatter power. It depends only on the relative relationship between the back scattered power and the wave displacement, because, as seen in equation (3.1), the bias is normalized by the mean back scattered power. Figure 3.9 shows a clear relationship between the back scatter coefficients and the RMS short wave height. The physical optics integral accurately represents the relative relationship between the Ku band back scatter coefficient and the short wave RMS height. The measured C band back scatter coefficient versus RMS short wave height has a slightly smaller slope, especially for smaller RMS short wave heights, than the physical optics integral estimate.

A correspondence between RMS short wave height and wind speed can also be seen in figure 3.8. An increase in wind speed causes a corresponding increase in short wave height. A direct comparison between the short wave height and wind speed is shown in figure 3.10. A fit to the data indicated by the solid line is given by

$$\sigma_m = 0.0116\ U_{25}^{0.24}. \qquad (3.24)$$

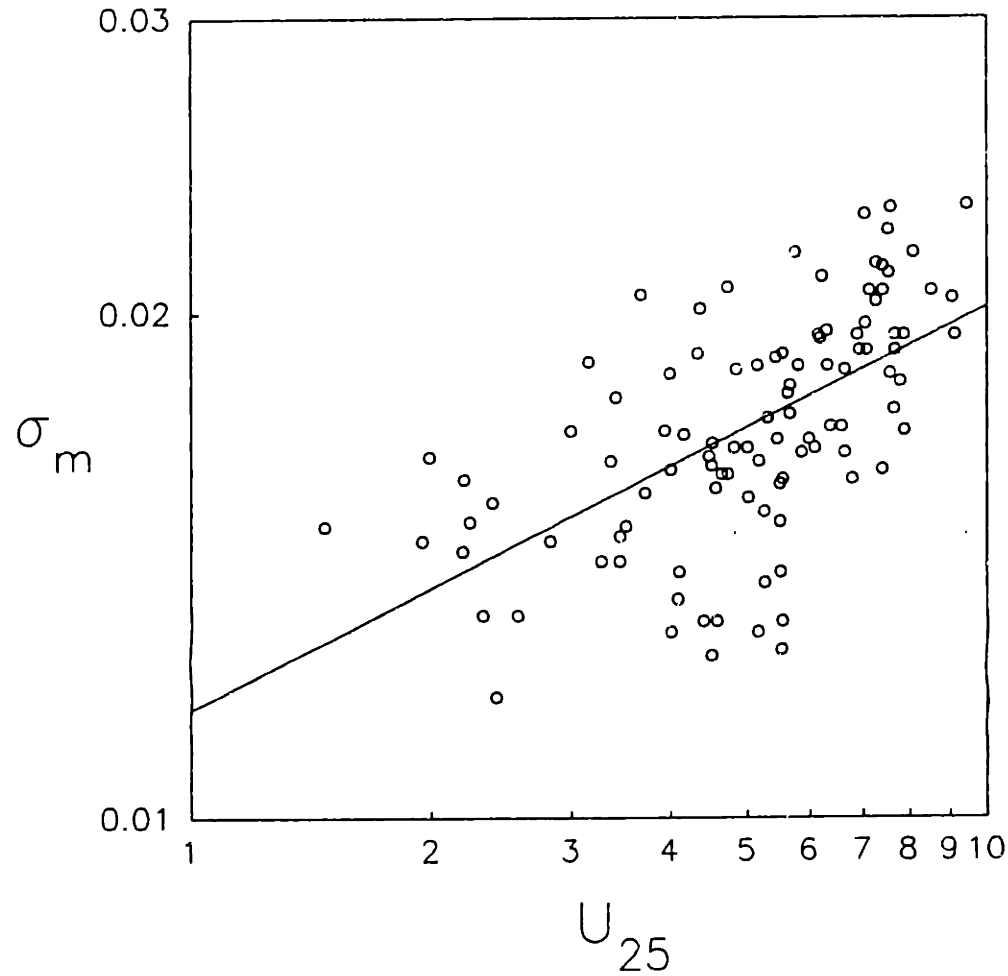

Figure 3.10: Short wave RMS height (m) as a function of wind speed (m/s). The solid line is given by equation (3.24).

Physical optics, the short wave model, and the preceeding expression can be used to estimate the relationship between the back scatter coefficient and the wind speed. The relationship between the back scatter coefficient and the RMS short wave height is given approximately by

$$\sigma^o = C_1 \sigma_m^{-\alpha} \tag{3.25}$$

where α is given by equation (3.23). For Ku band with p = 2.5, α was found to be 1.39 where the measured global short wave RMS height was 1.7 cm. Combining the last two equations gives

$$\sigma^o_{Ku} = C_2 U_{25}^{-0.33}. \tag{3.26}$$

The Ku band scatter coefficient versus wind speed is shown in figure 3.11. The solid line indicates the relationship given by the last equation, which agrees with the measurements. This result also agrees with measurements taken by *Melville et al.* [1991] during the SAXON-CLT experiment. They found

$$\log \sigma^o = 1.389 - 0.364 \log U_{10} \tag{3.27}$$

which is in close agreement. *Chelton and McCabe* [1985] found

$$\log \sigma^o = 1.502 - 0.468 \log U_{10} \tag{3.28}$$

based on an analysis of satellite altimetry data from Seasat.

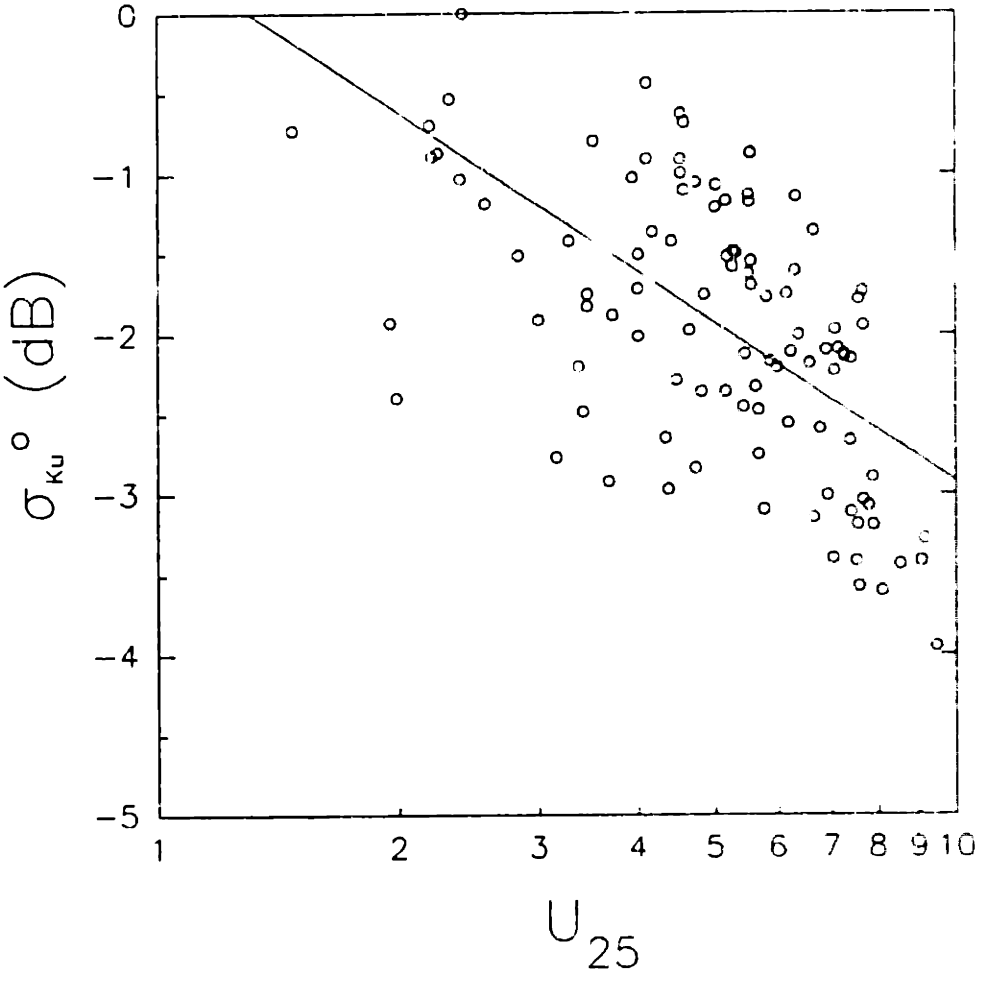

Figure 3.11: Ku band back scatter coefficient as a function of wind speed (m/s). The solid line is given by equation (3.26).

The difference from *Chelton and McCabe's* [1985] result may be due to the small number of samples at low wind speeds as noted in *Melville et al.* [1991].

Now that a relationship between scatter coefficient and RMS short wave height has been established, the effect of short wave modulation will be investigated. We begin by examining in detail two ten minute data records. One record corresponds to a large bias and the other to a small bias.

For the large bias record, a thirty second time series of measured wave displacement is shown in figure 3.12, along with the envelope of the short waves (frequency > 0.88 Hz). A visual inspection shows the short wave amplitude being modulated by the long wave displacement. The short waves are clearly larger at the crests of the long waves than in the troughs.

The modulation can also be seen by looking at the RMS short wave height versus the long wave displacement as in figure 3.13. It is seen that within two standard deviations of the mean sea level, the modulation appears to be linear with wave displacement.

The relative back scatter coefficient profile can be estimated

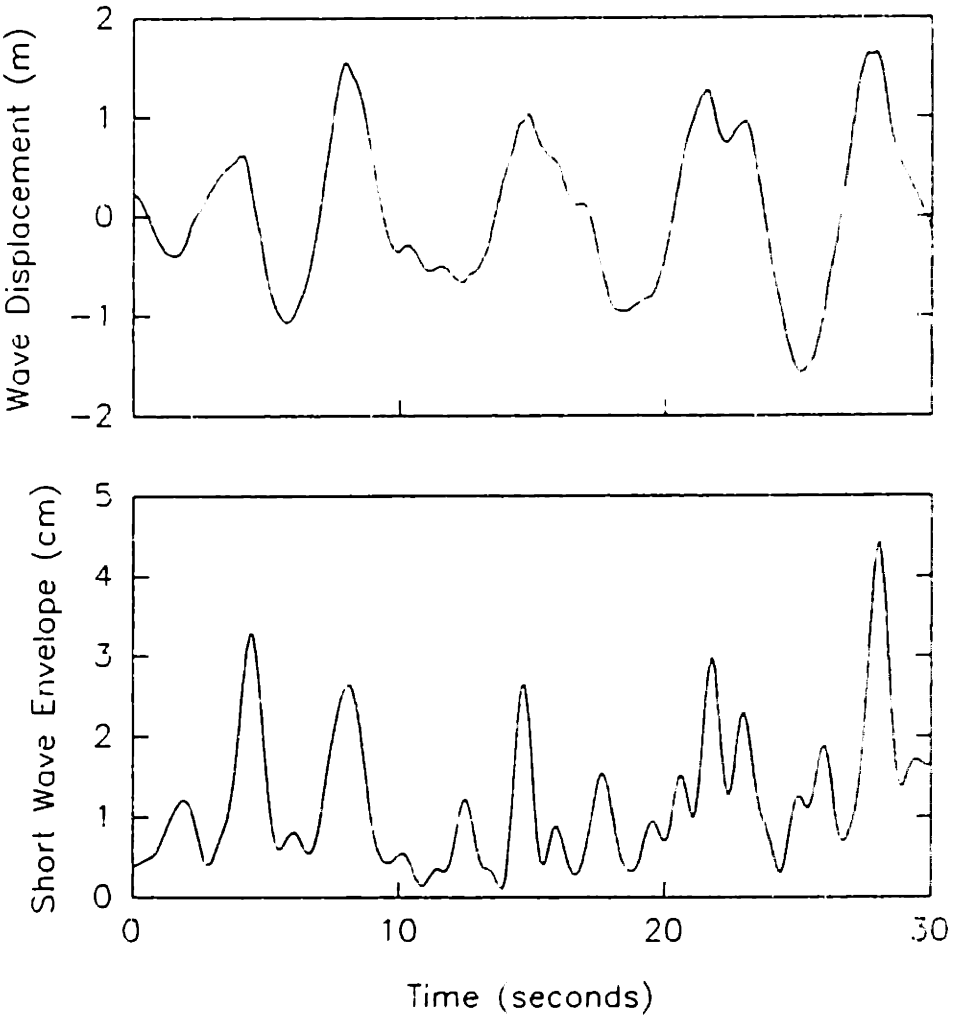

Figure 3.12: Time series of long wave displacement and short wave envelope for a large EM bias case.

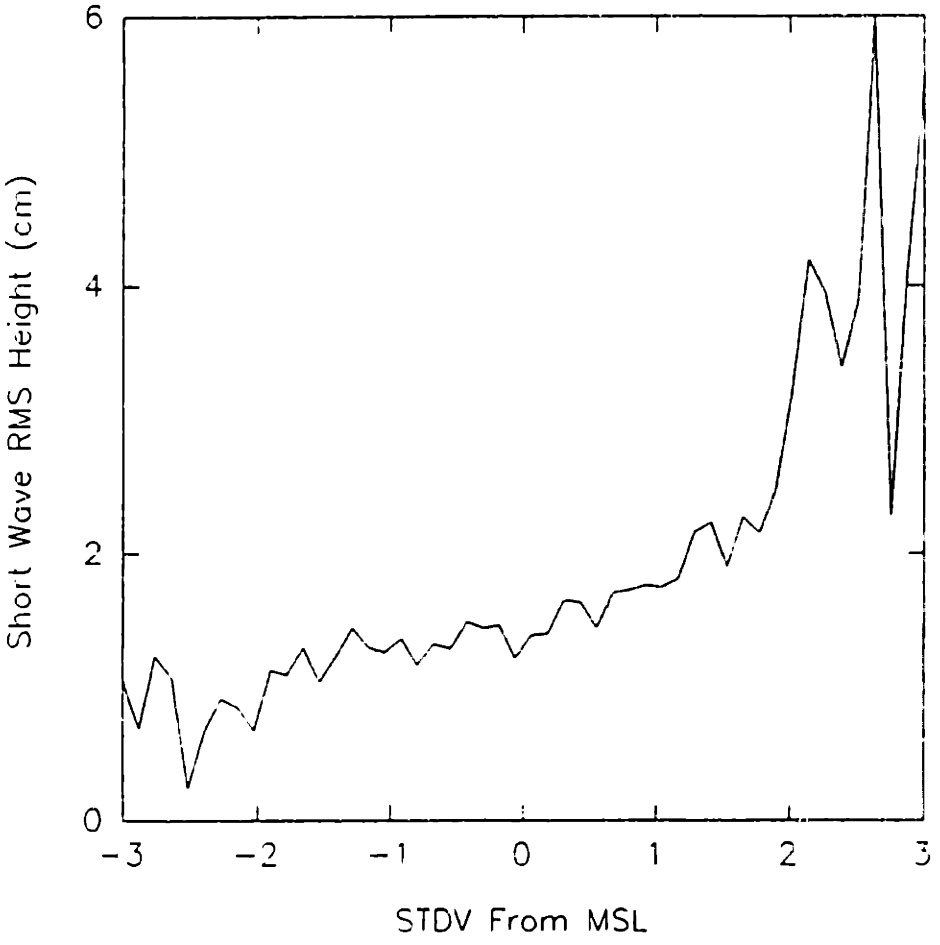

Figure 3.13: Short wave RMS height as a function of surface displacement from mean sea level in standard deviations for a large EM bias case.

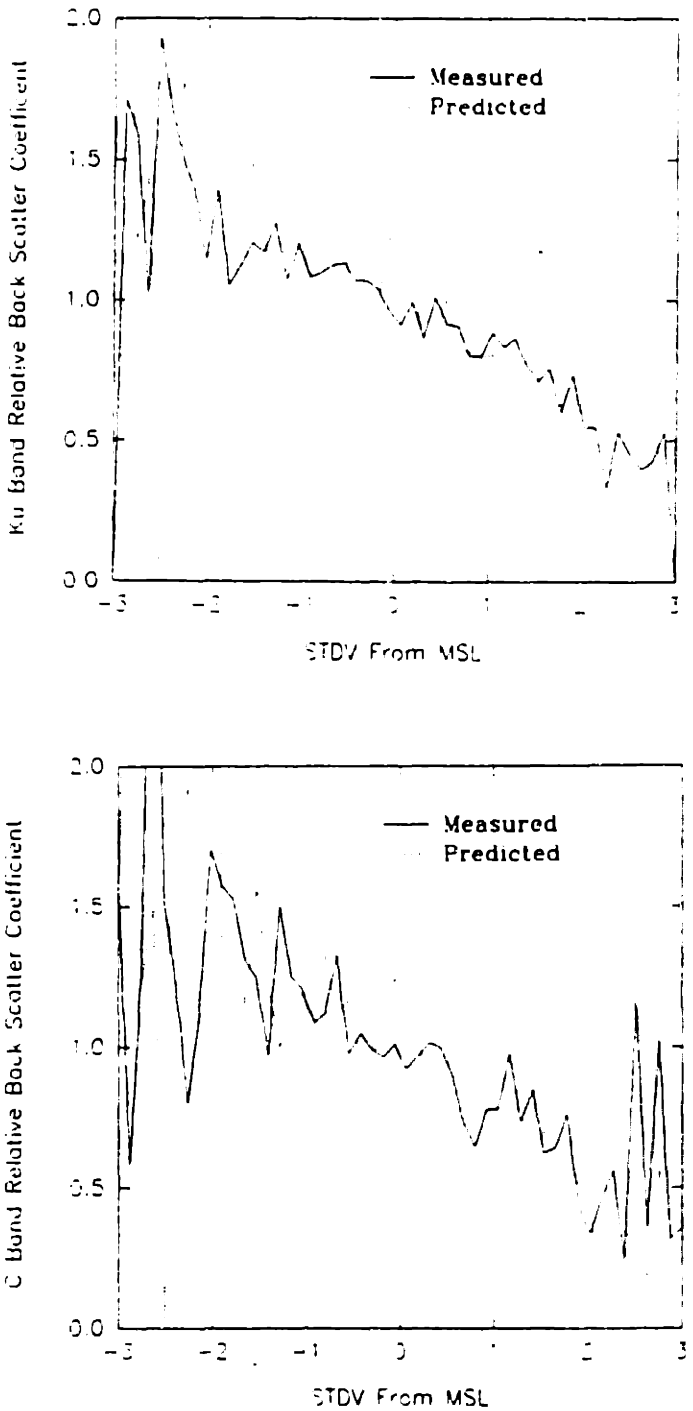

Figure 3.14: Ku band (top) and C band (bottom) relative back scatter coefficient as a function of surface displacement from mean sea level in standard deviations for a large EM bias case. The solid curves were measured. The dashed curves were estimated using physical optics scattering and the measured short wave RMS height profile.

from the short wave modulation profile by using the physical optics integral of equation (3.9) and the short wave model of section 3.1.1. The estimated and measured relative back scatter coefficient profiles for C and Ku bands are shown in figure 3.14. The estimated profiles show that the short wave modulation correctly predicts more scatter from the troughs of the long waves than the crests, which is in good agreement with the measured profiles.

To provide a contrast, figure 3.15 shows the envelope of the short waves for a time of small bias. It is no longer clear from a visual inspection that modulation is occuring, but an examination of figure 3.16 giving the corresponding short wave height versus long wave displacement again shows a modulation. The modulation is smaller, as expected, and continues to be linear within two standard deviations of the mean sea level. The estimated scatter coefficient profile, as shown in figure 3.17 for Ku band, again provides a reasonable estimate of the measured profile.

As noted above, the short wave modulation can be represented by a linear profile as given in equation (3.18). This allowed the modulation strength, defined as $M = m/4$ where m is defined in equation (3.18), to be computed for each remaining record for the 7 days of the experiment. The modulation strength is

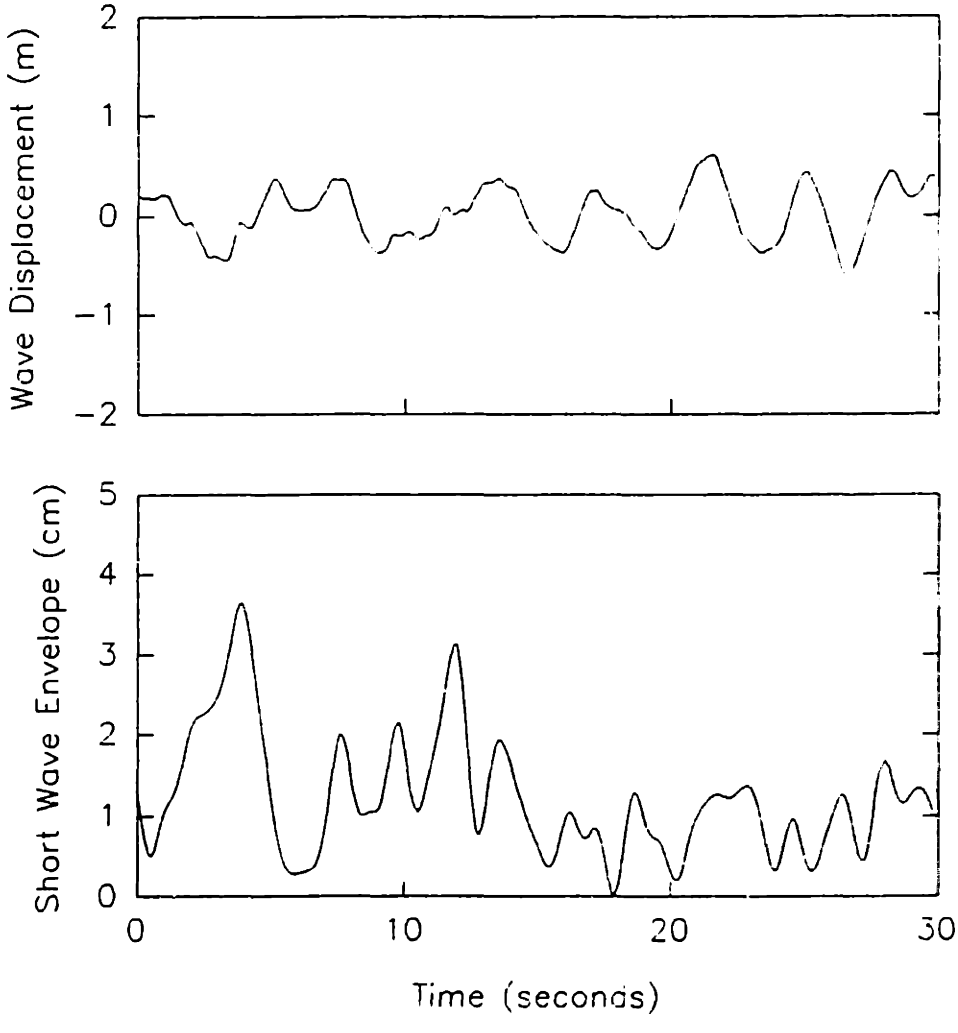

Figure 3.15: Time series of long wave displacement and short wave envelope for a small EM bias case.

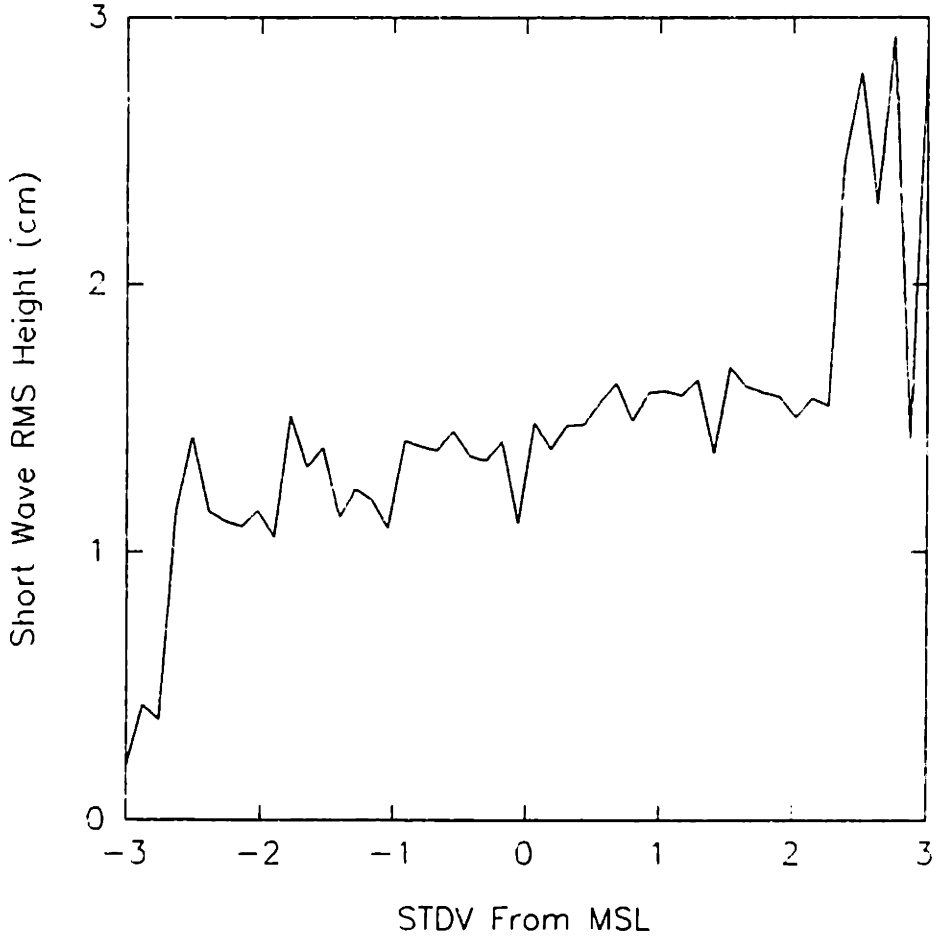

Figure 3.16: Short wave RMS height as a function of surface displacement from mean sea level in standard deviations for a small EM bias case.

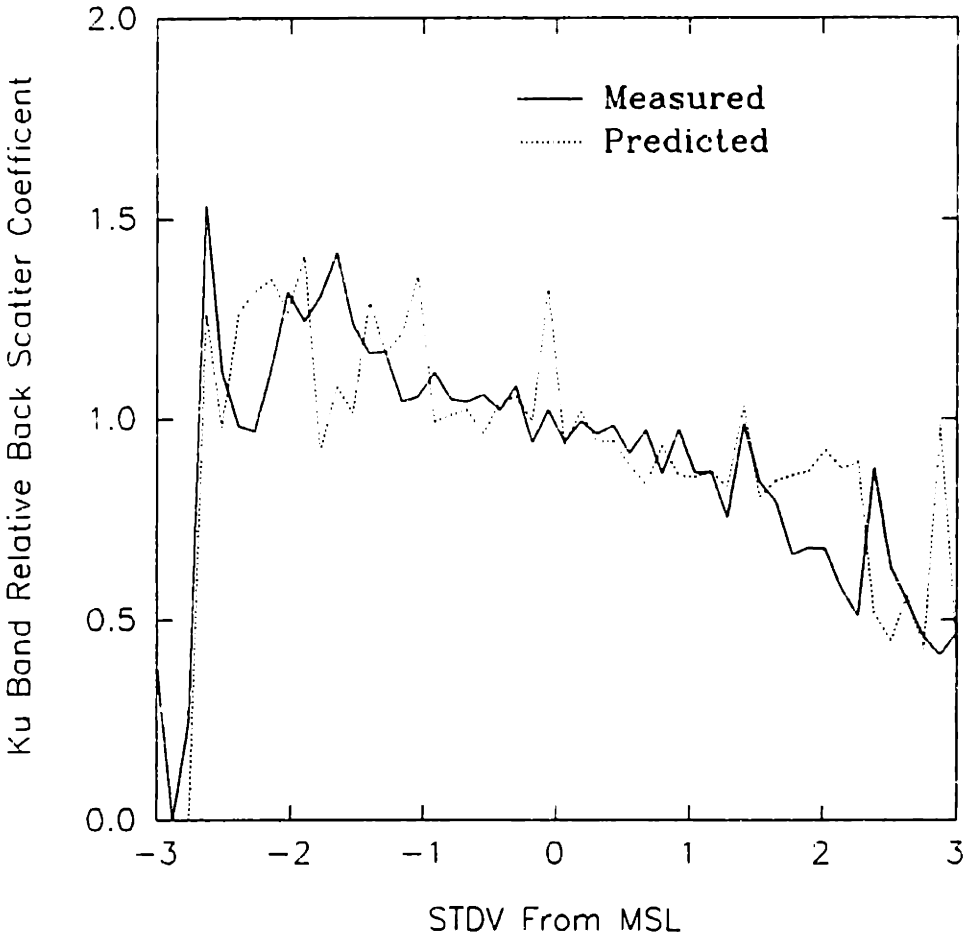

Figure 3.17: Ku band relative back scatter coefficient as a function of surface displacement from mean sea level in standard deviations for a small EM bias case. The solid curve was measured. The dashed curve was estimated using physical optics scattering and the measured short wave RMS height profile.

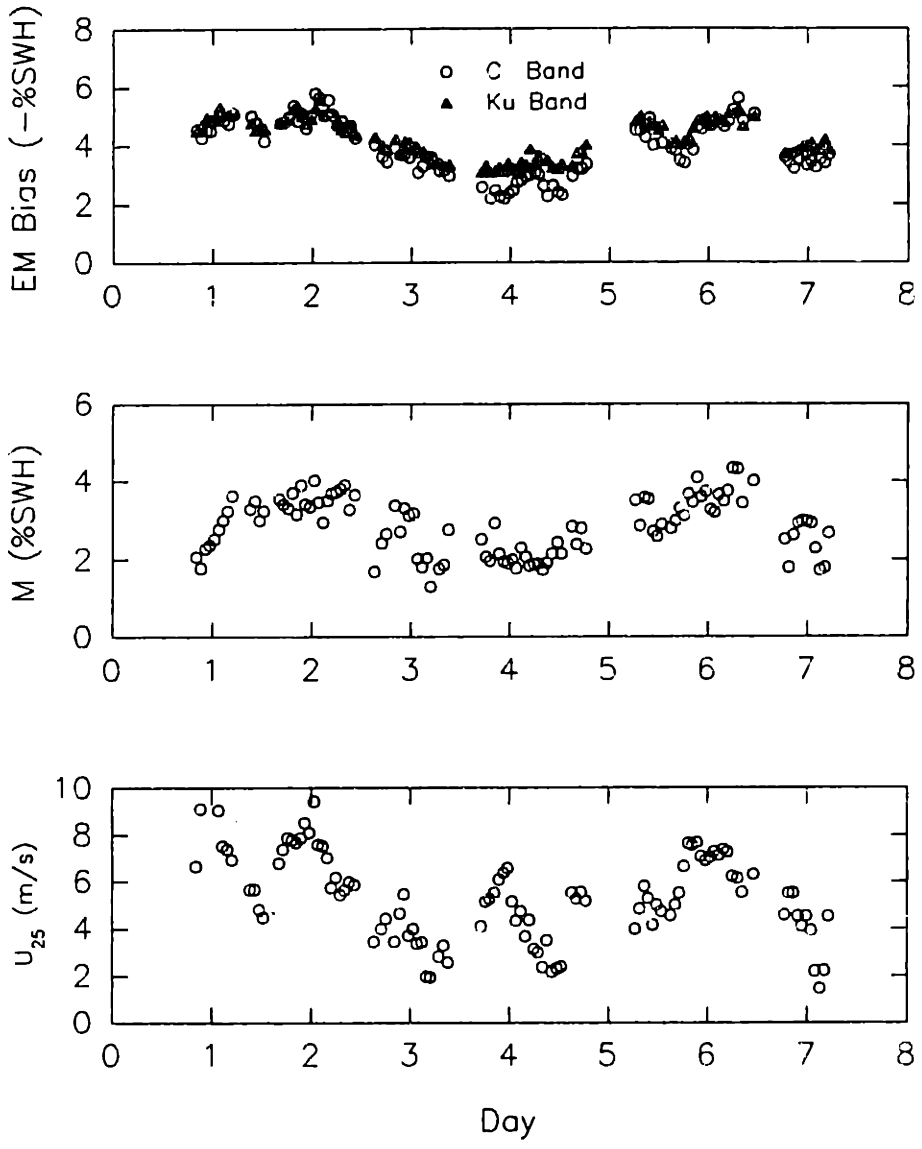

Figure 3.18: Time series of normalized electromagnetic bias, short wave modulation strength, and wind speed (m/s) recorded during the 7 days of the experiment.

measured using the wire wave gauge and is measured independently from the scatterometer measurements. Hourly averages of the modulation strength and normalized bias are shown in figure 3.18. It is easily observed that the normalized bias increases as the modulation strength increases. The bias is given by equation (3.22) in terms of the short wave modulation, which can be rewritten in terms of the significant wave height as

$$\epsilon = -\alpha M H_{\frac{1}{3}}. \qquad (3.29)$$

This shows the normalized bias is proportional to the modulation strength as observed in figure 3.18.

As seen in figure 3.18, the normalized bias and modulation strength are correlated with wind speed. However, at low wind speeds near days 3 and 7, the modulation strength has sudden drops, and the corresponding short wave modulation profiles become more random. This probably indicates that, at low wind speeds, the dominant scatterers are waves with lengths less than one meter. The cause of the differences between the bias and modulation strength at the beginning of day one is not known. The modulation strength and C and Ku band biases are shown versus wind speed in figures 3.19 and 3.20. A visual inspection shows a similar correlation of the modulation and the bias with the wind speed.

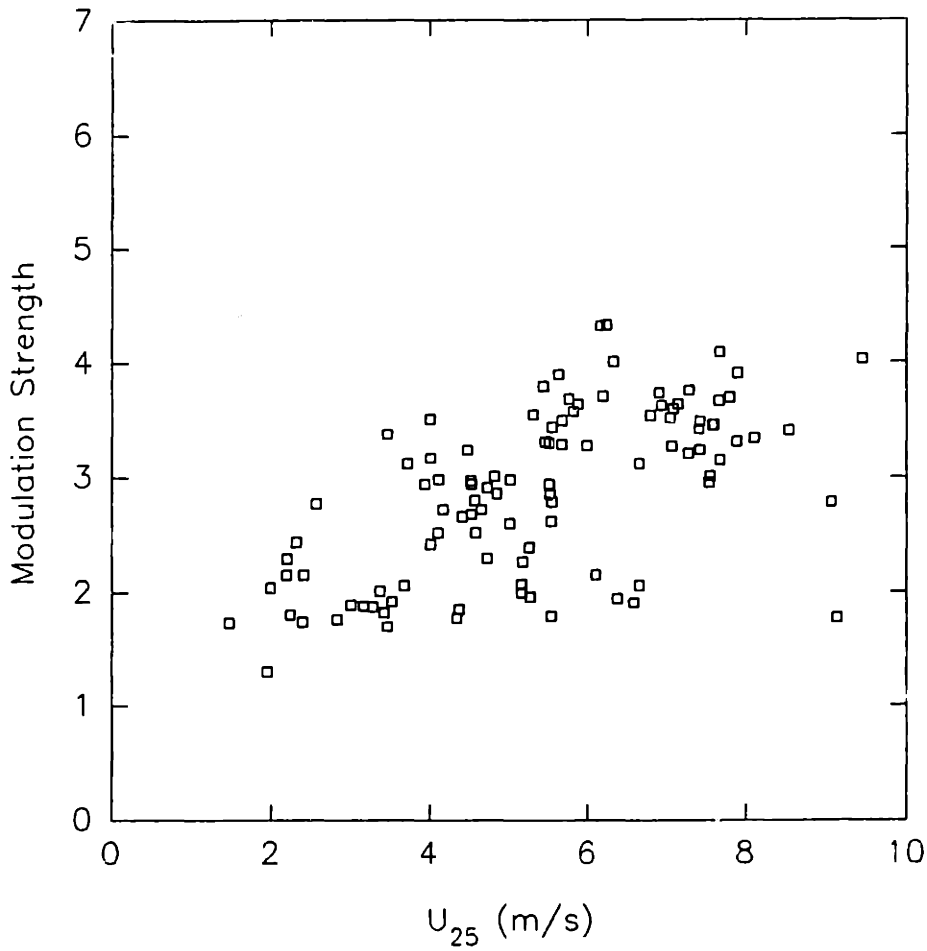

Figure 3.19: Short wave modulation strength as a function of the wind speed (m/s).

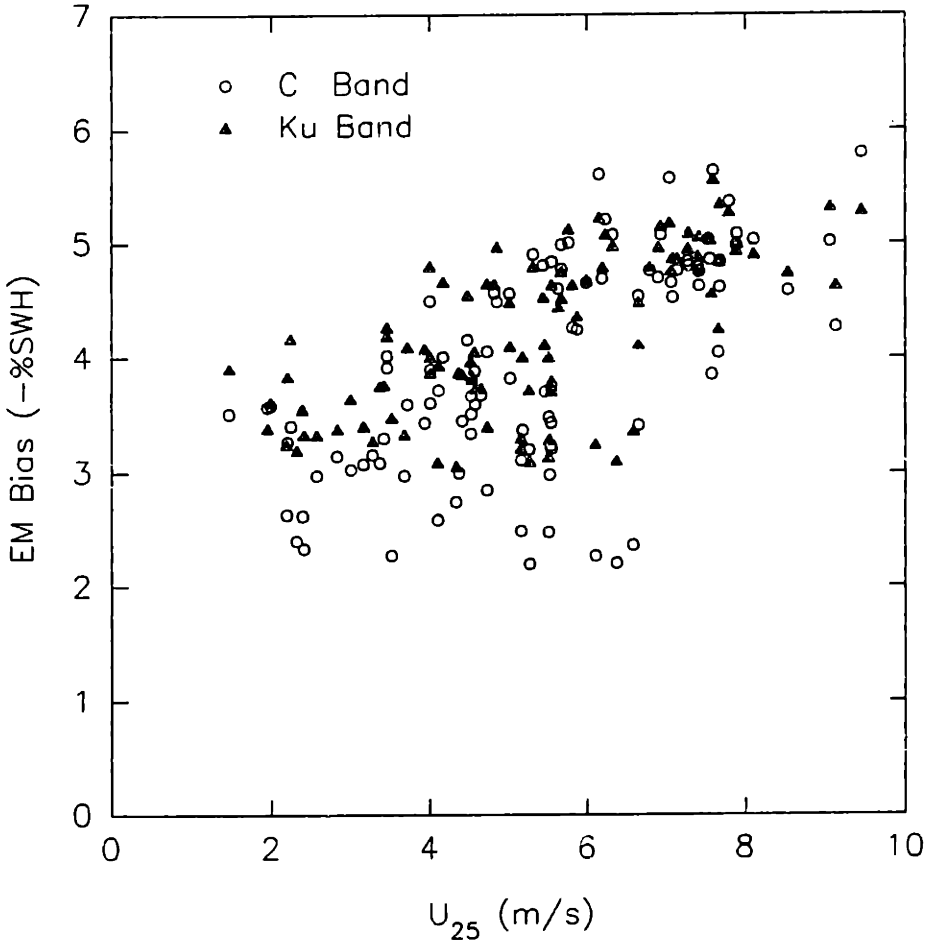

Figure 3.20: Normalized electromagnetic bias as a function of wind speed (m/s).

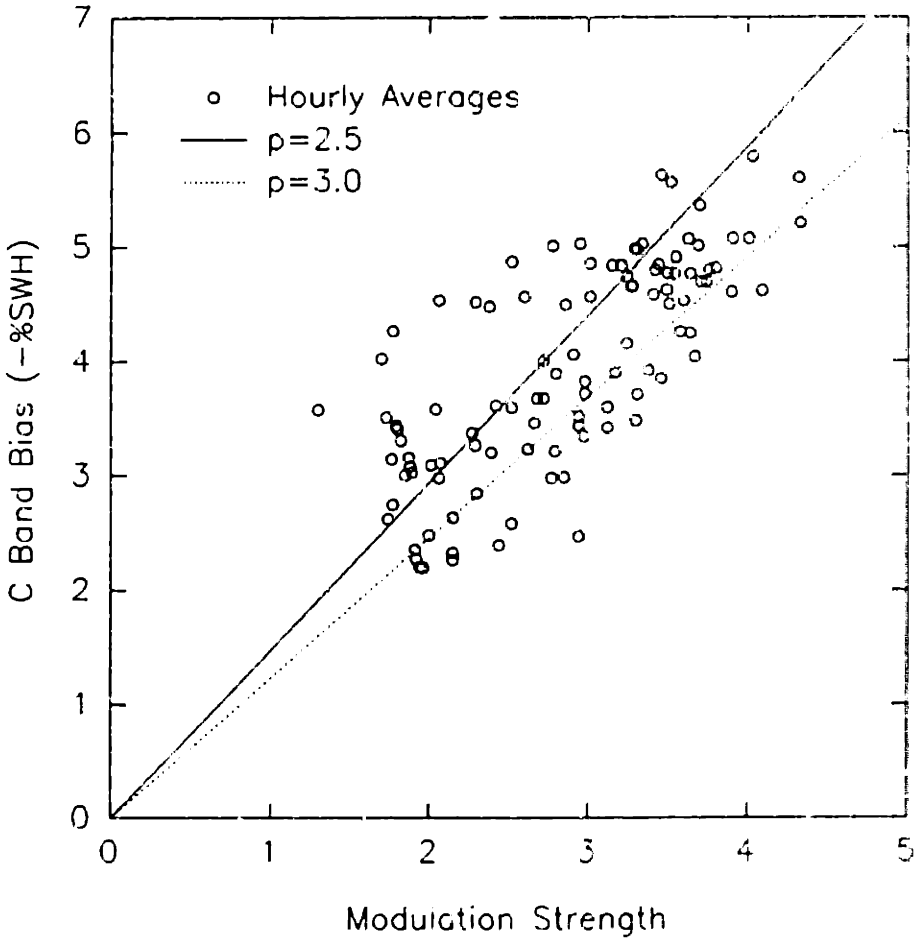

Figure 3.21: C band normalized electromagnetic bias as a function of short wave modulation strength. The lines show the ideal dependence of the bias on the modulation strength (see the text for details).

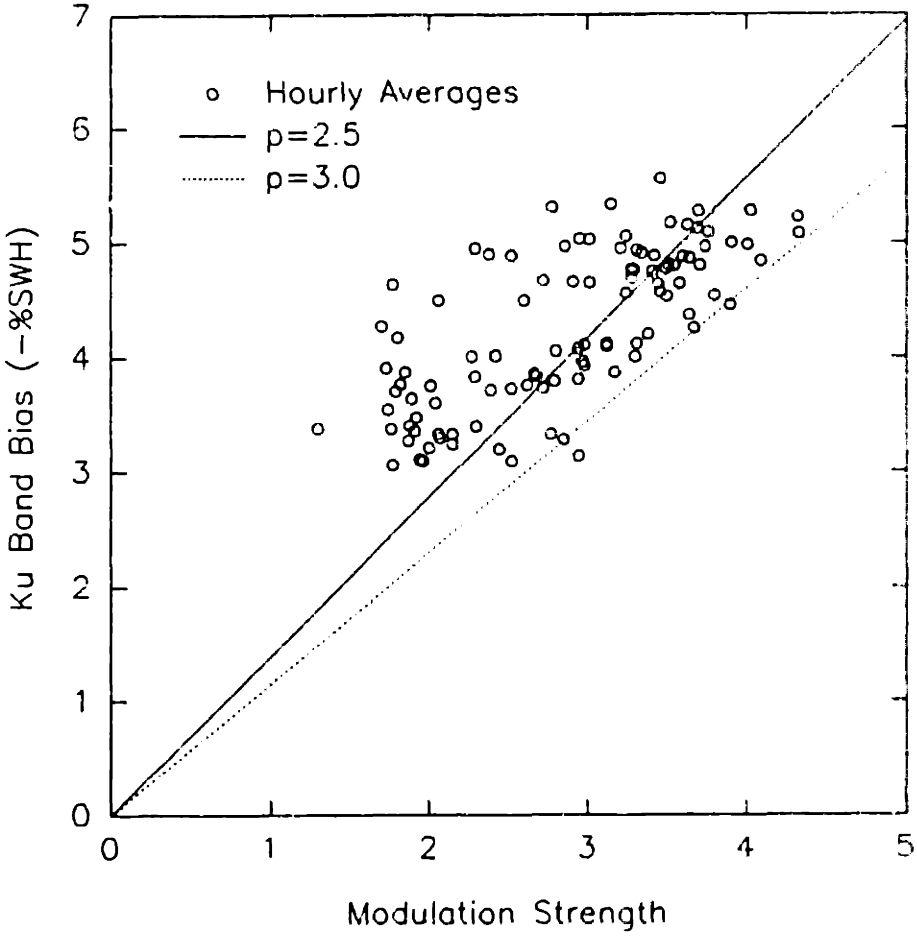

Figure 3.22: Ku band normalized electromagnetic bias as a function of short wave modulation strength. The lines show the ideal dependence of the bias on the modulation strength (see the text for details).

The C band bias versus modulation strength is shown in figure 3.21. The normalized bias appears to be a linear function of the modulation strength as predicted by equations (3.22) and (3.29). The constant α_c for 1.7 cm global RMS short wave height (the average, short wave RMS height for the 7 days of data) is 1.47 and 1.23 for p = 2.5 and 3.0 respectively. The lines in figure 3.21 show the ideal dependence of the bias on modulation strength according to equation (3.29) and the stated values of α_c. Figure 3.22 shows the Ku band bias versus the modulation strength. The lines in figure 3.22 correspond to α_{Ku} = 1.39 and 1.15 for p = 2.5 and 3.0 respectively. Some of the scatter in figures 3.21 and 3.22 is due to the sudden drops in the modulation strength at low wind speeds noted earlier.

Hourly averages of significant wave height, wind speed and measured and estimated bias are shown in figure 3.23. The estimated biases were computed from equation (3.29), equation (3.23), and the measured modulation strength. The estimated bias is in good agreement with the measured bias except near the beginning of days 1, 3 and 7, which is due to the difference in modulation strength as noted earlier.

A more direct comparison of the estimated and measured bias is shown in figure 3.24. The Ku bias is underestimated for low

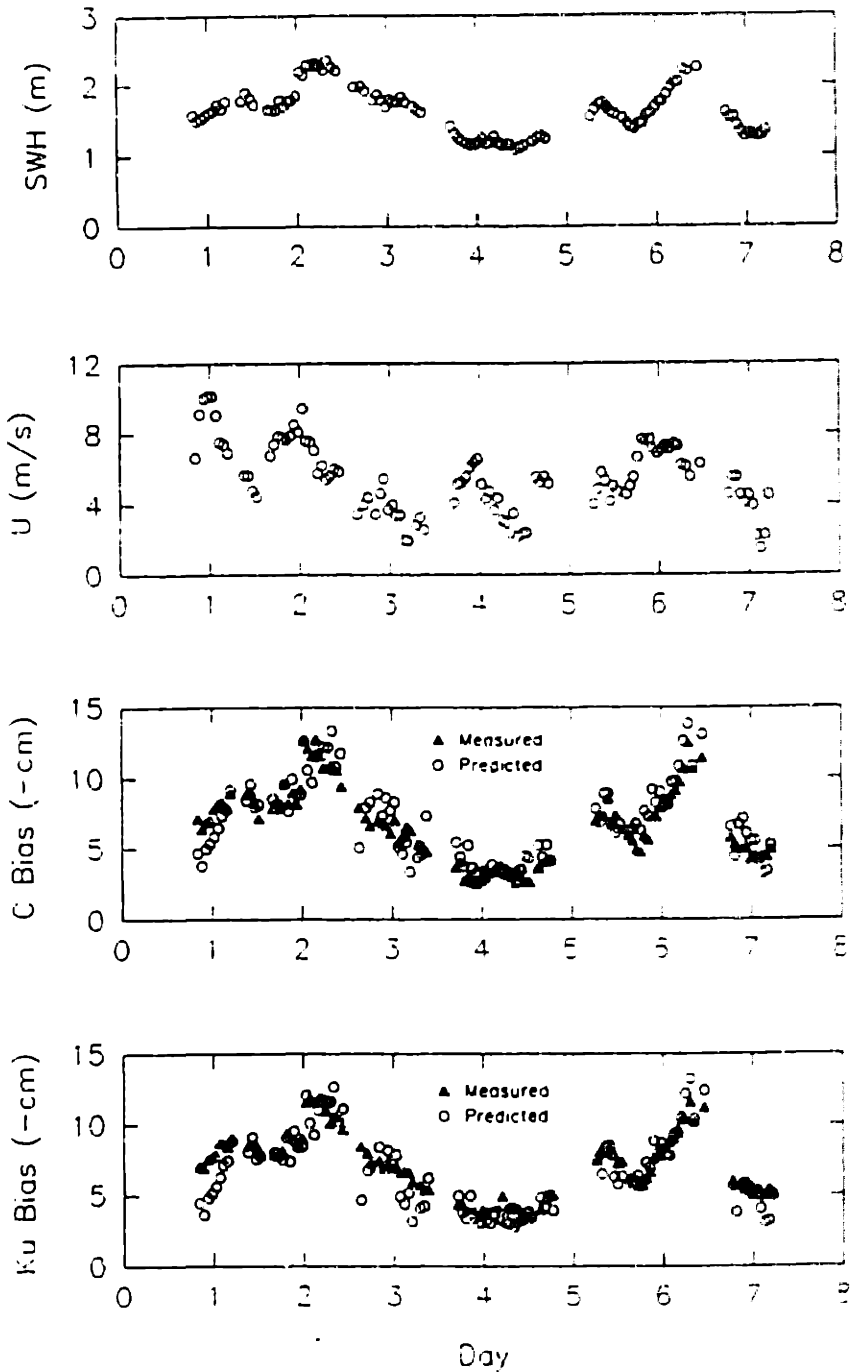

Figure 3.23: Time series of significant wave height, wind speed, and C and Ku band biases for the 7 days of the experiment. The predicted electromagnetic bias is found using the short wave modulation strength and equations (3.23) and (3.29).

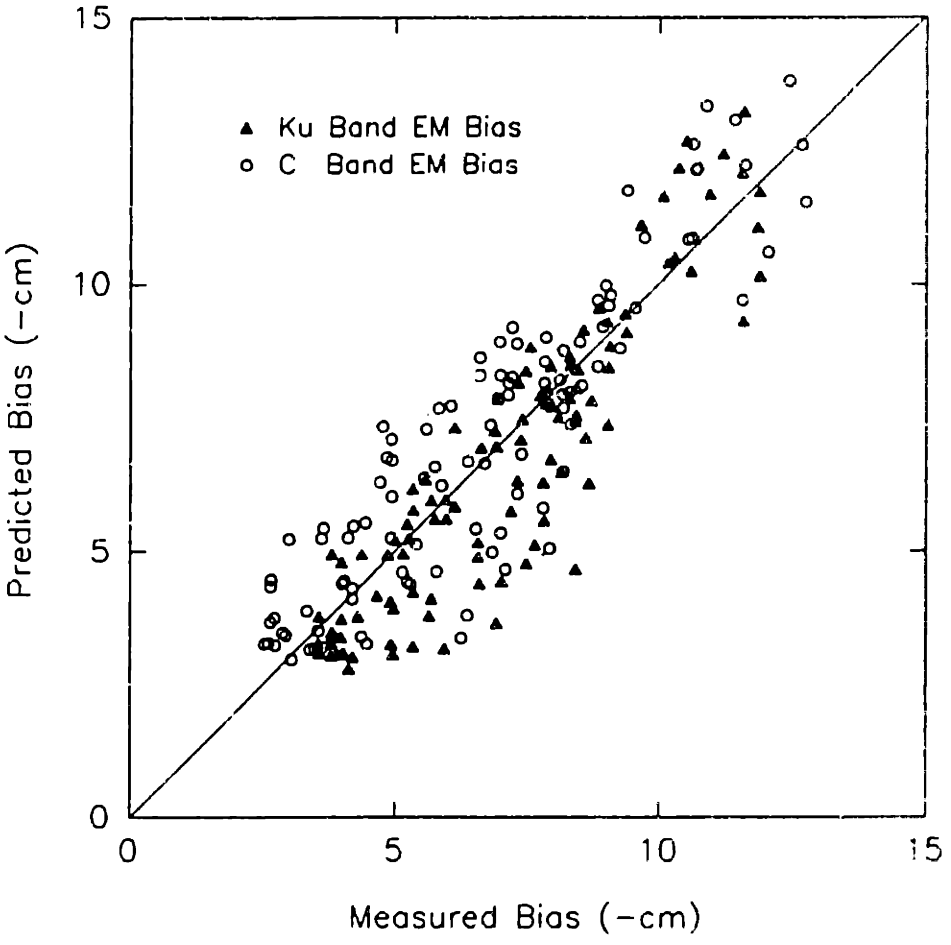

Figure 3.24: A comparison of the measured and predicted electromagnetic biases. The predicted bias is found using the short wave modulation strength and equations (3.23) and (3.29).

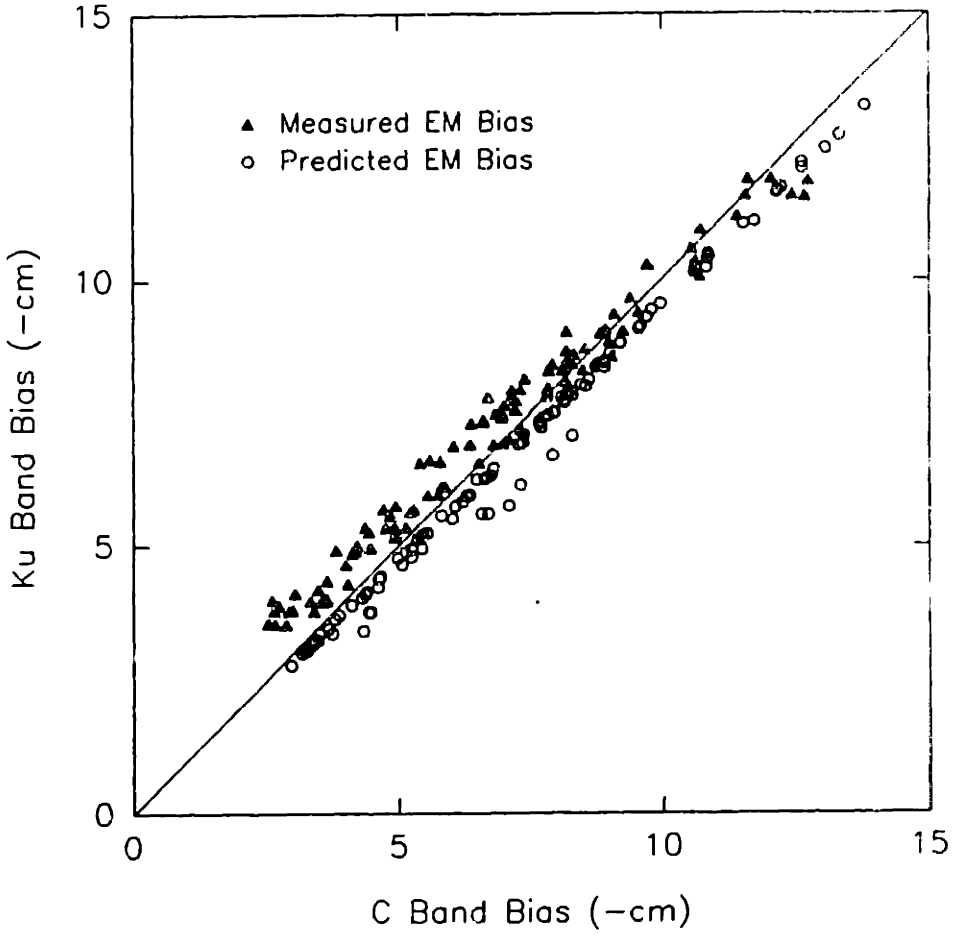

Figure 3.25: A comparison of the Ku and C band electromagnetic biases. The predicted bias is found using the short wave modulation strength and equation (3.23) and (3.29).

values of bias. This is at least partly due to the low modulation strength at low wind speeds as noted earlier.

The C band versus Ku band bias is shown in figure 3.25. As found earlier in chapter 2, the Ku band bias is larger than the C band bias for small values of bias and smaller for large values of bias. The biases, as predicted from the modulation strength, show the C band bias to be slightly larger than the Ku bias. The differences between the measured and predicted biases are partly explained by figure 3.9. The parameter α is the local slope of σ° versus $\sigma_m k$. The Ku band data is accurately represented by the physical optics integral of equation (3.9) indicated by the solid line, but the C band data has a smaller slope. This causes the physical optics scattering theory and the short wave modulation model to overestimate the C band bias at small short wave heights which correspond to small biases.

3.4 Discussion

The validity of using physical optics scattering for the employed short wave spectrum was established by comparison with method of moment calculations as shown in figures 3.4 and 3.5. The relationship between the high frequency wave energy and the back scatter coefficient as described by equation

(3.9) was established by the results shown in figures 3.8 thru 3.11. This led to the most fundamental result of this research, namely, the prediction of the electromagnetic bias based on the modulation of the short waves.

The effect of the short wave modulation on the bias is shown in figures 3.12 thru 3.18. These results show the short wave modulation to be the dominant cause of the electromagnetic bias at C and Ku bands for moderate wind and wave conditions. The results of figures 3.21 and 3.22 show a linear dependence of the normalized bias on short wave modulation strength. The observed linear dependence is described by the theoretical bias of equation (3.29).

The EM bias at C and Ku bands was found to depend on wave height and wind speed by *Melville et al.* [1991] and *Walsh et al.* [1991], where the dependence was found empirically to be of the form

$$\frac{\epsilon}{H^{\frac{1}{3}}} = a_0 + a_1 U + \ldots \qquad (3.30)$$

The results of this paper show the cause of these observed dependencies. From equation (3.29) the normalized bias is given by

$$\frac{\epsilon}{H_{\frac{1}{3}}} = -\alpha M. \qquad (3.31)$$

As indicated in figures 3.18, 3.19, and 3.20, the short wave modulation strength has the same dependence on wind speed as the observed normalized bias. Thus, the dependence of the bias on wave height and wind speed can be attributed to the short wave modulation.

The frequency dependence of the EM bias has only been partially addressed. A better explanation probably lies in a better short wave modulation model.

The employed short wave modulation model contains no dependence on wave number. This is clearly an oversimplification. For example, consider the measurements of EM bias at ultraviolet by *Walsh et al.* [1989]. They found the UV EM bias to be biased above mean sea level rather than below, as in the case of microwave frequencies. This implies that the modulation of short capillary waves is opposite in sign to the modulation of short gravity waves. The much smaller Ka band bias as measured by *Walsh et al.* [1989, 1991] might also imply a decrease in modulation with increasing wave number, causing a larger decrease in bias with increasing electromagnetic frequency.

Other limitations of this work include the spectral model employed, the neglect of long wave tilt and curvature and the unidirectional wave assumption. Figures 3.21 and 3.22 show the sensitivity of the bias to the choice of the power spectrum exponent in k^{-p}. The long wave tilt and curvature will have the effect of increasing the bias. The possible effects of the long wave curvature were discussed in chapter 2. The effect of the long wave tilt will be discussed below. The unidirectional wave assumption could cause an underestimation of the bias. In the high frequency limit σ^o is inversely proportional to the standard deviation and variance of the surface height respectively for a unidirectional and isotropic surface. For small modulation strengths this will cause the bias for an isotropic surface to have twice the bias as a unidirectional surface.

In light of the results presented in this paper two concerns are raised in the theoretical EM bias papers of *Jackson* [1979], *Huang* [1984], *Barrick and Lipa* [1985] and *Srokosz* [1986]. First, the spectral filter function used by those studies is of questionable validity. The common practice of equally weighting waves having wave number less than the electromagnetic wave number, may lead to overemphasizing the high frequency waves as indicated in figure 3.5. Second, since these theories depend on the joint height slope

probability density function, the development of this function should include the effect of the short wave modulation.

There are several differences between this work and the theoretical bias paper of *Rodriguez et al.* [1992]. First and most important is the difference between the measured dependence of the bias on short wave modulation and that predicted by *Rodriguez et al.* Figure 3.18, 3.21, and 3.22 of this work show that the observed normalized bias increases with short wave modulation strength. However, figures 4 and 9d of *Rodriguez et al.* (see figures 1.6 and 1.7), show the normalized bias remaining the same or decreasing with increasing short wave modulation strength.

The conclusion of *Rodriguez et al.*, concerning the cause of the wind speed and frequency dependence of the bias, is also different from this work. They found the wind speed dependence to be due to the increased modulation of large surface tilt as a function of wind speed, and the frequency dependence of the EM bias was explained in terms of the sensitivity of radar cross section to surface tilt and the modulation of tilt variance. This work has explained both the wind speed and frequency dependence of the bias in terms of the short wave modulation. The experimental evidence shown indicates that the model presented in this work gives better

agreement with measured data at C and Ku bands than does the model of *Rodriguez et al.* However, a combination of the two theories would likely lead to a better result.

Chapter 4

Summary

It has been shown from measurements that the electromagnetic bias depends primarily upon the wave height, the wind speed and the electromagnetic frequency. All of the EM bias experiments to date have shown a linear dependence of the bias on wave height.

The measurements of the present work, *Melville et al.* [1991], and *Walsh et al.* [1991] have shown a similar dependence of normalized bias on wind speed. For wind speeds less than 10 m/s the measured bias increases linearly with wind speed. At wind speeds above 10 m/s the bias saturates in the case of C band, and saturates and then decreases in the case of Ku band. The more extensive data set of the present work shows the Ku band bias saturating at 9-10 m/s, whereas the C band bias saturates at 11-12 m/s.

The tower measurements of the present work and *Melville et al.* [1991] exhibit two differences from the aircraft measurements of *Walsh et al.* [1991]. First, for the wind speed less than 3-4 m/s the tower measurements show the bias to be constant,

whereas the aircraft measurements show bias continuing to decrease for wind speeds less than 3-4 m/s. Second, the measurements of *Melville et al.* [1991] show a bias nearly a constant 1% of significant wave height larger than the aircraft measurements of *Walsh et al.* [1991], and the measurements of the present work show a bias nearly a constant 0.3% of significant wave height larger than the measurements of *Melville et al.* [1991]. This difference may be due to the different heights from the surface at which the measurements were taken as explained in chapter 2.

All of the EM bias experiments to date have shown a general increase in bias with decreasing frequency. The measurements of the present work show the C band bias to be larger than the Ku band bias for wind speeds greater than 10 m/s, but for wind speeds less than 10 m/s the Ku band bias is larger than the C band bias.

The measurements of the short wave modulation and the theory of chapter 3 demonstrated a linear dependence of the normalized bias on the short wave modulation strength. The fact that the short wave modulation strength was shown to have the same dependence on the wind speed as the normalized bias shows that the wind speed dependence of the bias is mostly accounted for by the short wave modulation. While other

effects such as long wave tilt and curvature will effect the bias, the primary cause of the EM bias has been shown to be due to the short wave modulation. The main weakness of the theory of chapter 3 was its simple model for the short wave modulation. There is evidence of a wave number dependence of the short wave modulation which would likely explain the frequency dependence of the EM bias.

Now that the primary dependencies and causes of the EM bias have been identified, the second order effects need to be explored. The effect of the long wave tilt and curvature, and the directionality of the waves should be included in the theory of chapter 3. A better model for the short wave modulation would greatly improve the electromagnetic frequency dependence prediction capability of the theory of chapter 3. While analyzing the measured EM bias, the normalized bias was found to be larger during periods of wave growth, indicating a dependence on the wave development. This effect should be fully investigated.

Appendix A

Measurements of Electromagnetic Bias in Radar Altimetry[1]

The accuracy of satellite altimetric measurements of sea level is limited in part by the influence of ocean waves on the altimeter signal reflected from the sea surface. The difference between the mean reflecting surface and mean sea level is the electromagnetic bias. The bias is poorly known, yet for such altimetric satellite missions as the Topography Experiment (TOPEX)/Poseidon it is the largest source of error exclusive of those resulting from calculation of the satellite's ephemeris. Previous observations of electromagnetic bias have had a large, apparently random scatter in the range of 1-5% of significant wave height; these observations are inconsistant with theoretical calculations of the bias. To obtain a better understanding of the bias, we have measured it directly using a 14-GHz scatterometer on the Chesapeake Bay Light Tower. We find that the bias is a

---

[1]This paper,"Measurements of electromagnetic bias in radar altimetry," by W. K. Melville, R. H. Stewart, W. C. Keller, J. A. Kong, D. V. Arnold, A. T. Jessup, M. R. Loewen and A. M. Slinn was published in *Journal of Geophysical Research*, Vol. 96, pp. 4915-4924, in March 1991.

quadratic function of significant wave height $H_{1/3}$. The normalized bias β, defined as the bias divided by the significant wave height, is strongly correlated with wind speed at 10 m, U_{10}, and much less strongly with significant wave height. The mean value for β is -0.034, and the standard deviation of the variability about the mean is ±0.0097. The standard deviation of the variability after removing the influence of wind and waves is ±0.0051 = 0.51%. The results are based on data collected over a 24-day period during the Synthetic Aperture Radar and X-Band Ocean Nonlinearities (SAXON) experiment from September 19 to October 12, 1988. During the experiment, hourly averaged values of wind speed ranged from 0.2 to 15.3 m/s, significant wave height ranged from 0.3 to 2.9 m, and air minus sea temperature ranged from -10.2° to 5.4°C. Because U_{10} can be calculated from the scattering cross section per unit area σ_o of the sea measured by spaceborne altimeters, we investigated the usefulness of σ_o for calculating bias. We find that β is strongly correlated with σ_o and much less strongly with $H_{1/3}$. The standard deviation of the variability after removing the influence of the radio cross section and waves is ±0.0065 = 0.65%. The results indicate that electromagnetic bias in radar altimetry may be reduced to the level required by the TOPEX/Poseidon mission using only altimetric data. We find, furthermore, that the relationship between σ_o and wind speed agrees with

previously published power law relationships within the accuracy of the measurement. The mean value of β, its variability, and the sensitivity of β to wind speed all agree well with previous measurements made using a 10-GHz radar carried on a low-flying aircraft. The mean value of β, its variability, and the sensitivity to wind were all significantly larger than previous measurements made using a 39-GHz radar also carried on a low-flying aircraft. All experiments included a similar range of wind speeds and wave heights. The SAXON data were, however, much more extensive, and the statistical relationships correspondingly more significant. The mean value of β is very close to the mean value determined from global measurements of sea level made by Geosat.

A.1 INTRODUCTION

The next generation of oceanographic satellites promises to make accurate measurements of wind velocity and sea level using advanced spaceborne radars. The accuracy of the proposed new measurements will depend critically on the interpretation of the radar signals scattered from the sea surface. We know enough about radar scatter from the sea to proceed with the design of the radars and satellite systems, but important aspects of our understanding of radar scatter seem to be lacking. Consider the important example of radar

altimetry for measuring sea level.

A spaceborne, radar-altimetric system measures sea level through a radar altimeter used for determining the height of a satellite above the sea and through tracking systems used for determining the height of the satellite above the center of the Earth, the difference in the two measurements being the sea level. While simple in principle, the measurement of sea level is difficult in practice because the measurements must have a precision and an accuracy of a few centimeters for studies of oceanic dynamics. This requires careful attention to many possible sources of error.

The influence of ocean waves on the altimeter's determination of the height of the satellite above the sea surface is an important source of error. There are two aspects to the sea state induced error: (1) waves distort the altimeter pulse, producing errors in the altimeter's determination of the distance of the satellite above the sea surface, and (2) waves cause the mean reflecting surface sensed by the radar to differ from mean sea level. The former is an instrumental error that varies with the design of the radar. The latter is common to all altimeters and is an intrinsic property of the sea surface. For consistency with *Chelton et al.* [1989] we call the latter the electromagnetic bias and the former the

instrumental error. The term sea state bias is used to describe the sum of the instrumental and sea state biases.

Electromagnetic bias arises from a correlation between the reflectivity of the sea surface and the deviation of the sea surface from its mean value. For radio signals with wavelengths of a few centimeters the trough of a wave tends to be a slightly better reflector than the crest, and the mean reflecting surface is biased toward the wave's trough by an amount equal to a few percent of the wave's height.

Our present understanding of the electromagnetic bias is based on (1) direct observation of radar scatter at vertical incidence, (2) studies of the correlation between altimeter errors and sea state, and (3) application of the theory of radar scatter from rough surfaces using a statistical description of the distribution of waves on the sea surface.

A.1.1 DIRECT OBSERVATIONS OF ELECTROMAGNETIC BIAS

Electromagnetic bias can be calculated from direct observations at vertical incidence of the radar reflectivity from a small area on the sea surface as a function of the deviation of the sea surface from mean sea level. The distribution of radar reflectivity as a function of deviation from mean sea level is then compared with the distribution of

sea surface elevation [*Jackson,* 1979]. The difference in the mean of the two distributions is the electromagnetic bias.

The first study of electromagnetic bias, by *Yaplee et al.* [1971], used a 10-GHz radar on the Chesapeake Bay Light Tower about 15 miles (24 km) east of Virginia Beach. The radar transmitted 1-ns pulses and recorded the distance to the water surface and the reflectivity of the surface at the same time that the wave height was independently recorded by three wave poles surrounding the area observed by the radar. An analysis of the observations, reported by *Jackson* [1979], showed that radar reflectivity increased nearly linearly from the wave crest to the trough and the electromagnetic bias was 5% of significant wave height.

Later studies used airborne radars for profiling the radar reflectivity at nadir at the same time that the wave height was measured either by the radar or by a laser profilometer [*Walsh et al.,* 1984; *Choy et al.,* 1984; *Hoge et al.,* 1984]. The results of these studies indicated that (1) electromagnetic bias was a function of frequency, being roughly -3.3 ± 1.0% of significant wave height at 10 GHz, -1.1 ± 0.4% at 36 GHz, and 1.4 ± 0.8% for ultraviolet light, (2) bias at 10 GHz ranged from 1% to 5% of significant wave height, and (3) the variability in the bias was apparently

unpredictable, being only weakly correlated with variations of wavelength, wave slope, skewness and kurtosis of sea surface elevation, and wind speed. It is not clear how much of the variability of electromagnetic bias measured in these experiments was real and how much was due to experimental error such as aircraft motion or distortion of the airflow around towers. The lack of correlation with any variable other than wave height and the difference in measured values for nearly identical conditions cast some doubt on the results.

A.1.2 SATELLITE OBSERVATIONS OF ELECTROMAGNETIC BIAS

Satellite altimeter measurements of the temporal variability of sea level have also been used for determining electromagnetic bias. Because satellite measurements include both electromagnetic bias and instrumental errors induced by waves, the studies are less direct than those based on data from surface experiments. They do, however, place bounds on the magnitude of the error.

Born et al. [1982] used Seasat altimeter measurements of sea level and wave height along repeated subsatellite tracks for determining the correlation between changes of sea level and changes of wave height observed during different repetitions of the track. The changes of sea level measured by the

altimeter were due to true changes of sea level, which tend to be small over many oceanic areas, and to errors in the corrections applied to the altimeter measurements, including the error due to sea state bias. Assuming that only the sea state induced errors were correlated with sea state, the correlation between the measurements of sea level and sea state gives the electromagnetic bias plus instrumental errors. The sum of the two errors was found to be 7% of significant wave height on the average for data from Seasat, but it ranged from 2.9% to 13.4%; the correlation accounted for only 50% of the variability of sea level attributable to variability of the surface wave field. This result was later refined by *Douglas and Agreen* [1983], who analyzed a much larger set of Seasat and GEOS 3 altimeter data and determined that the electromagnetic bias plus instrumental errors was 6.4 ± 0.6% of significant wave height for Seasat and 1.9 ± 1.1% of significant wave height for GEOS 3.

Further work based on Seasat altimeter data by *Hayne and Hancock* [1982] and *Lipa and Barrick* [1981] led to an independent estimate of the instrumental error due to sea state. This was calculated to be 5-5.5% of significant wave height; hence the electromagnetic bias determined from the Seasat data is 1.5-2.0% of significant wave height.

This result may be questionable, however. The work by *Hayne and Hancock,* based on a careful analysis of the Seasat altimeter's received waveforms, showed that the instrumental error is a nonlinear function of wave height. Their nonlinear equation for instrumental bias gives values of -0.3% for 1-m waves and 3.7% for 4-m waves. This implies that the electromagnetic bias may range from 7.3% to 3.3% of wave height for low waves. We note, however, that the error in determining the influence of waves on the satellite altimeter measurements is greatest for small wave heights and that the above results may not be statistically significant for smaller waves.

In addition, *Douglas and Agreen* [1983] argue that studies of the variability of ocean currents by *Douglas and Cheney* [1981] do not support a value of electromagnetic bias as large as 5%. Indeed, the maps of global mesoscale variability published by *Cheney et al.* [1983] show great areas of the Pacific and Atlantic oceans having a variability of mean sea level that is less than 5 cm during times when the wave height varied by many meters. This supports the contention that electromagnetic bias was correctly removed from the Seasat data and that it must be close to the values reported by *Born et al.* [1982] and *Douglas and Agreen* [1983].

More recently, several authors have calculated sea state bias from Geosat altimeter observations of sea level. R. D. Ray and C. J. Koblinsky (personal communication, 1990), using data from repeated tracks, found that the bias was 2.6 ± 0.2% of significant wave height. *Merem et al.* [1990], using simultaneous solutions for oceanic topography, Earth's geopotential, and errors, calculated a sea state bias of 3.6 ± 1.5% of significant wave height. Assuming that the instrumental bias is small for Geosat, these values give an upper bound for the electromagnetic bias of 2.5-5% of significant wave height.

In conclusion, the analyses of satellite altimeter data lead to an estimate of electromagnetic bias that is about 2-4% of significant wave height, but the result is not conclusive.

A.1.3 THEORETICAL BASIS OF ELECTROMAGNETIC BIAS

The inconclusive and sometimes inconsistent results of the analyses of satellite and aircraft radar observations of the electromagnetic bias are not clarified by an appeal to theory. Using the approximations of physical optics, *Barrick* [1968, 1972] showed that a radar pulse incident on the sea surface at angles close to vertical is reflected by mirrorlike facets that are randomly scattered over the sea surface within the field of view of the radar and are oriented perpendicular to

the radar beam. The theory gives the reflectivity of each facet, and if the number of facets is known, the vector sum of the reflection from the facets gives the reflectivity of the surface.

Jackson [1979] and *Barrick and Lipa* [1985] calculated the distributions of facets over the sea surface from the joint probability density of wave slope and elevation evaluated from zero slope in two horizontal dimensions. The distribution was calculated with partial success from the theory for the statistics of nonlinear waves using second- and third-order moments of the sea surface elevation [*Barrick and Lipa*, 1985; *Srokosz*, 1986] together with a model for the spectrum of sea surface elevation such as the JONSWAP (Joint North Sea Wave Project) model. Using this distribution, *Barrick and Lipa* [1985] calculated an electromagnetic bias of 2-3% of significant wave height for heights of 1.0-5.0 m with an uncertainty of at least 20% for the estimate of electromagnetic bias. They implicitly assumed a weak dependence on radio frequency because their theory assumed that waves shorter than some fraction of a radio wavelength do not contribute to the scatter, an assumption consistent with the results of *Tyler* [1976]. The basis for the assumption was that the sea surface appears to be smooth (mirrorlike) even if it has small irregularities, provided that the wave length of

the irregularities is small enough.

Despite the apparent success of the theory, important difficulties remain. First, the theory for nonlinear waves assumed that the wave system conserved energy. Wave breaking and the growth of waves by the wind were both avoided to simplify the analysis. Yet wind blowing over long waves is known to change the distribution of short waves on long waves, producing part of the modulation of radar reflectivity which allows synthetic aperture radars to image long waves [*Weissman and Johnson*, 1986]. Second, the analysis assumed that certain integrals in the analysis could be truncated at an arbitrary upper bound to ensure convergence. The upper bound for wavelengths contributing to the integrals was assumed to be some multiple of the radar wavelength, although the exact relationship between smoothness of the wave facet and the wavelengths of the short waves on the facet is not precise. Third, the theory predicts that the bias should be a function of wave skewness because both skewness and bias are directly related to the nonlinearity of the wave field and vanish for linear waves. Hence this result conflicts with the direct measurements of the bias which showed that it was nearly independent of skewness.

A.1.4 SUMMARY OF PREVIOUS WORK

Direct observations of electromagnetic bias ranged from 1% to 5% of significant wave height, and the variability of the bias was only weakly correlated with other variables describing the sea state. Analyses of satellite data indicate that the bias is less than 5% of significant wave height and that it is around 2-4% of wave height. The theory for electromagnetic bias gives a bias of 2-3% of wave height, but various assumptions used in deriving the results are questionable.

Barrick and Lipa [1985] and others have clearly recognized the limitations of the present theory and experiments useful for understanding the electromagnetic bias. *Barrick and Lipa* [1985, p. 61] state,

Electromagnetic bias is a height error not easily removed. Although it varies with sea state, it is seen to depend significantly on other factors also. Quantitative estimates of these dependencies from both theoretical and experimental investigations are as yet incomplete. Since altimeter-measured surface heights can be in error by as much as 15-25 cm because of [electromagnetic] bias, further investigations are necessary if accurate sea surface topography is to be realized from future altimeters.

A.2 DESCRIPTION OF THE EXPERIMENT AND DATA PROCESSING PROCEDURES

To determine the relationship of electromagnetic bias to environmental conditions, we made direct measurements of the bias during the Synthetic Aperture Radar and X-Band Ocean Nonlinearities (SAXON) experiment [*Shemdin and McCormick*, 1988] at the United States Coast Guard's Chesapeake Bay Light Tower for a 24-day period from September 19 to October 12, 1988. The platform is located at 36°55'N and 75°43'W, 24 km offshore of Cape Henry, Virginia, at the mouth of the Chesapeake Bay in water 12 m deep (Figure A.1). The site is in the open ocean with long fetches over a wide range of angles. The water depth was sufficient that almost all waves recorded during the experiment were only slightly influenced by the bottom. The platform has an open design leading to relatively little distortion of the air flow at sea level while providing support for environmental instrumentation mounted on the light tower high above the sea (Figure A.2).

A nadir-looking, 14-GHz, continuous-wave, coherent scatterometer designed and built at the U.S. Naval Research Laboratory was mounted 22 m above mean sea level at the end of a boom which extended 6.6 m out from the southern end of the eastern side of the tower. The scatterometer is an instrument which transmits a radio signal and then measures the power

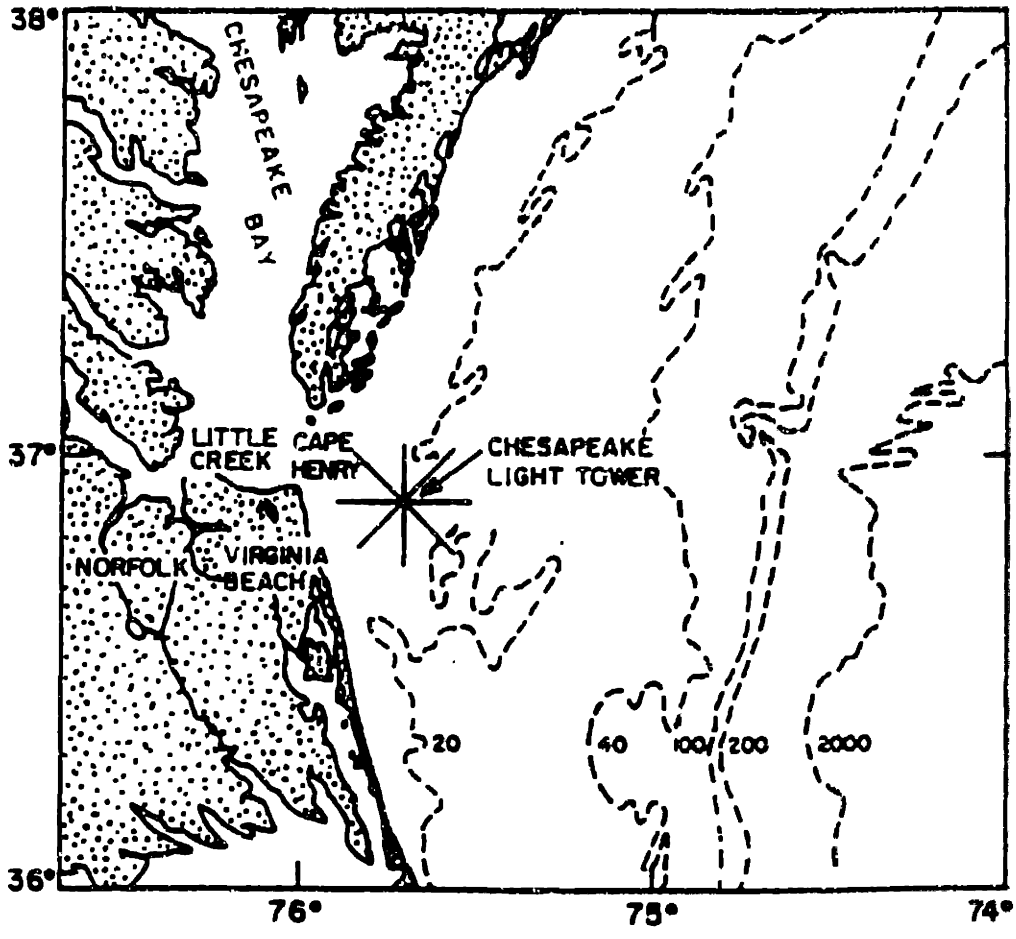

Figure A.1: Map showing the location of the Chesapeake Bay Light Tower off the east coast of North America and the surroundings. Depths are in meters; 1 m = 0.55 fathom. (Figure from O. Shemdin, personal communication, 1988.)

Appendix A. Measurements of EM Bias

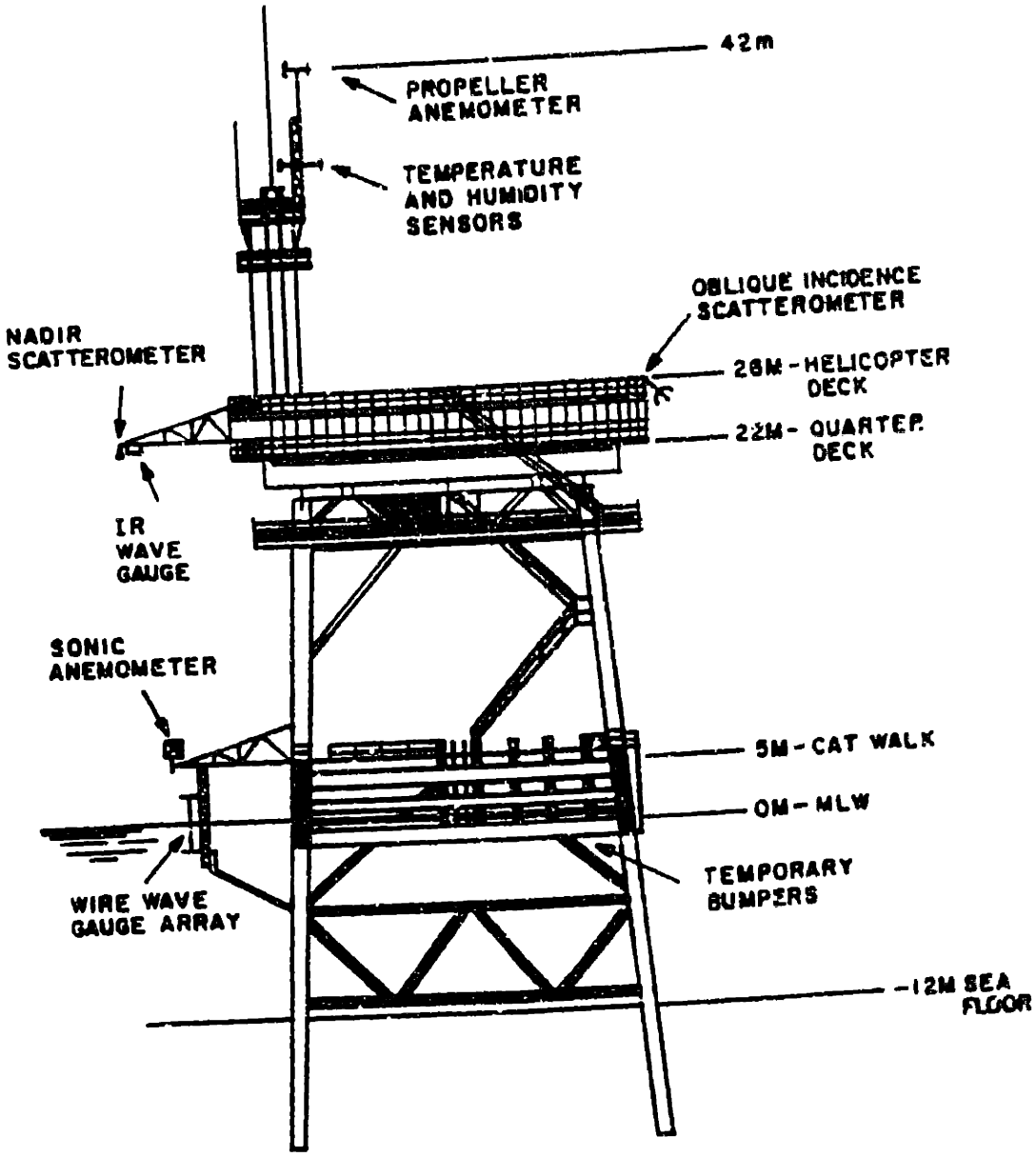

Figure A.2: Side view of the Chesapeake Bay Light Tower as seen from the north showing typical dimensions and the location of instruments.

reflected from a target. It differs from a radar only in being unable to measure range. The scatterometer illuminated an area of sea 1.7 m in diameter defined by the two-way, 3-dB beam width of the transmitting and receiving antennas. A Thorn/EMI infrared (IR) wave gauge was colocated with the scatterometer. The gauge had a beam width of 1°, illuminating a spot 0.4 m in diameter. A three-element, capacitance wire wave gauge was mounted on an identical boom attached to the lowest catwalk on the tower, 5 m above mean sea level. The boom was covered with microwave-absorbing material and was positioned just outside the main lobe of the scatterometer.

The scatterometer was calibrated before and after deployment using corner reflectors of known radio cross section in a calibration range of the U.S. Naval Research laboratory. The wire wave gauges, which do not directly contribute to the measurements reported here, were calibrated at the R. M. Parsons Laboratory of the Massachusetts Institute of Technology to confirm their linear response. They were dynamically calibrated in the field using the IR wave gauge as a reference. The field calibrations of the wire gauges (based on the IR wave gauge) were within 10% of those established in the laboratory. The wire gauges were used for providing a check on the spectral response of the IR wave gauge, which was found to be flat to a frequency of approximately 1 Hz.

Wind speed and direction, air temperature, and relative humidity were measured with an R. M. Young meteorological package mounted on a tower extending 16 m above the helicopter deck at the top of the platform, 42 m above mean sea level. Manufacturers' calibrations were used for this package. Water temperature was measured at a depth of 1 m immediately below the platform. Additional weather and wave data were obtained from a standard instrument package operated by the U.S. National Oceanographic and Atmospheric Administration. The package included meteorological instruments mounted 40 m above the sea, a Baylor wave gauge, and an experimental IR wave gauge. A sonic anemometer operated by Risoe National Laboratory, Denmark, was mounted at the end of the lower boom at 5 m above mean sea level. The anemometer was used for measuring wind velocity U_5 and the friction velocity of the wind, u^*, close to the sea surface.

The usefulness and reliability of the measurements reported here were strengthened by intercomparison among measurements of the same variable made by the different equipment described above. The intercomparisons led to the identification of outliers (measurements with large errors), which were removed from the data set. For example, we investigated the influence of the platform on wind speed at the water surface near the area illuminated by the scatterometer by plotting wind speed

from the sonic anemometer, U_5, minus wind speed at 42 m, U_{42}, as a function of wind direction. We found unexpected differences only for a narrow range of wind directions near 220°, consistent with being in the wake of the nearest leg of the platform. These data were not used in the following analyses.

The digital data acquisition system sampled one channel of the scatterometer, the IR wave gauge, and the environmental instruments at 60 Hz. Data were processed in real time to produce 10-min averages of backscattered power σ_0, significant wave height $H_{1/3}$, electromagnetic bias B, wind speed U_{42}, wind direction, air temperature T_a, sea temperature T_s, and relative humidity H. Raw data were also recorded on an eight track analog tape recorder with a bandwidth of 625 Hz. The analog tapes were later digitized at 1 kHz, and hourly averages of the observations were computed and compared with averages over six continuous 10-min averages of data processed in real time. No significant differences were observed.

The real-time calculation did not correct the measurements of the backscattered power measured by the scatterometer, σ_m, for wave-induced changes in range between the scatterometer and the sea surface. The correction is small but important. The change in backscattered power due to change in range is

proportional to r^{-4}, while the change in scattering area is proportional to r^2. Hence the change in backscattered power per unit are σ_o is proportional to r^{-2} and

$$\sigma_o = [K(z_o - \zeta)^2/z_o^2]\,\sigma_m$$

where z_o = 22 m is the height of the scatterometer above mean sea level, ζ is the displacement of the sea surface from mean sea level, and K is the absolute calibration constant of the scatterometer. Data were corrected for the change in range before further analyses described below.

Electromagnetic bias B was calculated from the digitized values of σ_o and the displacement of the sea surface measured by the IR wave gauge using

$$B = \left(\frac{1}{N}\Sigma\sigma_o\zeta\right)\left(\frac{1}{N}\Sigma\sigma_o\right)^{-1}$$

where N is the number of samples in the averaging interval.

Preliminary comparisons of the wind measurements from the sonic anemometer at 5 m and from the propeller anemometer at 42 m indicated that the lower measurements were much more variable. We therefore correlated electromagnetic bias with U_{10} and u^* calculated from U_{42} using bulk formulas together with other environmental measurements. The profile of wind above

the sea surface is well approximated by the logarithmic profile:

$$U_z = \frac{u^*}{\kappa}\{\ln(z/z_o) - \Psi(z/L)\}$$

where $\kappa = 0.40$ is Karman's constant, z_o is the roughness height of the surface, and L is the Monin-Obukov stability length. Values of friction velocity u^* and wind speed at 10 m, U_{10}, were iteratively computed using 10-min averages of wind speed, air-sea temperature difference, and relative humidity. For the computation the roughness height was taken to be the sum of a smooth-surface contribution z_s, and an aerodynamic roughness contribution z_c as outlined by *Smith* [1988]:

$$z_o = z_s + z_c$$
$$z_s = 0.11\nu/u^*$$
$$z_c = au^{*2}/g$$

where ν is the kinematic viscosity of air and g is the gravitational acceleration. The value $a = 0.0185$ proposed by *Wu* [1980] was used because of the limited fetch and shallow depth at the light tower. The bulk stability parameter z/L was calculated from the formula proposed by *Large and Pond* [1981] in the last equation, unnumbered, in their section 3c combined with their equation 13. The computed results were

then used for computing hourly averaged values for U_{10} and u^*.

A.3 RESULTS

During the experiment, hourly averaged values of wind speed ranged from 0.2 m/s to 15.3 m/s, significant wave height ranged from 0.3 m to 2.9 m, air minus sea temperature ranged from -10.2°C to 5.4°C, and electromagnetic bias varied from -0.6 cm to -15 cm or from -1.3% to -5.8% of significant wave height (Figure A.3). The values for wind, waves, and temperature and the spectra of wave displacement are typical of open-ocean conditions.

To confirm the correlation between electromagnetic bias and cross section measured by the scatterometer, several hours of data from the experiment were processed to obtain cross section as a function of displacement from mean sea level (Figure A.4). The cross section was an almost linear function of displacement of the sea surface from mean sea level. The slope of the function is the electromagnetic bias.

The SAXON data were then used for investigating the relationships between bias B and wind speed at 10 m, U_{10}; the wind stress u^*, including the effects of stability; significant wave height $H_{1/3}$; and the nonlinearity of the wave field. An analysis of variance showed that the only

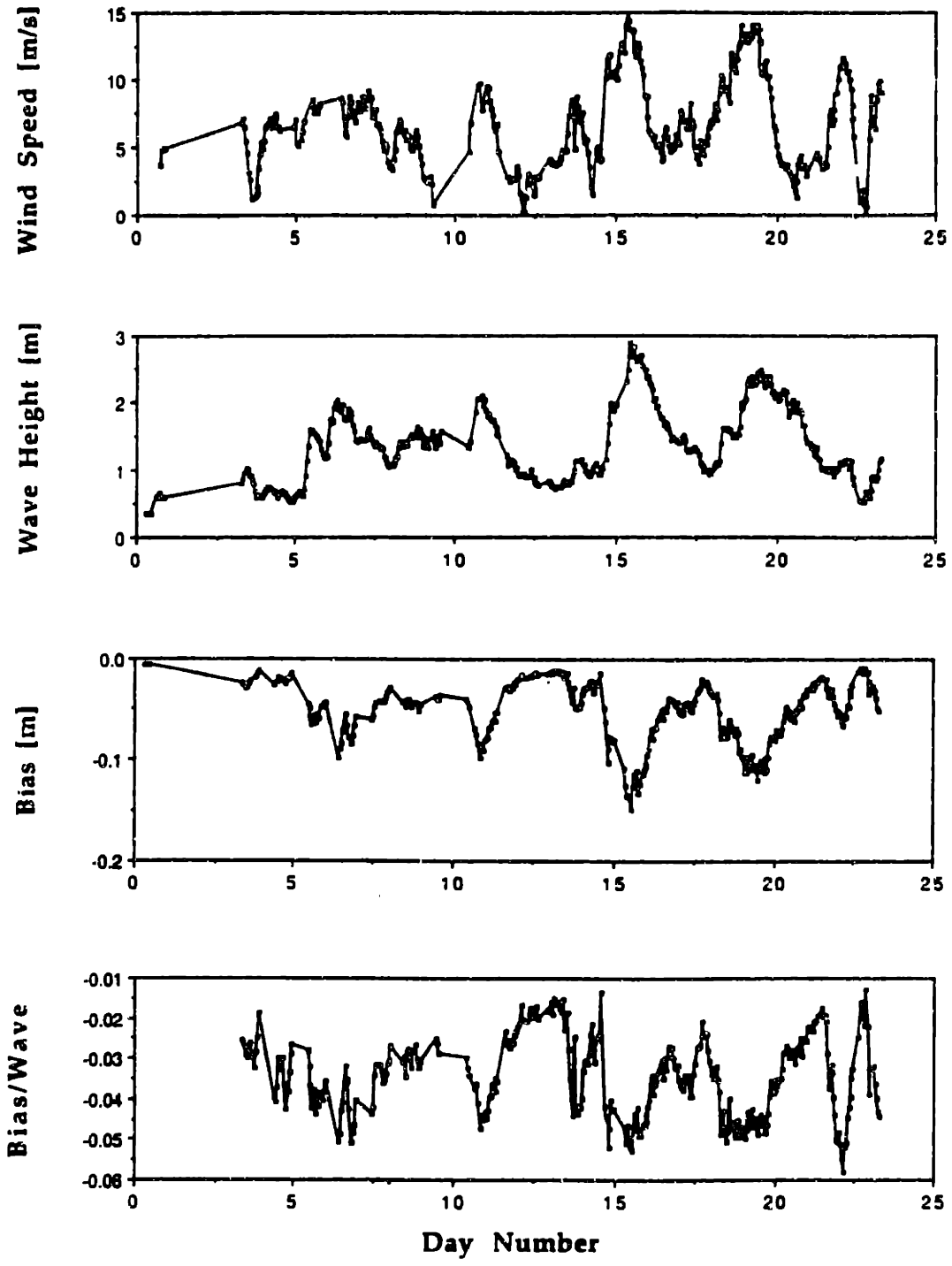

Figure A.3: Time series of wind speed at 10 m, U_{10}; significant wave height $H_{1/3}$; electromagnetic bias B; and bias divided by wave height, β, recorded during the SAXON experiment.

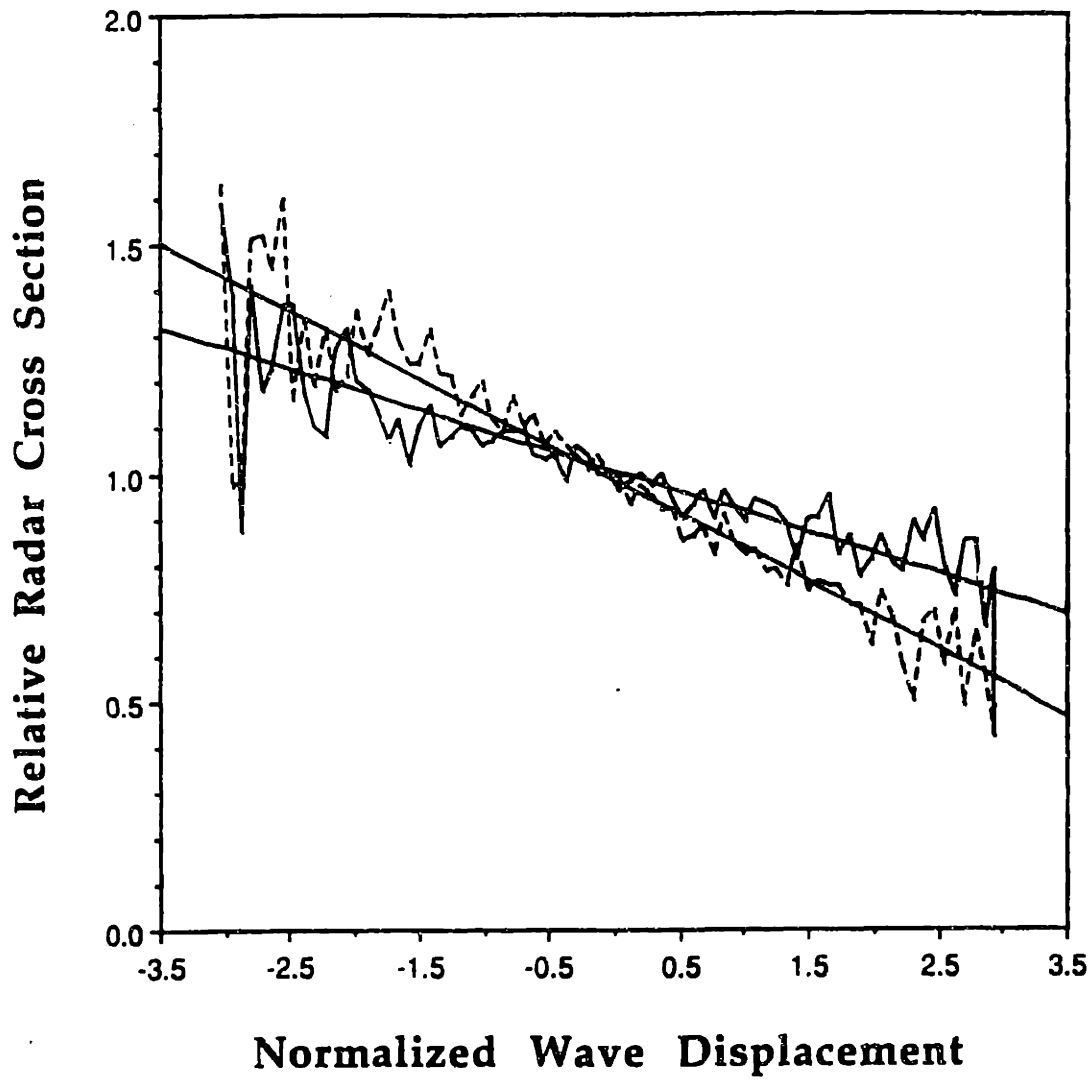

Figure A.4: Two examples of averaged radio cross section of the sea as a function of the displacement of the sea surface from mean sea level. The displacement is normalized by the standard deviation of the displacement. Note that the cross section is a nearly linear function of displacement, whose slope increases with normalized electromagnetic bias. Solid line denotes bias = 1.85 cm, $H_{1/3}$ = 0.92 m, β = -0.020, and U_{10} = 2.8 m/s. Dashed line denotes bias = -2.9 cm, $H_{1/3}$ = 0.85 m, β = -0.034, and U_{10} = 9.6 m/s.

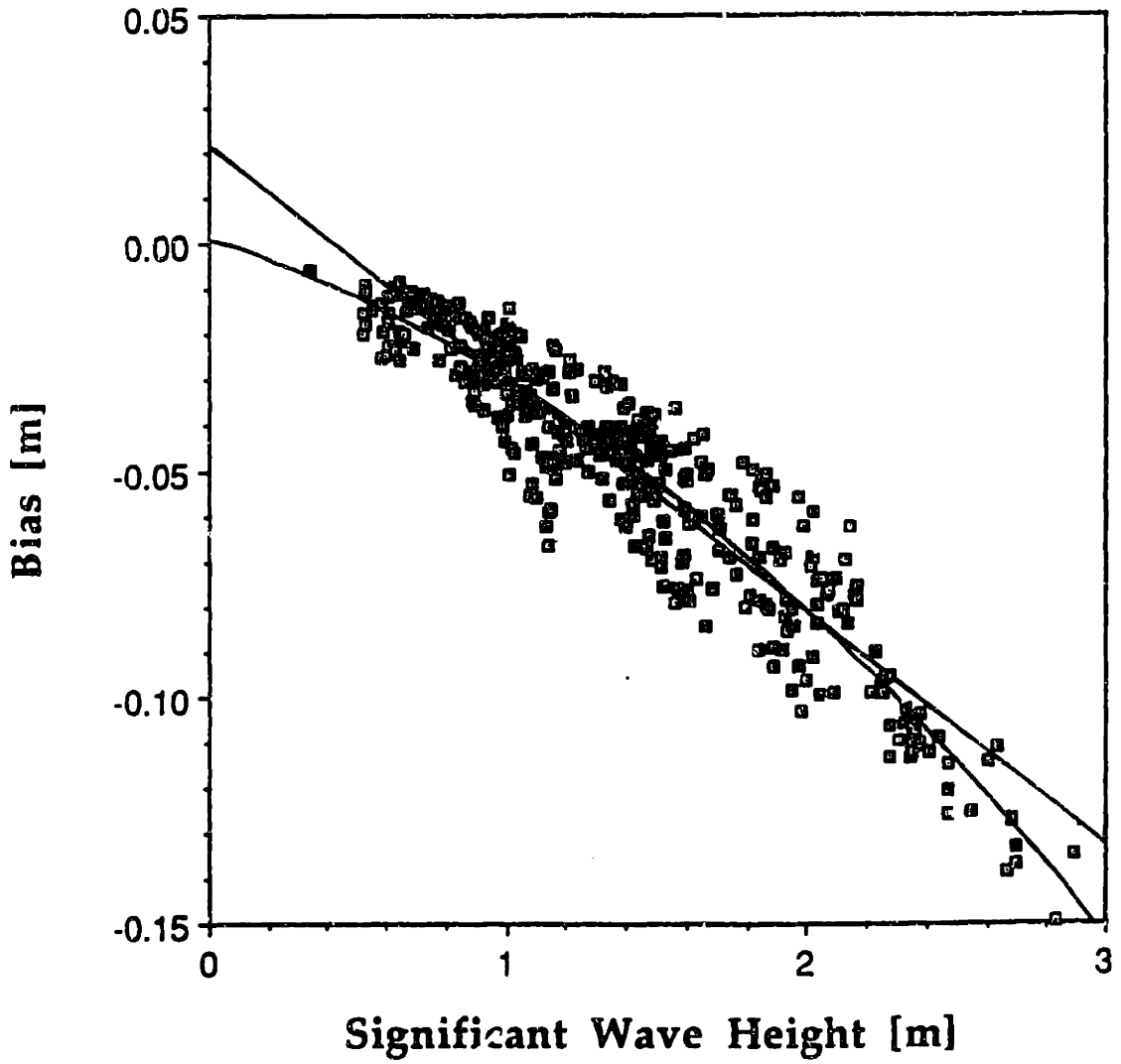

Figure A.5: Electromagnetic bias B as a function of significant wave height $H_{1/3}$ together with the least squares linear and quadratic fit to the data. The best fitting linear equation is $B = 0.00216 - 0.0517H_{1/3}$ ($r^2 = 0.873$), and the best fitting quadratic equation is $B = 0.00100 - 0.210H_{1/3} - 0.0104(H_{1/3})^2$ ($r^2 = 0.887$) for wave height in meters. Both correlations are statistically significant at the 99% level.

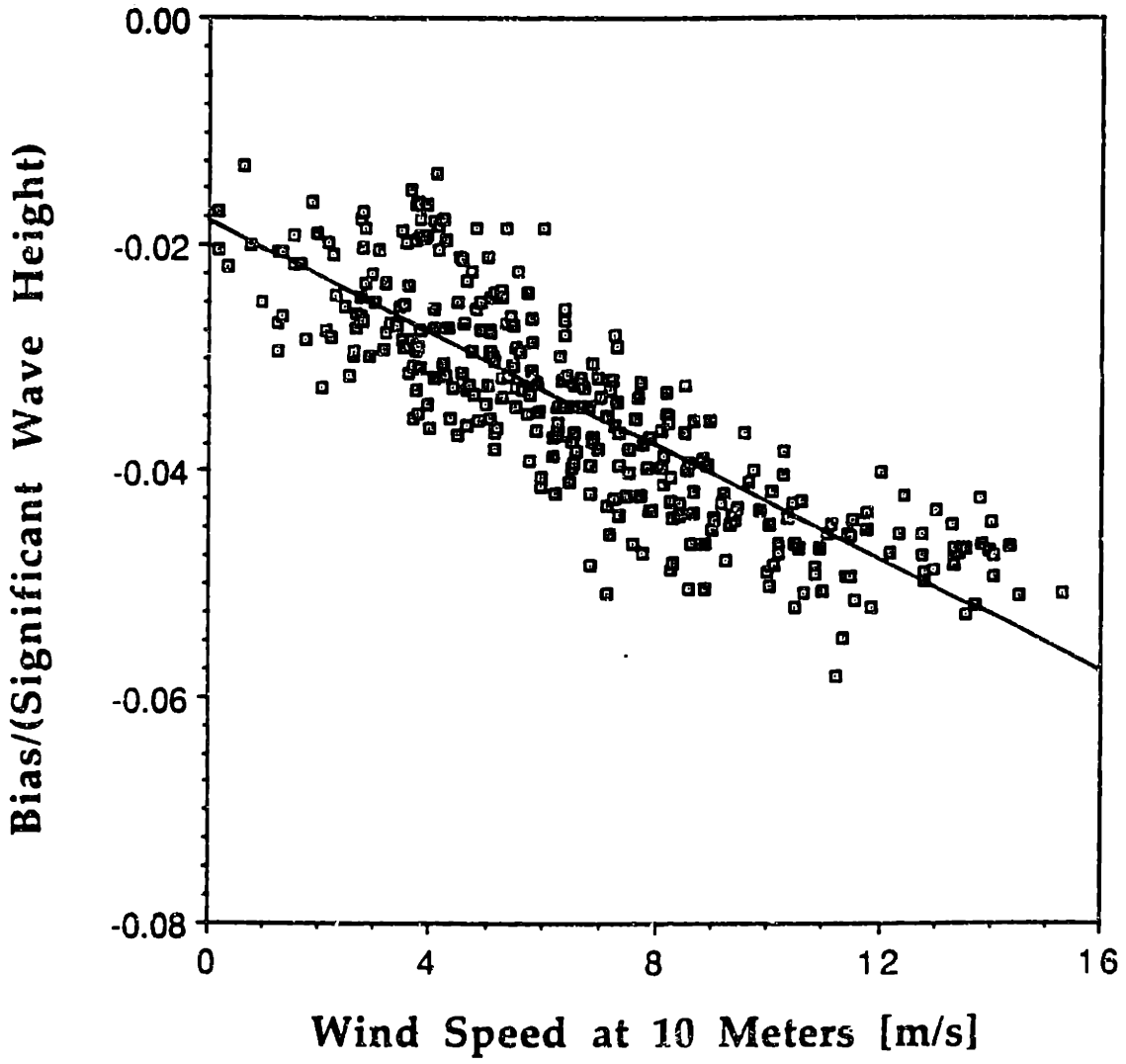

Figure A.6: Normalized electromagnetic bias β, which is bias B divided by significant wave height $H_{1/3}$, as a function of wind speed 10 m above the sea surface, U_{10}. The line through the data is the least squares regression line $\beta = -0.0179 - 0.00250U_{10}$ ($r^2 = 0.707$) for wind speed in meters per second.

statistically significant correlations were with wind speed, significant wave height, and significant wave height squared (Figures A.5 and A.6). Because the strongest correlation by far was with significant wave height, we used the dimensionless bias, $\beta = B/H_{1/3}$, in the following analysis of the residual correlations of bias with other variables. The quadratic dependence on wave height, which is evident in Figure A.5, is accounted for by correlating β with $H_{1/3}$.

Before describing the correlations with other variables, we note that the mean value of β averaged over 347 hours of data was -0.0342 and the standard deviation was 0.0097. Thus electromagnetic bias observed at the SAXON experiment was 3.5% of significant wave height with variability of 1% of significant wave height. Therefore significant wave height alone is not sufficient for accurately predicting electromagnetic bias for radar altimetry.

Dimensionless bias β was well correlated with wind speed at 10 m, U_{10}, the correlation coefficient being $r^2 = 0.706$, and with significant wave height $H_{1/3}$, the correlation coefficient being $r^2 = 0.343$. All correlations had approximately 315 or more degrees of freedom. The latter correlation includes the quadratic dependence of bias on wave height (compare Figure A.5) as well as the dependence of wave height on wind speed.

The two influences cannot be uniquely determined from the SAXON data, but the large number of independent observations of winds and waves and the weak correlation between them (r^2 = 0.279 with 380 degrees of freedom) allows a good separation of the dependence of β on U_{10} and $H_{1/3}$. In addition, the predicted value of β calculated from U_{10} and $H_{1/3}$ has much less error than that of β calculated from $H_{1/3}$ alone. Because of the strong dependence of β on wind, we have chosen to investigate the wind's influence first before considering the multiple correlation of β with wind and waves.

The most significant correlations of bias with the wind were with U_{10} (Figure A.6) and with friction velocity calculated from the bulk formulas, u^* (Figure A.7). Wind speed at 42 m, U_{42}, and friction velocity measured directly by the sonic anemometer, u^* (sonic), were only slightly less well correlated with β. In searching for power relationships among measured variables we found that dimensionless bias was also well correlated with the square root of the wind speed and with the square root of the friction velocity. Both correlations were about the same as the correlation with wind speed.

After removing the latter sample correlation of β with wind speed we found that β was still weakly but significantly

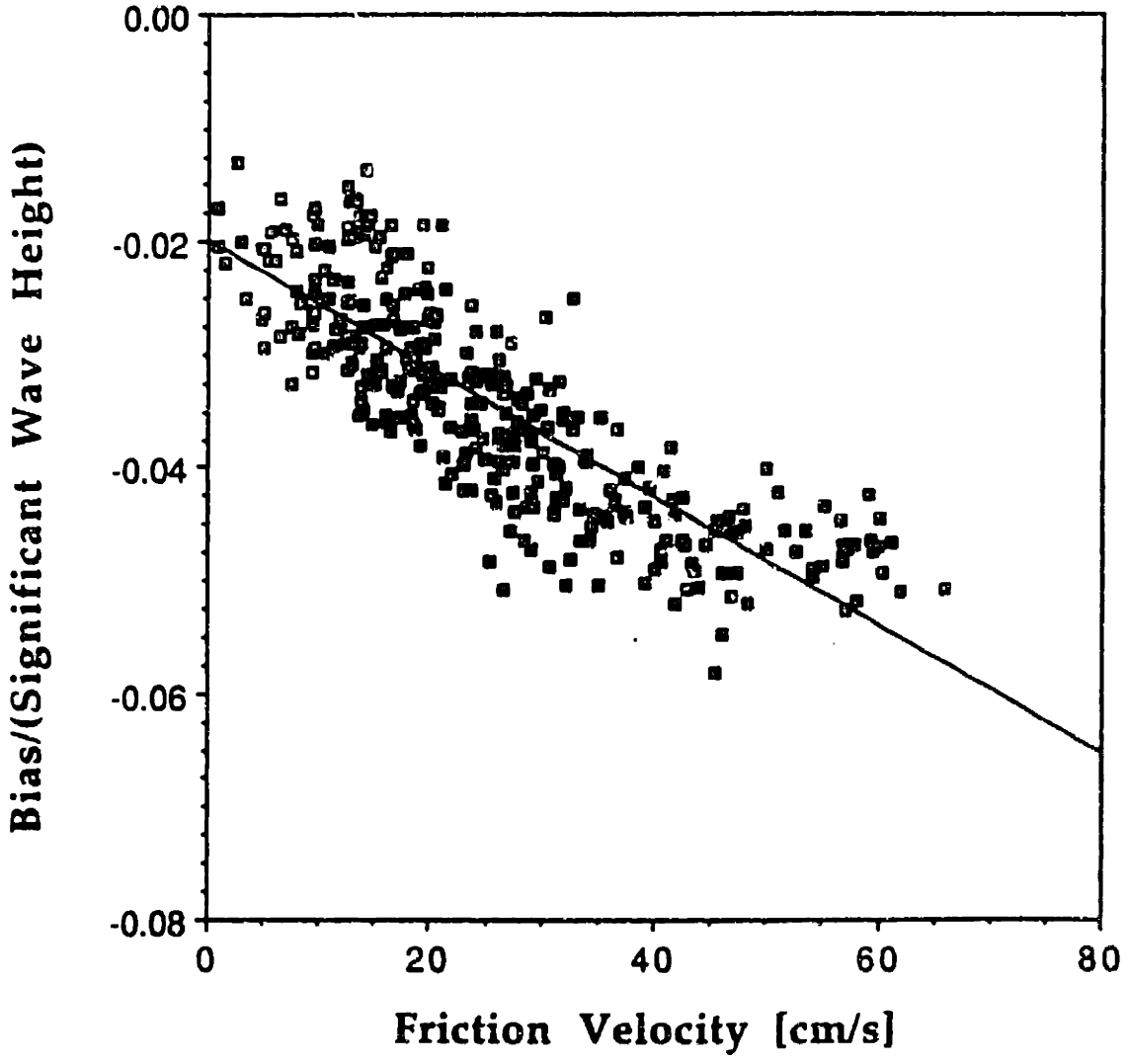

Figure A.7: Normalized electromagnetic bias β, which is electromagnetic bias B divided by significant wave height $H_{1/3}$, as a function of friction velocity u^*. The friction velocity was calculated from U_{10} using a bulk formula. The line through the data is the least squares regression line $\beta = -0.0199 - 0.0565u^*$ ($r^2 = 0.686$) for friction velocity in centimeters per second.

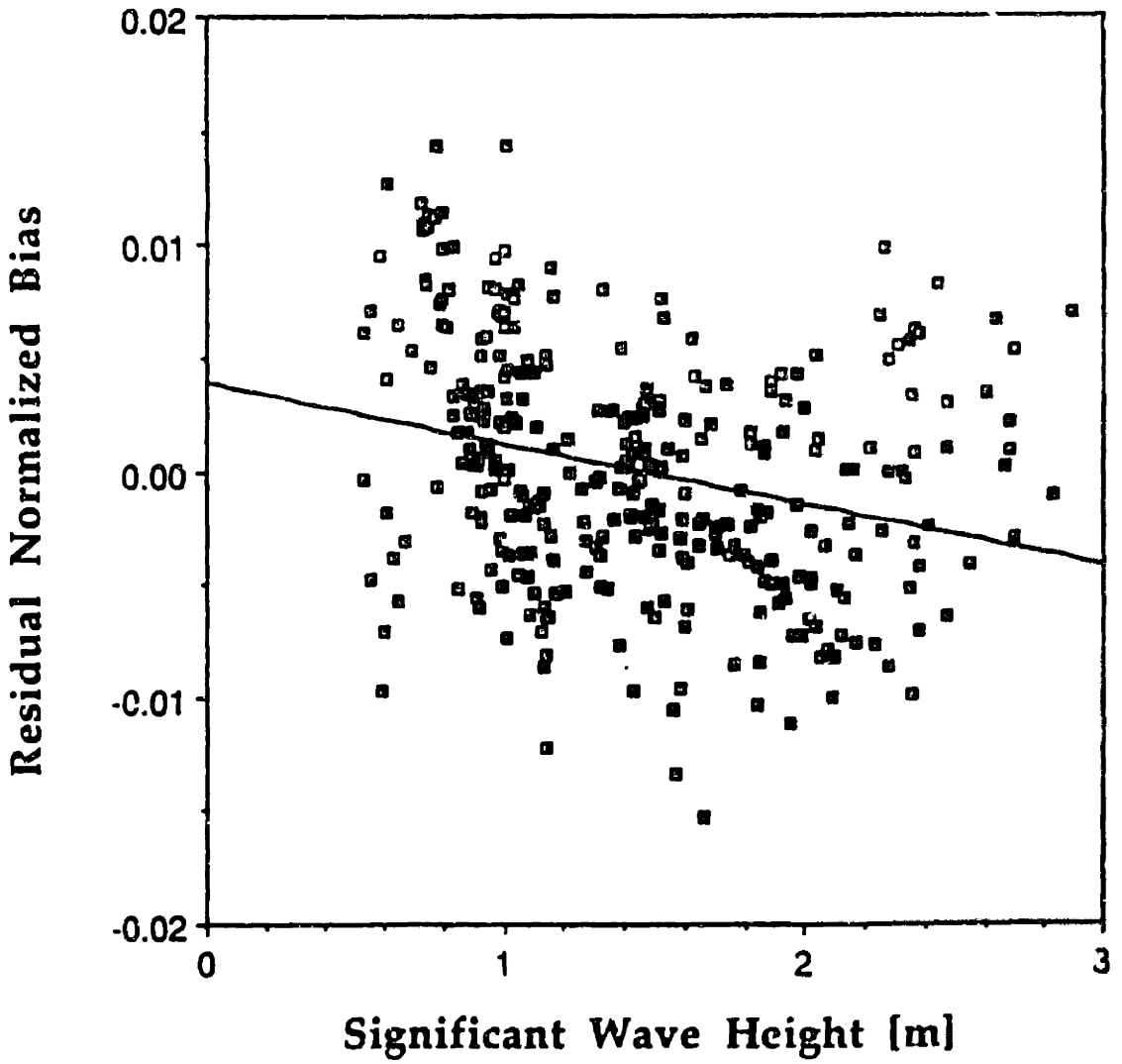

Figure A.8: The residual normalized electromagnetic bias as a function of significant wave height $H_{1/3}$. The residual is the normalized bias β minus the correlation with wind speed calculated from the SAXON data (see Figure A.6). The line through the data is the least squares regression line, residual = $0.00387 - 0.00270H_{1/3}$ ($r^2 = 0.075$), for wave height in meters. The correlation is statistically significant at the 99% confidence level even though the correlation coefficient is small.

correlated with significant wave height, $r^2 = 0.075$ (Figure A.8).

Combining the influence of wind speed and wave height, the multiple correlation of β with U_{10} and $H_{1/3}$ yielded

$$\beta = -0.0146 - 0.00215U_{10} - 0.00389H_{1/3} \qquad r^2 = 0.737$$

for wind speed in meters per second and wave height in meters. The coefficients are significant at the 99% confidence level. The use of wind information significantly improves the estimation of β. The correlation of β with $H_{1/3}$ has a correlation coefficient of only $r^2 = 0.343$ with 345 degrees of freedom, as compared with $r^2 = 0.737$ above.

The residual bias, after removing the observed correlation of β with U_{10} and $H_{1/3}$ (Figure A.9), had a standard deviation of ± 0.0051, but it was not a random function of time. Rather, its structure suggests that it has a component that may be predictable using variables not considered in the multiple regression. The residual was not correlated with wind direction, which would indicate errors caused by the platform distorting the wind flow, nor was it correlated with the stability of the atmospheric boundary layer. Regardless of the cause of the residual, it is small, and the data indicate that wind speed and wave height alone can be used for

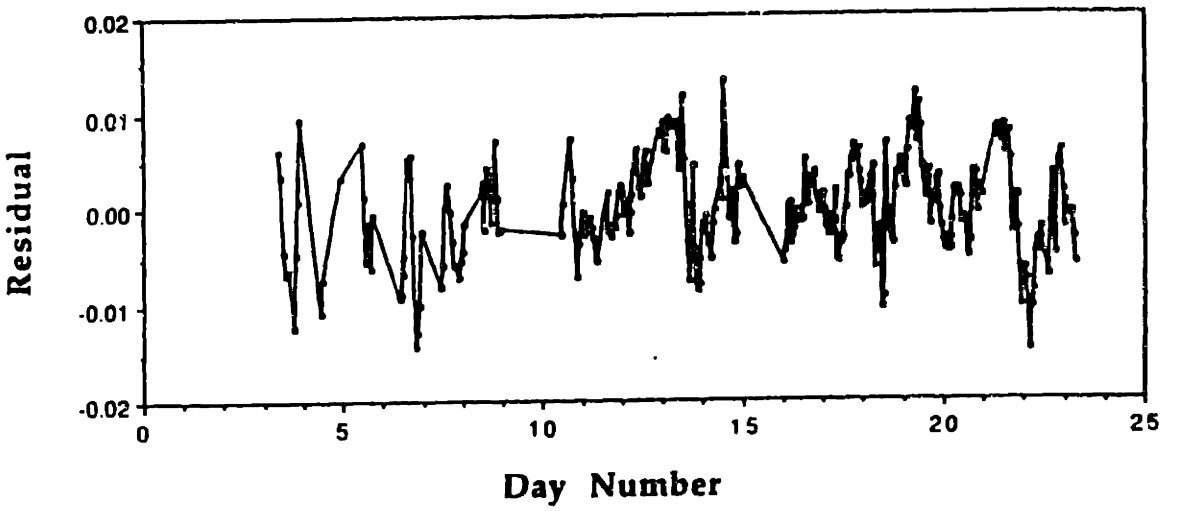

Figure A.9: The residual normalized bias as a function of time in days. The residual is the normalized bias β minus the correlations with U_{10} and $H_{1/3}$. The residual has a weak but systematic structure suggesting that other variables not considered in the multiple regression may be used for further reducing the uncertainty in β. Day 1 is September 19, 1988.

predicting normalized bias with an uncertainty of 0.5% for the SAXON data.

Because wind speed can be calculated from measurements of the scattering cross section per unit area σ_o made by satellite altimeters, we investigated the relationship between σ_o and dimensionless bias. But first we compared the relationship between σ_o measured by the SAXON scatterometer and U_{10} measured by an anemometer with previously published data in order to understand the accuracy of our scatterometer measurements.

A plot of σ_o in decibels as a function of 10 log U_{10} together with σ_o in decibels calculated from U_{10} using the algorithm proposed by *Chelton and McCabe* [1985] showed that the two differ by 1.08 dB, a difference well within the uncertainty of the calibration of the Seasat altimeter and our scatterometer. The difference in the two calibrations is estimated to be ±2-3 dB. After reducing our measurements by 1.08 dB, we found (Figure A.10)

$$\sigma_o(dB) = 10[1.389 - 0.364 \log U_{10}] \qquad r^2 = 0.655$$

for wind speed in meters per second, compared with *Chelton and McCabe* [1985], who found

$$\sigma_o(dB) = 10[1.502 - 0.468 \log U_{10}]$$

based on an analysis of global altimetric satellite data. The

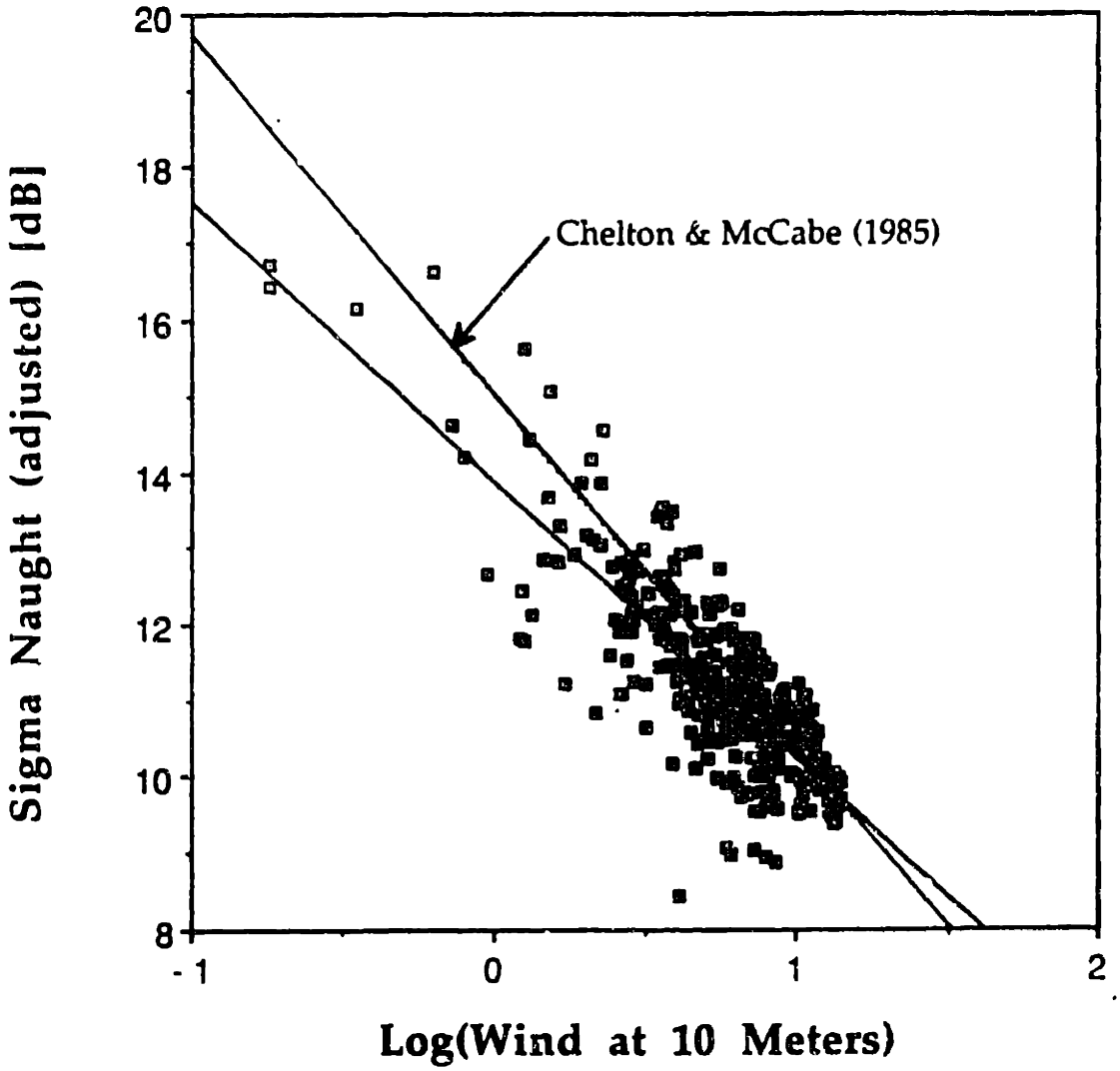

Figure A.10: Adjusted scattering cross section per unit area σ_o (sigma naught) in decibels as a function of the logarithm of wind speed at 10 m, U_{10}. The data have been adjusted by 1.08 dB for better agreement with the curve proposed by *Chelton and McCabe* [1985] based on an analysis of altimetric satellite data. The adjustment is within the uncertainty of the calibration of the altimeter and the tower scatterometer. The other line through the data is the least squares regression σ_o(dB) = 13.9 - 3.64 log U_{10} (r^2 = 0.655) for wind speed in meters per second.

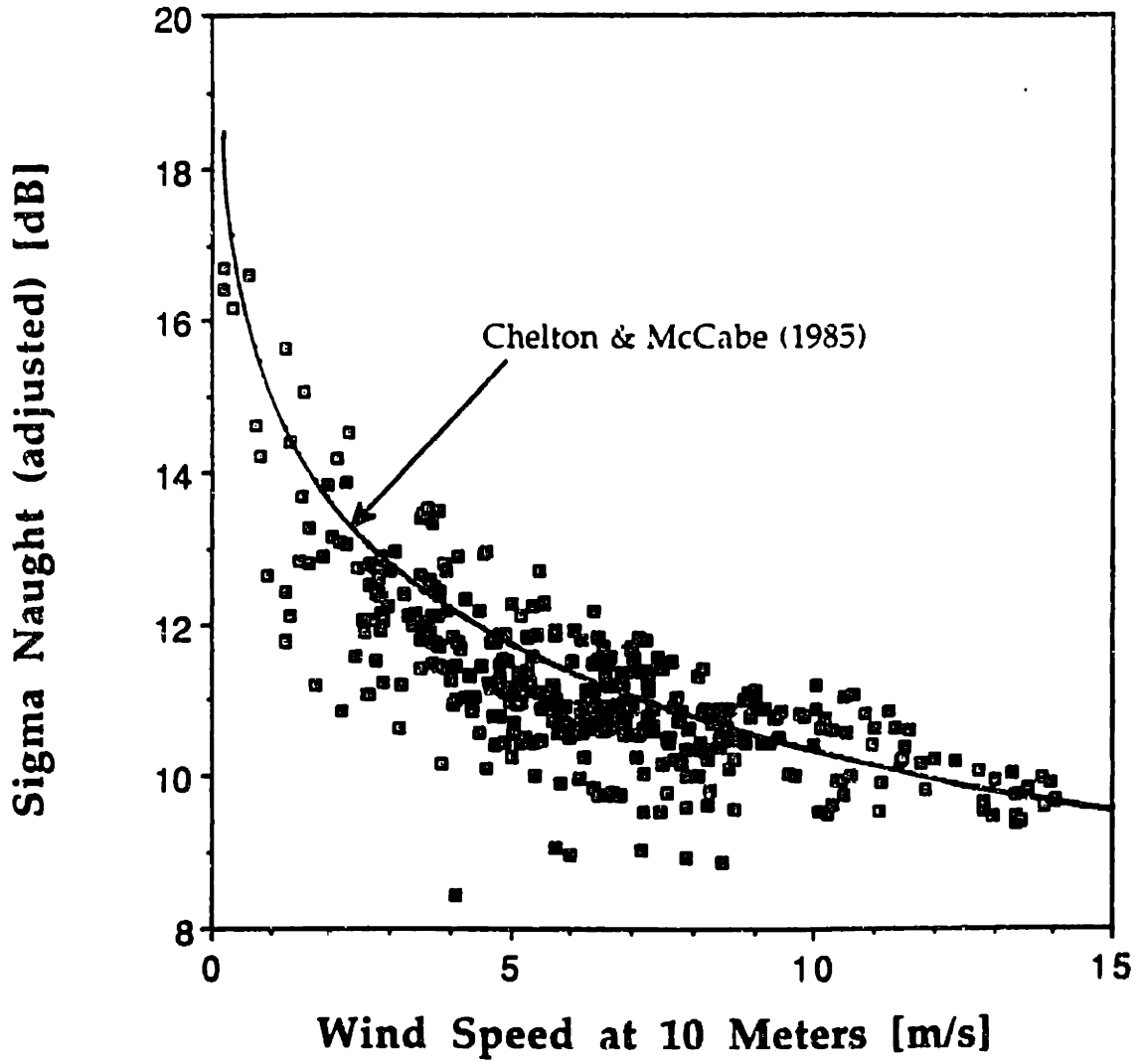

Figure A.11: Adjusted scattering cross section per unit area σ_o (sigma naught) in decibels as a function of wind speed at 10 m, together with the relationship proposed by *Chelton and McCabe* [1985] based on an analysis of altimetric satellite data.

two sets of coefficients differ by 4-5 times their small standard error, but Figure A.10 shows that the linear regression for SAXON data is dominated by relatively few observations at low wind speed. A plot of the same data in linear form (Figure A.11) shows a close agreement between the SAXON data and the global observations. The agreement suggests that relationships between β and σ_o based on SAXON data would provide corrections useful for satellite altimetry.

To determine β from σ_o, we used σ_o directly rather than convert σ_o to wind speed for use in the correlation of β with U_{10}. This provides a less noisy variable for predicting β. We found previously that $\beta \sim U_{10}$ and $\sigma_o^{-1} \sim (U_{10})^2$; therefore we expected $\beta \sim 1/\sigma_o^2$. This was verified by the correlation of β with σ_o, which yielded (Figure A.12)

$$\beta = -0.0183 - 2.46/\sigma_o^2 \qquad r^2 = 0.516.$$

Other power laws had poorer fit to the data. The multiple regression of β with $1/\sigma_o^2$ and $H_{1/3}$ yielded

$$\beta = -0.0163 - 2.15/\sigma_o^2 - 0.00291 H_{1/3} \qquad r^2 = 0.528$$

for wave height in meters. The correlation is nearly as good as that between β and U_{10} and $H_{1/3}$. The standard deviation of the variability after removing the influence of the cross

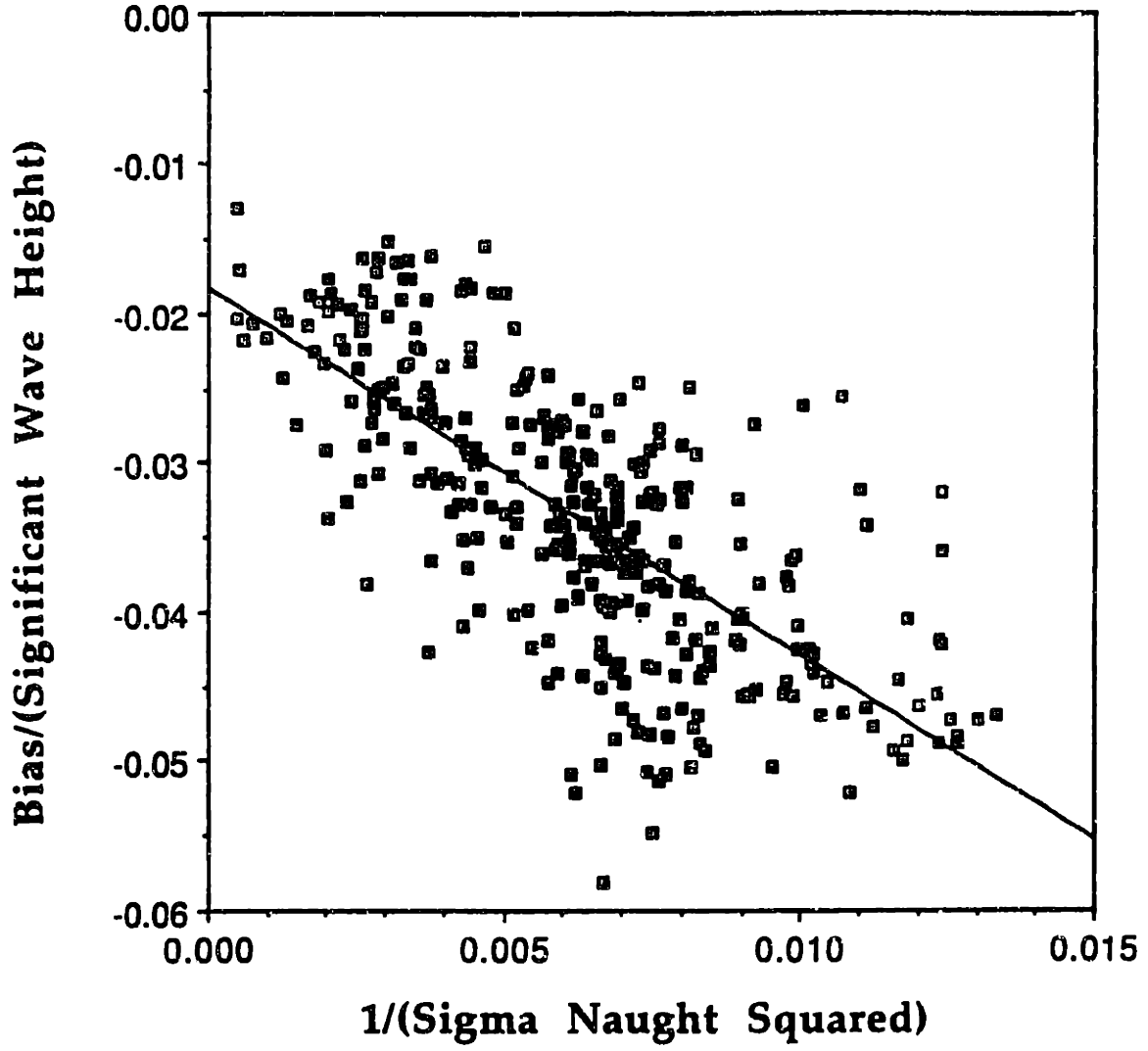

Figure A.12: Normalized electromagnetic bias β as a function of the inverse square of the scattering cross section per unit area σ_o (sigma naught). The line through the data is a linear least squares regression $\beta = -0.0183 - 2.46\sigma_o^{-2}$ ($r^2 = 0.516$).

section and waves is ±0.0065 = 0.65%. The results are important for the TOPEX/Poseidon mission. The TOPEX/Poseidon satellite will carry an altimeter for measuring sea level with an accuracy of ±14 cm, of which ±2 cm is allocated to errors due to electromagnetic bias for 2-m waves [*Stewart et al.*, 1986]. Our results indicate that the bias could be reduced to the required level using only data from the satellite.

A.4 DISCUSSION

The mean value of our measurements of electromagnetic bias is the same, within experimental error, as that of the measurements by *Choy et al.* [1984] using a 10.0-GHz radar flown on an aircraft at a height of 150-230 m. Both sets of measurements yielded a bias of -3.3% of significant wave height with a variability of ±1.0%. These values are substantially larger than the mean value of -1.1% and the variability of ±0.4% measured by *Walsh et al.* [1984] using a 36-GHz radar also flown on an aircraft at about the same altitude.

Our measurement of the sensitivity of dimensionless bias to wind speed was nearly the same as that calculated from the data in Table 2 of *Choy et al.* [1984]. We found (Figure A.6)

$$\beta = -0.0179 - 0.0025 U_{10} \qquad r^2 = 0.707$$

while data in the work by *Choy et al.* [1984] gives

$$\beta = -0.00075 - 0.0028 U_{150} \qquad r^2 = 0.258$$

for winds in meters per second. Because there were no winds less than 7.5 m/s in Choy et al.'s data, their value of $\beta(U = 0)$ was not well defined. There were insufficient data for converting wind speed at aircraft altitude, U_{150}, to wind at 10 m, U_{10}, so we used only the correlation with uncorrected wind speed. The dimensionless bias measured at 36 GHz was much less sensitive to wind. All data were observed over approximately the same range of wind and wave conditions. The SAXON data were, however, much more extensive, and the statisitcal relationships correspondingly more significant. For example, *Choy et al.* [1984] reported only 23 values of wind and bias in their Table 2, as compared with 316 values in Figure A.6 this paper.

The close agreement between measurements made at 10 and 14 GHz and the large difference compared with measurements at 36 GHz indicates that measurements of β should be made close to the frequency used by spaceborne altimeters if the measurements will be used for determining corrections to the satellite data.

Our value for the electromagnetic bias is also nearly

identical to the 3.6% value for the bias calculated from Geosat data by *Nerem et al.* [1990], and it is slightly higher than the 2.6% value calculated from Geosat data by R. D. Ray and C. J. Koblinsky (personal communication, 1990). It is also within the range of values calculated from Seasat altimeter data. The satellite data, however, yield only the sea state bias, and the uncertainty in the determination of the instrumental errors in the satellite observations makes the comparison less clear.

The analysis of the SAXON data and the agreement with 10-GHz radar measurements suggests that electromagnetic bias in radar altimetry can be corrected with useful accuracy using only data from the altimeter. The instrument measures significant wave height and scattering cross section per unit area, from which U_{10} can be calculated. Either the cross section or the wind speed could be used for calculating the bias. If the correlations observed in the SAXON data hold also for spaceborne radars, then the bias could be calculated with an accuracy of 0.6%. This would be an improvement over existing corrections, and it would be sufficiently accurate for many studies of ocean dynamics.

Acknowledgments. We thank Omar Shemdin for facilitating our participation in SAXON and Les McCormick for the logistical support on the tower. These measurements would not have been possible without the generosity of Ted Blanc of the U.S. Naval Research Laboratory, who lent us the Thorn/EMI wave gauge. Feng Chi Wang and Jack Crocker designed and built the wire wave gauge array based on a design by colleagues at the Applied Physics Laboratory of the Johns Hopkins University. We thank Francis Felizardo for assistance with the acquisition of the environmental data. The work was supported by NASA grants NAGW-1272 to the Massachusetts Institute of Technology, NAGW-1836 to Texas A & M University, and NAGW-1271 to the Univeristy of California, and by a NASA Graduate Researcher's Fellowship NGT-40292 to A. T. J.

REFERENCES

Barrick, D. E., Rough surface scattering based on the specular point theory, *IEEE Trans. Antennas Propag.*, AP-16, 449-454, 1968.

Barrick, D. E., Remote sensing of sea state by radar, in *Remote Sensing of the Troposphere*, edited by V. E. Derr, pp. 12-1-12-46, U.S. Government Printing Office, Washington, D. C., 1972.

Barrick, D. E., and B. J. Lipa, Analysis and interpretation of altimeter sea echo, *Adv. Geophys.*, 27, 61-100, 1985.

Born, G. H., M. A. Richards, and G. W. Rosborough, An empirical determination of the effects of sea state bias on Seasat altimetry, *J. Geophys. Res.*, 87(C5), 3221-3226, 1982.

Chelton, D. B., and P. J. McCabe, A review of satellite altimeter measurement of sea surface wind speed: With a proposed new algorithm, *J. Geophys. Res.*, 90(C3), 4707-

4720, 1985.
Chelton, D. B., E. J. Walsh, and J. L. MacArthur, Pulse compression and sea level tracking in satellite altimetry, *J. Atmos. Oceanic Technol.*, 6, 407-438, 1989.
Cheney, R. E., J. G. Marsh, and B. D. Beckley, Global mesoscale variability from collinear tracks of Seasat altimeter data, *J. Geophys. Res.*, 88(C7), 4343-4354, 1983.
Choy, L. W., D. L. Hammond, and E. A. Uliana, Electromagnetic bias of 10-GHz radar altimeter measurements of MSL, *Mar. Geod.*, 8(1-4), 297-312, 1984.
Douglas, B. C., and R. W. Agreen, The sea state correction for GEOS 3 and Seasat satellite altimeter data, *J. Geophys. Res.*, 88(C3), 1655-1661, 1983.
Douglas, B. C., and R. E. Cheney, Ocean mesoscale variability from repeat tracks of GEOS 3 altimeter data, *J. Geophys. Res.*, 86(C11), 10, 931-10,937, 1981.
Hayne, G. S., and D. W. Hancock, Sea-state-related altitude errors in the Seasat radar altimeter, *J. Geophys. Res.*, 87(C5), 3227-3231, 1982.
Hoge, F. E., W. B. Krabill, and R. N. Swift, The reflection of airborne UV laser pulses from the ocean, *Mar. Geod.*, 8(1-4), 313-344, 1984.
Jackson, F. C., The reflection of impulses from a nonlinear random sea, *J. Geophys. Res.*, 84(C8), 4939-4943, 1979.
Large, W. G., and S. Pond, Open Ocean momentum flux measurements in moderate to strong winds, *J. Geophys. Oceanogr.*, 11, 324-336, 1981.
Lipa, B. J., and D. E. Barrick, Ocean surface height-slope probability density function from Seasat altimeter echo, *J. Geophys. Res.*, 86(C11), 10,921-10,930, 1981.
Nerem, R. S., B. D. Tapley, and C. K. Shum, Determination of the ocean circulation using Geosat altimetry, *J. Geophys. Res.*, 95(C3), 3163-3179, 1990.
Shemdin, O. H., and L. D. McCormick, SAXON I 1988/1990 science plan, report, 85 pp., Ocean Res. and Eng., Pasadena, Calif., 1988.
Smith, S. D., Coefficients for sea surface wind stress, heat flux, and wind profiles as a function of wind speed and temperature, *J. Geophys. Res.*, 93(C12), 15,467-15472, 1988.
Srokosz, S. A., On the joint distribution of surface elevation and slopes for a nonlinear random sea, with an application to radar altimetry, *J. Geophys. Res.*,91(C1), 995-1006, 1986.
Stewart, R., L.-L. Fu, and M. Lefebvre, Science opportunities from the TOPEX/Poseidon mission, *JPL Publ.*, 86-18, 62 pp., 1986.
Tyler, G. L., Wavelength dependence in radio-wave scattering and specular-point theory, *Radio Sci.*, 11(2), 83-91,

1976.

Walsh, E. J., D. W. Hancock, D. E. Hines, and J. E. Kenney, Electromagnetic bias of 36-GHz radar altimeter measurements of MSL, *Mar. Geod.*, 8(104), 265-296, 1984.

Weissman, D. E., and J. W. Johnson, Measurements of ocean wave spectra and modulation transfer function with the airborne two-frequency scatterometer, *J. Geophys. Res.*, 91(C2), 2450-2460, 1986.

Wu, J., Wind-stress coefficients over sea surface near neutral conditions-A revisit, *J. Phys. Oceanogr.*, 10, 727-740, 1980.

Yaplee, B. S., A Shapiro, D. L. Hammond, B. D. Au, and E. A. Uliana, Nanosecond radar observations of the ocean surface from a stable platform, *IEEE Trans. Geosci. Electron.*, GE-9, 17-174, 1971.

Appendix B

Correlation Coefficient

For a surface spectrum given by

$$S_p(k,\eta) = \begin{cases} (p-1)\,\sigma_s^2(\eta)\,k_s^{p-1}k^{-p} & k \geq k_s = \frac{2\pi}{L} \\ 0 & k < k_s \end{cases} \qquad \text{(B.1)}$$

for p greater than one, the correlation coefficient is given by

$$C_p(x) = \int_{k_s}^{\infty} dk\,(p-1)\,k_s^{p-1}k^{-p}\cos kx. \qquad \text{(B.2)}$$

Making a change of variable gives the correlation coefficient as

$$C_p(z) = (p-1)\,z^{p-1}\int_{z}^{\infty} du\; u^{-p}\cos u. \qquad \text{(B.3)}$$

where $z = k_s x$. The last equation can be written in terms of the incomplete gamma function

$$\gamma(a,x) = \int_0^x dt\, e^{-t} t^{a-1} \tag{B.4}$$

as

$$\begin{aligned} C_p(z) &= (p-1)\cos\left[\frac{\pi}{2}(p-1)\right]\Gamma(1-p) \\ &- \frac{1}{2}(p-1)\, z^{p-1}\left[i^{1-p}\,\gamma(1-p,-iz) + (-i)^{1-p}\,\gamma(1-p,iz)\right] \end{aligned} \tag{B.5}$$

Expanding the incomplete gamma function about x equal zero gives

$$\gamma(a,x) = x^a \sum_{n=0}^{\infty} \frac{(-1)^n x^n}{n!\,(a+n)}. \tag{B.6}$$

Substituting the last equation into equation (B.5) gives an expression for the correlation function for small argument as

$$\begin{aligned} C_p(z) &= 1 + (p-1)\cos\left[\frac{\pi}{2}(p-1)\right]\Gamma(1-p)\,|z|^{p-1} \\ &+ (1-p)\sum_{m=1}^{\infty} \frac{(-1)^m z^{2m}}{(2m-p+1)\,(2m)!}. \end{aligned} \tag{B.7}$$

The last expression is valid for fractional p. For p equal to an even integer, the appropriate limit of the cosine and gamma

term must be taken, yielding

$$C_{2n}(z) = 1 + \frac{(-1)^n \pi |z|^{2n-1}}{2(2n-2)!} + (1-2n)\sum_{m=1}^{\infty} \frac{(-1)^m z^{2m}}{(2m-2n+1)(2m)!}. \tag{B.8}$$

For p equal to an odd integer, equation (B.3) can be expressed in terms of an exponential integral [Abramowitz and Stegun, 1975] and represented in terms of its series expansion about zero as

$$C_{2n+1}(z) = 1 + \frac{(-1)^n z^{2n}}{(2n-1)!}\left[-\gamma + \sum_{k=1}^{2n} \frac{1}{k} - \ln|z|\right] - \sum_{m=1, m\neq n}^{\infty} \frac{n(-1)^m z^{2m}}{(m-n)(2m)!}. \tag{B.9}$$

For large argument, equation (B.3) can be integrated using integration by parts, giving

$$C_p(z) = -(p-1)\frac{\sin z}{z}\left[1 - \frac{p(p+1)}{z^2} + \ldots\right] + (p-1)\frac{\cos z}{z}\left[\frac{p}{z} - \frac{p(p+1)(p+2)}{z^3} + \ldots\right]. \tag{B.10}$$

Appendix C

Physical Optics Formulation

Physical optics is described by *Beckman and Spizzichino* [1963], *Tsang et al.* [1985], *Kong* [1986] and *Holliday et al.* [1986], but since the derivation is short it is given here for application to a unidirectional surface and to illustrate the approximations that are made. For a perfectly conducting surface, the back scattered electric field at normal incidence from an L by L patch on a unidirectional surface ($\delta\eta/\delta y = 0$) is found from the electric surface current K in terms of a Green's function as

$$\overline{E}(r) = ik\eta_o L \int_{-L/2}^{L/2} dx' \left(1 + \left[\frac{\partial \eta(x')}{\partial x}\right]^2\right)^{\frac{1}{2}} g(r,x')\,\overline{K}(x') . \qquad (C.1)$$

The far field (r >> x') Green's function is given by

$$g(r,x') = e^{-ikz'} \left.\frac{e^{ikr}}{4\pi r}\right|_{z'=\eta(x')} . \qquad (C.2)$$

The electromagnetic wave number is given by k, the surface displacement by η and the impedence of free space by η_o. The

physical optics or tangent plane approximation is used to estimate the surface current as

$$\overline{K}(x') = 2\hat{n} \times \overline{H}_i = \frac{2E_o}{\eta_o}\left(1 + \left[\frac{\partial \eta(x')}{\partial x}\right]^2\right)^{-\frac{1}{2}} e^{-ik\eta(x')}. \qquad (C.3)$$

The unit vector normal to the surface is given by $\mathbf{n}$, and the incident electric and magnetic fields are given by E_o and H_i. For this approximation to provide an accurate estimate of the surface current, the surface must be sufficiently smooth. A criteria for the surface smoothness is given by equation 3.10.

The back scatter coefficient is given by

$$\sigma^2 = \frac{1}{L^2}\left\langle \frac{4\pi r^2 \overline{E} \cdot \overline{E}^*}{E_o^2} \right\rangle = \frac{k^2}{\pi} \int_{-L/2}^{L/2} \int_{-L/2}^{L/2} dx dx' \langle e^{i2k[\eta(x) - \eta(x')]} \rangle. \qquad (C.4)$$

Assuming the surface displacement has a Gaussian probability density function, the average term can be expressed in terms of the surface correlation function and variance σ^2 as [*Tsang et al.*, 1985, p. 79 or *Kong*, 1986, p. 535]

$$\langle e^{i2k[\eta(x) - \eta(x')]} \rangle = e^{-4\sigma^2 k^2 [1 - C(x - x')]}. \qquad (C.5)$$

The double integral can be reduced to a single integral as

$$\int_{-L/2}^{L/2}\int_{-L/2}^{L/2} dx dx' f(x-x') = L\int_{-L}^{L} dx(1-|\alpha|/L)\, f(\alpha)\,. \qquad (C.6)$$

The back scatter coefficient is given by

$$\sigma^{o} = \frac{k^2 L}{\pi}\int_{-L}^{L} dx(1-|x|/L)\, e^{-4\sigma^2 k^2[1-C(x)]}\,. \qquad (C.7)$$

By making the integration variable nondimensional and rearranging, the back scatter coefficient is given by

$$\sigma^{o} = \left(\frac{k^2 L^2}{\pi}\right)\int_{-1}^{1} du(1-|u|)\, e^{-4\sigma^2 k^2[1-C(Lu)]}\,. \qquad (C.8)$$

References

Abramowitz, M. and I.A. Stegun, Handbook of mathematical functions with formulas, graphs, and mathematical tables, 568 pp, New York, Academic Press, 1975.

Arnold, D.V., J.A. Kong, W.K. Melville, and R.W. Stewart, Theoretical prediction of EM bias, Proc. Progress in Electromagnetics Research Symposium, 354-355, Boston, Mass., 1989.

Arnold, D.V., W.K. Melville and J.A. Kong, Theoretical prediction of EM bias, Conference Proc. Oceans 90, 253-256, Washington, D.C., 1990.

Arnold, D.V., J.A. Kong, and W.K. Melville, Physical optics prediction of EM bias, Proc. Progress in Electromagnetics Research Symposium, 169, Cambridge, Mass., 1991.

Axline, R.M. and A.K. Fung, Numerical computation of scattering from a perfectly conducting rough surface, IEEE Trans. Antennas and Propag., 26, 482-488, 1978.

Banner, M.L., I.S.F. Jones and J.C. Trinder, Wavenumber spectra of short gravity waves, J. Fluid Mech., 198, 321-344, 1989.

Barrick, D.E., Rough surface scattering based on the specular point theory, IEEE Trans. Ant. Propag., 16, 449-454, 1968.

Barrick, D.E., Unacceptable height correlation coefficients and the quasi-specular component in rough surface scattering, Radio Science, 5, 647-654, 1970.

Barrick, D.E. and E. Bahar, Rough surface scattering using specular point theory, IEEE Trans. Ant. Propag., 29, 798-800, 1981.

Barrick, D.E. and B.J. Lipa, Analysis and interpretation of altimeter sea echo, Advances in Geophysics, 27, 61-100, 1985.

Beckmann, P. and A. Spizzichino, The scattering of electromagnetic waves from rough surfaces, Macmillan Co., New York, N.Y., 503 pp., 1963.

Born, G.H., M.A. Richards and G.W. Rosborough, An empirical determination of the effects of sea state bias on SEASAT altimetry, J. Geophys. Res., 87, 3221-3226, 1982.

Chan, M.F. and A.K. Fung, A numerical study of the regions of validity of the Kirchhoff and the small-perturbation rough surface scattering models, Radio Science, 23, 163-170, 1988.

Chelton, D.B. and P.J. McCabe, A review of satellite altimeter measurement of sea surface wind speed: With a proposed new algorithm, J. Geophys. Res., 90, 4707-4720, 1985.

Choy, L.W., D.L. Hammond and E.A. Uliana, Electromagnetic bias of 10 GHz radar altimeter measurements of MSL, Mar. Geod., 8(1-4), 297-312, 1984.

Desanto, J.A. and G.S. Brown, Analytical techniques for multiple scattering from rough surfaces, Progress in Optics, 23, 1-62, 1986.

Donelan, M.A., J. Hamilton and W.H. Hui, Directional spectra of wind-generated waves, Phil. Trans. R. Soc. Lond. A, 315, 509-562, 1985.

Donelan, M.A. and W.J. Pierson, Jr., Radar scattering and equilibrium ranges in wind-generated waves with application to scatterometry, J. Geophys. Res., 92, 4971-5029, 1987.

Douglas, B.C. and R.W. Agreen, The sea state correction for GEOS 3 and SEASAT satellite altimeter data, J. Geophys. Res., 88, 1655-1661, 1983.

Doviak, R.J. and D.S. Zrnic, Meteorological radar signal processing, in Doppler Radar and Weather Observations, 91-120, Academic, San Diego, Calif., 1984.

Evans, D.D. and O.H. Shemdin, An investigation of the modulation of capillary and short gravity waves in the open ocean, J. Geophys. Res., 85, 5019-5024, 1980.

Fu, L. and R. Glazman, The effect of the degree of wave development on the sea state bias in radar altimetry measurement, J Geophys. Res., 96, 829-834, 1991.

Fung, A.K. and R.K. Moore, The correlation function in Kirchhoff's method of solution of scattering of waves from statistically rough surfaces, J. Geophys. Res., 71, 2939-2943, 1966.

Fung, A.K. and H.L. Chan, On the integral for backscattering from a randomly rough surface, Proc. IEEE, 59, 1280-1281, 1971.

Fung, A.K. and H.J. Eom, Note on the Kirchhoff rough surface solution in backscattering, Radio Science, 16, 299-302, 1981.

Hagfors, T., Relationship of geometric optics and autocorrelation approaches to the analysis of lunar and planetary radar, J. Geophys. Res., 71, 379-382, 1966.

Hasselmann, K., T.P. Barnett, E. Bouws, H. Carlson, D.E. Cartwright, K. Enke, J.A. Ewing, H. Gienapp, D.E. Hasselmann, P. Kruseman, A. Meerburg, P. Muller, D.J. Olbers, K. Richter, W. Swell and W. Walden, Measurements of wind-wave growth and swell decay during the Joint North Sea Wave Project, Deutsches Hydrographisches Institut, Hamburg, 1973.

Hayne, G.S. and D.W. Hancock, III, Sea-state-related altitude errors in the SEASAT radar altimeter, J. Geophys. Res., 87, 3227-3231, 1982.

Hoge, F.E., W.B. Krabill and R.N. Swift, The reflection of airborne UV laser pulses from the ocean, Mar. Geod., 8(1-4), 313-344, 1984.

Holliday, D., G. St-eyr and N.E. Woods, A radar ocean imaging model for small to moderate incidence angles, Int. J. Remote Sensing, 7, 1809-1834, 1986.

Huang, N.E., S.R. Long, L.F. Bliven and C. Tung, The non-gaussian joint probability density function of slope and elevation for a nonlinear gravity wave field, J. Geophys. Res., 89, 1961-1972, 1984.

Jackson, F.C., The reflection of impulses from a nonlinear random sea, J. Geophys. Res., 84, 4939-4943, 1979.

Jahne, B. and K.S. Riemer, Two-dimensional wave number spectra of small-scale water surface waves, J. Geophys. Res., 95, 11531-11546, 1990.

Jessup, A.T., Detection and characterization of deep water wave breaking using moderate incidence angle microwave backscatter from the sea surface, Ph.D. thesis, 344pp, Joint Program in Oceanogr. and Oceanogr. Eng., Mass. Inst. of Technol./Woods Hole Oceanogr. Inst., Woods Hole, Mass., 1990.

Jessup, A.T., W.K. Melville and W.C. Keller, Breaking waves affecting microwave backscatter, J. Geophys. Res., 96, 20547-20569, 1991.

Kodis, R.D., A note on the theory of scattering from an irregular surface, IEEE Trans. Ant. Propag., 14, 77-82, 1966.

Lipa, B.J. and D.E. Barrick, Ocean surface height-slope probability density function from SEASAT altimeter echo, J. Geophys. Res., 86, 10921-10930, 1981.

Longuet-Higgins, M.S., The effect of non-linearities on statistical distributions in the theory of sea waves, J. Fluid Mech., 17, 459-480, 1963.

Melville, W.K., D.V. Arnold, R.H. Stewart, W.C. Keller, J.A. Kong, A.T. Jessup and E. Lamarre, Measurements of EM bias at Ku and C bands, Conf. Proc. Oceans 90, 181-186, Washington, D.C., 1990.

Melville, W.K., R.H. Stewart, W.C. Keller, J.A. Kong, D.V. Arnold, A.T. Jessup, M.R. Loewen and A.M. Slinn, Measurements of electromagnetic bias in radar altimetry, J. Geophys. Res., 96, 4915-4924, 1991.

Nerem, R.S., B.D. Tapley and C.K. Shum, Determination of the ocean circulation using GEOSAT altimetry, J. Geophys. Res., 95, 3163-3179, 1990.

Reece, A.M., Jr., Modulation of short waves by long waves, Boundary Layer Meteorol., 13, 203-214, 1978.

Rodriguez, E., Y. Kim and J.M. Martin, The effect of small-wave modulation on the electromagnetic bias, J. Geophys. Res., 97, 2379-2389, 1992.

Shemdin, O.H., H.M. Tran and S.C. Wu, Directional measurement of short ocean waves with stereophotography, J. Geophys. Res., 93, 13891-13901, 1988.

Slinn, A., M.S. Thesis, Mass. Inst. of Technol., 1990.

Srokosz, M.A., On the joint distribution of surface elevation and slopes for a nonlinear random sea with application to radar altimetry, J. Geophys. Res., 91, 995-1006, 1986.

Tyler, G.L., Wavelength dependence in radio-wave scattering and specular-point theory, Radio Science, 11, 83-91, 1976.

Valenzuela, G.R., Theories for the interaction of electromagnetic and ocean waves - a review, Boundary Layer Meteorol., 13, 61-85, 1978.

Walsh, E.J., D.W. Hancock, D.E. Hines and J.E. Kenney, Electromagnetic bias of 36 GHz radar altimeter measurements of MSL, Mar. Geod., 8, 265-296, 1984.

Walsh, E.J., F.C. Jackson, E.A. Uliana and R.N. Swift, Observations on electromagnetic bias in radar altimeter sea surface measurements, J. Geophys. Res., 94, 14575-14584, 1989.

Walsh, E.J., F.C. Jackson, D.E. Hines, C. Piazza, L.G. Hevizi, D.J. McLaughlin, R.E. McIntosh, R.N. Swift, J.F. Scott, J.K. Yungel and E.B. Frederick, Frequency dependence of electromagnetic bias in radar altimeter sea surface range measurements, J. Geophys. Res., 96, 20571-20583, 1991.

Yaplee, B.S., A. Shapiro, D.L. Hammond, B.D. Au and E.A. Uliana, Nanosecond radar observations of the ocean surface from a stable platform, IEEE Trans. Geosci. Electron., 9, 170-174, 1971.